GEOCHEMICAL ANALYSIS OF FOUR LATE MIDDLE PENNSYLVANIAN CORES FROM SOUTHERN INDIANA

Clinton M. Broach

Submitted to the faculty of the University Graduate School
in partial fulfillment of the requirements
for the degree
Master of Science
in the Department of Earth Sciences,
Indiana University

December 2014

Accepted by the Graduate Faculty, of Indiana University, in partial fulfillment of the requirements for the degree of Master of Science.

_____

William Gilhooly III, PhD, Chair

_____

Greg Druschel, PhD

Master's Thesis
Committee

_____

Kathy Licht, PhD

DEDICATION

This work and the degree which it confers are dedicated to my children,

Ethan Morris and Elayne Adele.

ACKNOWLEDGEMENTS

I would like to acknowledge the stalwart dedication, commitment, and sense of professional responsibility shown by my advisor, Dr. William Gilhooly, III. Without his persistence and hard work in developing and moving both this project and myself on the right path, this research could never have been accomplished. I would also like to thank my other committee members, Dr. Greg Druschel and Dr. Kathy Licht; my undergraduate advisor and mentor Dr. William Elliott Jr.; and Dr. Christopher Smith of Weatherford International Ltd. for their patience, mentorship, funding and professional scrutiny of this document and research. Lastly, I would like to thank my wife and family for their enduring patience as I went through this research process; without their unflappable love, support, and understanding I would and could not have completed this document.

GEOCHEMICAL ANALYSIS OF FOUR LATE MIDDLE PENNSYLVANIAN CORES FROM SOUTHERN INDIANA

Clinton M. Broach

The shale and mudstone directly superjacent to Desmoinesian coal seams of southern Indiana (Springfield, Houchin Creek, Survant, and Seelyville coals) were initially deposited under marine waters and are shown to exhibit high concentrations of organic carbon, sulfur and redox-sensitive metals (Mo, V, Ni, Fe, and U) that were sequestered during times of benthic anoxia and intermittent to sustained euxinia (anoxic and sulfidic). Strata upsection display geochemical signatures that indicate increasingly oxic and nearshore sedimentation that mirrors cyclothemic sequence stratigraphic trends.

Carbon source, nearshore and offshore proximity, freshwater and marine influence, and redox conditions of the epeiric sea overlying southern Indiana during the Late Middle Pennsylvanian were identified and tracked throughout the deposition of four drill cores of the Petersburg, Linton and Staunton Formations. Carbon, nitrogen, and sulfur data (total organic carbon [TOC], total nitrogen [TN], and total sulfur [TS]); paleoredox proxies ([Mo/Al], [V/Al], [Th/U], [Fe_{tot}/Al]); organic carbon isotopes ($\delta^{13}C_{org}$); and detrital influx concentrations (Zr) were all used in conjunction with lithological and paleontological interpretations to better understand the mode of deposition in this unique midcontinent ancient epeiric sea. Geochemical results when combined with lithologic and paleontologic interpretations reveal a dynamic environmental system where water column geochemistry varies with the influence of

variable magnitudes of epeiric seawater flooding on the extensive peatlands of equatorial Late Middle Pennsylvanian southern Indiana.

William Gilhooly III, PhD

TABLE OF CONTENTS

1. INTRODUCTION

Pennsylvanian shales and mudstones within the midcontinent of North America were deposited under an equatorial epeiric sea, which at times of maximum transgression, extended from the Appalachian basin to the ancient western Panthalassic Sea (Algeo, 2008). This epeiric sea, named the Late Pennsylvanian Midcontinent Sea (LPMS), was a dynamic depositional environment characterized by marine sedimentation when sea levels were high and terrestrial peat accumulation and clastic sedimentation when they were low (Fig. 1). Detrital influxes from the Alleghenian and Ouachita orogenic highlands provided a large quantity of sediments that fed lowland deltaic environments along the coasts (Fig. 1). In addition, rapid sea level change driven by Gondwanan glacial and interglacial cycles resulted in dramatic shifts in the lateral position of LPMS coastlines of the midcontinent throughout the Pennsylvanian (Heckel, 2008). Indeed, at times of maximum glaciation the Gondwanan Ice Age was a global event comparable in extent to the northern hemisphere Pleistocene glacial maxima in terms of both ice volume and effects of global eustasy (Heckel, 2008; Algeo and Heckel, 2008; Falcon-Lang, 2012; Fig. 1). Equatorial

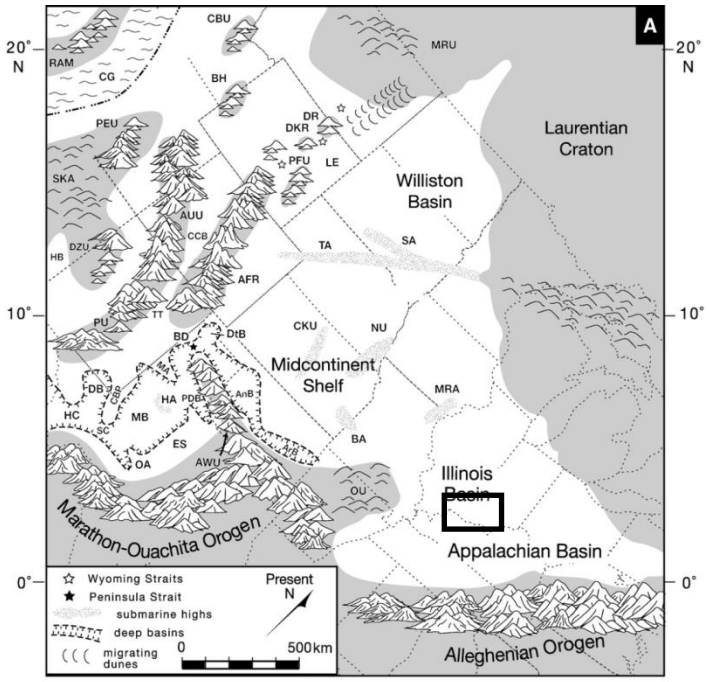

Figure 1. LPMS with box covering eastern portion of Illinois Basin, modified from Algeo and Heckel, 2008.

vegetation throughout the midcontinent produced laterally extensive Pennsylvanian tropical peat mires, which were potentially the largest peatlands ever produced in Earth history (Greb, et al., 2003). The coals produced from the diagenetic compaction and lithification of these peatlands have long been exploited as an energy resource and have thus been studied extensively (Phillips, et al., 1985; Jacobson, 1983, 1987; Treworgy and Jacobson, 1986; DiMichele and Nelson, 1989; Archer and Kvale, 1993; DiMichele, et al., 1996; Philips and DiMichele, 1998; Greb, et al., 2003; Heckel, 2008; Strapoc, et al., 2008). The organic-rich shale, that in many instances overlies these coals, has also recently drawn a lot of attention due to advances in hydraulic fracture technologies that allow for the hydrocarbons within them to be extracted economically (Loucks and Ruppel, 2007). But while the process of coal formation has been well studied, the sedimentary controls on this organic-rich black shale deposition are still somewhat enigmatic and resolving the geochemical conditions necessary for their formation is still under investigation (Rimmer, et al., 2004; Schultz, 2004; Lyons and Severmann, 2006). In addition to an economic incentive, resolving both black shale and mudstone depositional controls has broader implications for paleoclimate reconstructions and global climate change (Falcon-Lang, 2004; Heckel, 2008; Fielding, et al., 2008; Frank, et al., 2008).

Based on sedimentological and depositional analyses of modern environments, the model for black shale formation was traditionally interpreted to have been deposited under relatively ‘deep water’ anoxic conditions in basins with little exchange with the open ocean (Heckel, 1977; Schultz and Coveney, 1992; Schultz, 2004). Due to their prevalence across a range of geological environments, most notably in what are now

understood to be relatively shallow paleoenvironments, these interpretations have been reexamined (Hatch and Levanthal, 1992; Schultz and Coveney, 1992, Algeo and Heckel, 2008). An array of geochemical analyses, from metal enrichment proxies to stable isotope compositions, when used in conjunction with sedimentological and paleontological data can improve interpretations of environments of deposition and when analyzed stratigraphically can track these depositional controls through time (Schultz, 2004; Algeo et al., 2006; Scott and Lyons, 2012).

The development of geochemical models that discern between oxic and anoxic systems, marine and terrestrial carbon sources, and degrees of marine versus riverine water influx, are vital to the interpretations of paleoenvironmental basin development and contribute to a greater understanding of sedimentary deposition in aqueous environments both in ancient and modern systems. My research focuses on using geochemical tools in conjunction with sedimentological and paleontological data to reconstruct a more accurate depositional model for black and grey shale facies overlying four coal seams from southern Indiana. These sediments were deposited when transgressive LPMS marine waters flooded low-lying Illinois basin peat mires.

For my research I examined the geochemistry of these mudrock-rich drill cores from well USI 1-32. These geochemical analyses were compared with previously studied sedimentological and paleontological analyses on the LPMS coals and black shale (Broach and Elliott, 2011), in order to more accurately determine the depositional model and water chemistry for southern Indiana during the Late Middle Pennsylvanian. The combined approach of sedimentology and geochemistry provides insight into key differences between sediments deposited earlier (in Cores 4 and 5) and those deposited

later (Core 2 and 3). Of particular interest is the lack of black shale in Cores 4 and 5, which otherwise have similar facies observed within Cores 2 and 3. In addition, while the presence of marine fauna suggests marine conditions for the muds above Core 2 and Core 3 no such paleontological data was found in Core 4 and Core 5. My goal was to use the geochemical data to further characterize the muddy lithofacies to confirm initial observations and assess depositional models for these lithofacies, which occur in cyclothem-like depositional sequences.

2. BACKGROUND

2.1 Stratigraphy

Four cores of Late Middle Pennsylvanian (Desmoinesian Series) strata from southern Indiana with coal and superjacent mudrock were studied (Fig. 2). The general stratigraphy of each 20 ft. core is summarized as follows: Core 5 - 20 ft. of the Staunton Formation (Raccoon Creek Group) and consists of the Seelyville coal seam overlain by grey mudrock with no marine fossils; Core 4 – 20 ft. of the Linton Formation (Carbondale Group) and consists of the Survant coal seam overlain by grey mudrock with no marine fossils; Core 3 – 20 ft. of the Petersburg Formation (Carbondale Group) and consists of the Houchin Creek coal overlain by the Excello Shale (black shale) then grey mudrock with marine fossils; Core 2 – 20 ft. of the Petersburg Formation (Carbondale Group) and consists of the Springfield coal seam overlain by black then grey shale containing marine fossils (Fig. 2). Complete core descriptions are provided in the Results section.

Indiana Stratigraphy					
Period	Series	Group	Formation	Coal Member	USI 1-32 Cores
Middle Pennsylvanian	Desmoinesian	Carbondale	Petersburg	Springfield Coal	**Core 2 (395'-415')**
				Stendal Ls.	
				Excello Sh.	**Core 3 (495'-515')**
				Houchin Creek Coal	
			Linton		
				Survant Coal	**Core 4 (540'-560')**
				Velpen Ls.	
				Mecca Sh.	
				Colchester Coal	
				Coxville Ss.	
		Raccoon Creek	Staunton	Seelyville Coal	**Core 5 (655'-675')**

Figure 2. Portion of Middle Pennsylvanian stratigraphy of Indiana showing four coal-bearing cores of well USI 1-32. (Adapted from Indiana Geological Survey, Bulletin 59, Plate 2, Shaver, et al., 1986)

2.2 Paleogeography

The midcontinent of the US during the Late Middle Pennsylvanian (~300 Ma) was located at 5-10˚N latitude (Algeo, et al., 2004; Algeo and Heckel, 2008). The climate was tropical with limited seasonal temperature ranges and monsoonal precipitation fluxes (Algeo et al., 2004; Algeo, et al., 2007; Algeo and Heckel, 2008; Heckel, 2008). The LPMS covered a large portion of the midcontinent including the entirety of the Illinois basin (Fig. 3). At highstand (times of maximum sea level), waters reached as far inland as the Appalachian Basin. Eustatic response to glacial-interglacial cycles from the vast ice sheets covering Gondwana (Algeo et al., 2004; Algeo and Heckel, 2008; Falcon-Lang, 2012) caused midcontinent water depths in the Illinois basin to fluctuate between 0-70 m (Algeo and Heckel, 2008). These relatively shallow depths, combined with the paleoenvironmental and paleoclimatic conditions of the LPMS, are unusual relative to the traits of epeiric seas of today. Hudson Bay, the Black and Baltic Seas, and even Norwegian fjords, like Framvaren, have been identified as contemporary systems that provide insight into the

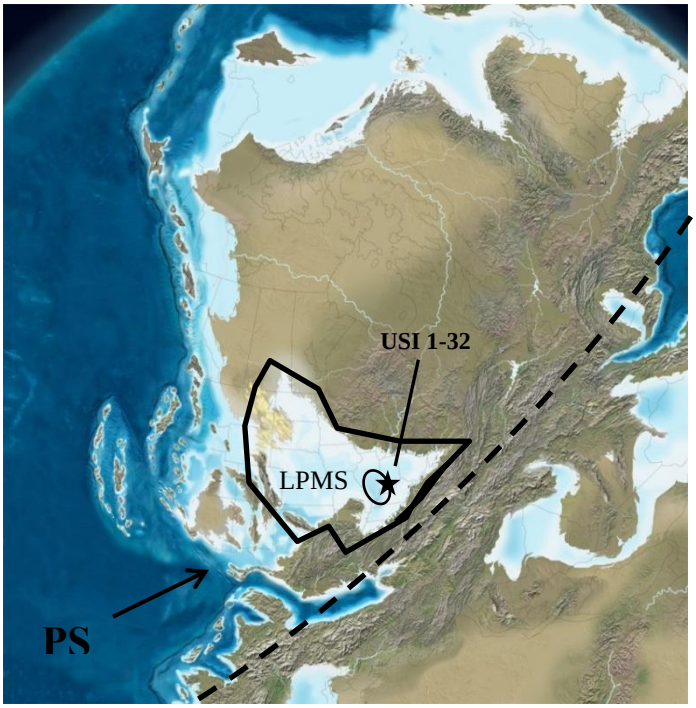

Figure 3: Paleogeographic reconstruction of Laurentia during the Middle to Late Pennsylvanian, ~300 Ma (Ron Blakey and Colorado Plateau Geosystems, Inc). The study site (USI 1-32; star) is located in the LPMS (solid line), north of the paleoequator (dashed line). The open marine waters (arrow) of the Panthalassic Sea (PS) enter the Illinois Basin (ellipse) from the west.

ways in which the hydrography and the water chemistry in the LPMS changed with sea-level fluctuations.

Laterally extensive anoxic sediment facies in the midcontinent, particularly black shales can be traced from the ancient west to east coasts of the LPMS. The lateral continuity of these facies indicate that the LPMS certainly contained anoxic bottom waters that were both present in large areas, and persistent and reoccurring throughout most of the Pennsylvanian (Algeo, 2004: Algeo, 2008). Modern anoxic settings with analogous sedimentation and water column chemistry include the Black Sea, the Baltic Sea, the Cariaco Basin, and the Framvaren fjord (Algeo, et al., 2006). Unlike these modern basins however, the LPMS was a vast (~2.1 x 10^6 km^2) epeiric sea that lacked a sill that would have impeded circulation. It is hypothesized that this seaway received oxygen-depleted water from an upwelling zone along the distant western margin, some 2000 km away, and then only through subsequent circulation and advection through the deepwater channel to the southwest, what would eventually form the Greater Permian Basin Seaway (Algeo, 2004, 2008; Algeo and Heckel, 2008). Thus, determining whether and when LPMS waters were ever fully oxygenated ('normal' marine) or whether they were dominated by sustained benthic anoxia, and possibly euxinia (both anoxic and sulfidic) is still unresolved. All of these conditions, along with its hypothesized 'super estuarine' system (Algeo, 2008) and equatorial location make the LPMS difficult to compare with modern analogs. Depositional models of the LPMS thus require a holistic approach with regards to proper characterization of the water chemistry and sedimentation behavior.

2.3 Depositional Environment

The coal seams, black shale, and grey shale contained in the four cores in this study contain portions of the cyclothemic stratigraphy (cyclothems) common to midcontinent Pennsylvanian strata. Cyclothems are characterized by strata displaying a 'cycle' of deposition - an underclay, or paleosol, followed by a coal seam, then a 'deep' water facies such as black shale or limestone with a subsequent shallowing upwards (regressive) sequence of lithologies, generally a grey silty shale and eventually a fluvial or deltaic sandstone or siltstone (Heckel, 2008). Depositional interpretations of these cyclothemic facies consist of: 1) a terrestrial underclay or paleosol formed from subaerial exposure, 2) followed by peat accumulation in a near shore paludal equatorial environment (coal), 3) flooded by a 'rapid' marine transgression depositing a fossiliferous limestone or fossil rich mud/shale directly over the peat and, 4) deposition of a relatively slower regressive sequence resulting in progressively shallower facies that transition into a repeat of the sequence (Heckel, 2008). Overlying the coal is a black shale or limestone, which are the cyclothem 'deepwater' facies. However, these deepwater facies are often 'missing' and the coals are often overlain by a grey shale/mudstone facies with no discernible unconformities. These grey shale facies have were originally interpreted to be the result of riverine crevasse splays and levee overbank discharge over surrounding peatlands (Eggert, 1982; Treworgy and Jacobson, 1985; DiMichele and Nelson, 1989). This nonmarine (fluvial) interpretation was later reclassified as a coastal environment of mixed deltaic to estuarial origin based on the evidence of tidally influenced sedimentary structures present in many grey shales superjacent to coal seams (Archer and Kvale, 1993). In addition, resolving mudrock

(shale and mudstone) depositional environments has always been difficult to ascertain due to the small grain size (silt and clay) of the muds in question which are not visible under ordinary petrographic microscopes (Boggs, 1995). Thus, those who study mudrocks are forced to use other tools, like geochemical data, to answer their depositional riddles and provide accurate interpretations. Regardless of the depositional affinity (marine or nonmarine), the grey and black cyclothemic shales facies overlying Middle Pennsylvanian coals in the Illinois Basin are evidence of a dramatic shift in deposition, from subaerial to subaqueous. The marine flooding event, and the depositional controls that determine shale lithofacies deposition within these cyclothems can be well characterized when a combined geochemical, lithological, and paleontological approach is utilized.

During interglacial periods of the Middle Pennsylvanian, sea levels rose in the LPMS and flooded low-lying peatlands. The seawater delivered metals, nutrients, marine organic matter, and a large reservoir of sulfate ions to coastal peatlands and deltas. The marine influx mixed with riverine and deltaic inputs characterized by large quantities of detrital minerals, low metal concentrations, terrestrial organic matter, and relatively low sulfur concentrations. Although sequence stratigraphic concepts explain these interactions in terms of large-scale lithofacies development (e.g. 1^{st} to 4^{th} order; Heckel, et al., 1998) the depositional controls at the sub-4^{th} order (cyclothem) sequence level recorded in the shale and mudstone are often not distinct.

Although the LPMS and its corresponding cyclothemic facies have been studied extensively (Greb, et al., 2003; Algeo and Maynard, 2004; Algeo, 2004, 2008; Algeo, et al., 2007; Algeo and Lyons, 2007; Heckel, 2008; Woodard, et al., 2013) and a picture of

the truly dynamic depositional character is beginning to emerge, most geochemical studies have focused on either the far easternmost strata in the Appalachian Basin or on the deeper water strata deposited in present Kansas and Oklahoma. Because of this focus on near-shore and outboard endmember environments, the intermediate Illinois Basin has been somewhat overlooked from a geochemical perspective. This research builds upon the current state of knowledge concerning Pennsylvanian deposition for the Illinois Basin and aids in filling in the gap regarding southern Indiana during the Late Middle Pennsylvanian.

2.4 Geochemical Proxies

The geochemical core analysis on the coals and mudrocks of USI 1-32 consisted of an array of geochemical techniques and proxies and three groupings of geochemical data. The first was metal and metalloid enrichment data, specifically Mo, Fe, V, Th, and U because these enrichments have been shown to track paleoredox conditions of the water column under which the sediment was deposited. The second group included total organic carbon (TOC), total inorganic carbon (TIC), total nitrogen (TN), and total sulfur (TS). The concentrations of carbon, nitrogen, and sulfur, used in conjunction with various metal data, can be used to determine the quantity of organic matter sequestered in the sediment, as well as the conditions necessary for this sequestration to occur, and the type of organic matter being deposited (terrestrial or marine). The third group included the isotopic composition of organic carbon ($\delta^{13}C_{org}$) and zirconium (Zr) concentrations, which can be used to track the source of the organic matter and proximity of shoreline relative to deposition.

2.4.1 Carbon, Sulfur, and Nitrogen

2.4.1.1 Organic Carbon

Organic matter is relatively scarce in sedimentary rocks. In general, sedimentary rocks contain only about 1% TOC (Degens, 1965). Coals on the other hand generally contain on average 70% organic carbon (Degens, 1965; Mastalerz, 2010). Mudrocks average 2.1% and of these, organic carbon concentrations in black shale (black due to the elevated presence of this organic matter) can be considerable, ranging 3-10% (Boggs, 1995). Organic carbon in coal is derived from plant matter in peat mires that has been compressed and diagenetically altered. Organic matter accumulates in shales as the result of far different processes. Organic carbon in sedimentary rocks is preserved when plant or animal tissue settles in a depositional basin and escapes microbial degradation (Boggs, 1995).

Research on ancient shale formation at first focused on two endmember processes to explain the presence of organic-rich black shales in general. The 'preservation' model proposes that restricted circulation within a basin caused by physical isolation and a permanent pycnocline promotes anoxic conditions. Bottom water anoxia within a stratified basin, such as the modern Black Sea, enhances organic matter preservation by inhibiting aerobic decomposition (Murphy et al., 2000). The 'productivity' model posits that high organic matter content is a consequence of enhanced surface water productivity and organic matter deposition into benthic zones followed by decomposition and rapid consumption of dissolved oxygen that exceeds the rate of advective resupply by water column mixing (Murphy et al., 2000; Schultz, 2004). It is important to note that both models posit that high organic matter sequestration in ancient sediments is possible only with benthic anoxia. The models differ only in how that benthic anoxic boundary or

chemocline is generated (by either stratification or productivity). The mechanisms of organic matter accumulation likely require a combination of both of these factors. Furthermore, the complex LPMS hydrography contributes an additional control, such as the potential for pre-conditioned oxygen-deficient water and the presence and magnitude of inorganic inputs (especially detrital or clastic dilution) (Calvert et al., 1996; Murphy et al., 2000; Rimmer, et al., 2004).

In the LPMS, Algeo and Heckel (2008) posit that even if productivity was low and seawater freely circulated, the waters were oxygen-depleted prior to arriving at central LPMS and eastern shores within the Illinois Basin (in present-day southern Indiana). They propose that seawater delivered from the Panthalassic Sea on the western margin of the North American continent supplied oxygen-deficient waters to the LPMS. In this model, oxygen concentrations were lowered within an oxygen minimum zone (OMZ) in the Panthalassic Sea, and remained at low levels because transport through the deep and narrow proto-Greater Permian Basin Seaway prevented mixing and replenishment of oxygen. These 'preconditioned' oxygen-deficient waters, when combined with relatively shallow bathymetry, elevated terrestrial runoff into a landlocked superbasin, a strong pycnocline, and estuarine-type circulation resulted in widespread benthic anoxia (Algeo and Heckel, 2008).

Assuming that black shale is the result of benthic anoxia then the Illinois Basin stratigraphy would suggest that benthic anoxia was both persistent and laterally extensive across the LPMS (Algeo and Heckel, 2008). Black shales, like the Excello Shale of the Petersburg Formation (Core 3), can be laterally traced over thousands of kilometers across the midcontinent of North America (Ece, 1987; Schultz and Coveney, 1992; Algeo

and Heckel, 2008). This lateral continuity of organic-rich thinly laminated black shales like the Excello across the entire LPMS indicates that benthic anoxia was certainly present and far-reaching. This work focuses on the determination of redox conditions for the mudrock present in LPMS over southern Indiana 300 Ma and whether some degree of seawater restriction and/or detrital influence (deltaic) was perhaps influencing the development of benthic anoxia and the sequestration of organic carbon of the mudrock overlying the coals of the Petersburg, Linton, and Staunton formations.

2.4.1.2 Inorganic Carbon

TIC is a measurement of the amount of carbonate in the sediment, predominantly calcium carbonate ($CaCO_3$). Calcium carbonate can be the result of biogenic calcite remains such as the shells, tests, reefs or other carbonate building organisms or could be the result of abiotic direct precipitation from the water column. Calcium carbonate production is generally promoted in shallow, warmer waters. Limestone benches, while not observed in this study, are found in the Petersburg, Linton, and Staunton Formations (Shaver, et al., 1986). While an acid test using dilute HCl to test for calcium carbonate was completed during the initial core description, no quantitative amounts were calculated, thus a measurement of TIC throughout each core is a check on this 'fizz' test so often done in the field to determine the presence of carbonates.

2.4.1.3 Total Sulfur

In the case of the LPMS, where hydrothermal sources are minimal, the sulfur inputs to coal and mudrock are likely derived from marine or nonmarine sources. The largest modern reservoir of sulfur is in seawater, where it is found overwhelmingly in its oxidized form as sulfate (Millero, 2008). Dissolved sulfate has the third highest ionic

concentration (2.7 parts per thousand; Castro and Huber, 2009) in modern seawater, surpassed only by dissolved sodium and chloride ions. Relative to seawater, rivers contain three orders of magnitude less sulfate ($8.25x10^{-3}$ parts per thousand; Meybeck, 1979; Millero, 2008). Another source of sulfur to coal and possibly to ancient shales could be the organic material itself; however, all modern organic matter today contains only about 1% sulfur by dry weight. Assuming that Pennsylvanian seawater and riverine concentrations of sulfur were equivalent to modern values, and that ancient organisms did not a have substantially higher sulfur content of those today, seawater inundation of peat mires is the mostly likely contribution to the high sulfur concentrations observed in coals and black shales, often 5-15% by weight (Mastalerz, 2010). Indeed it has been shown that when definite marine strata overlies coals, i.e. black shale or limestone, the underlying coal contains higher amounts of sulfur (>2.5%) than when overlain by nonmarine strata, such as grey silty shale (<2.5%; Gluskoter and Simon, 1968; Affolter and Hatch, 2002)

It is important to note that TS is a bulk measurement, which includes reduced sulfur (e.g., pyrite), oxidized sulfur (e.g., sulfate), and organic sulfur compounds. Pyrite that forms in aquatic settings provides a geochemical record of the sulfur source and chemical or biological processes that altered that source. Bacterial sulfate reduction produces dissolved sulfide in anoxic sediments (or water columns), which eventually reacts with iron minerals to form iron monosulfides and eventually FeS_2 (pyrite). Pyrite is thus a common component of black shale and is closely linked to the carbon and iron cycles (Berner and Raiswell, 1983; Murphy, et al., 2000). This bacterial sulfate reduction in turn is only accomplished by the oxidation of organic matter via the overall generalized reaction:

$$2CH_2O + SO_4^{2-} \rightarrow H_2S + 2HCO_3^-$$

Pyrite formation in marine black shale is controlled by sulfate availability, reactive iron delivery, and the quantity of organic matter (Berner and Raiswell, 1983; Schultz, 2004). The coupled carbon-sulfur-iron cycles thus can provide a metric for differentiating marine and freshwater depositional conditions. Marine systems have high sulfur concentrations but are low in reactive iron and organic matter. In contrast, freshwater systems tend to have low sulfur concentrations and high reactive iron and organic matter inputs. Thus determining which component is the limiting factor helps to interpret the chemical composition of the water column and the depositional context of the basin, whether marine or freshwater dominated. In addition to these source indices, the process of sulfate reduction can only proceed under anoxic conditions. The oxic/anoxic interface may occur within the sediment pore waters or within the water column. Euxinic water columns are relatively rare in the modern ocean but the extensive deposits of pyritic black shales in the Pennsylvanian suggest that this redox condition was more prevalent in ancient and shallow oceans like the LPMS (Schultz, 2004; Scott and Lyons, 2012). Evidence of euxinia was examined in all four cores and can be determined by plotting the C/S ratios in Cores 2-5 against known ratios between C and S for marine, freshwater, and modern settings.

2.4.1.4 Total Nitrogen

Nitrogen concentrations in mudrocks may be informative of ancient biogeochemical processes but the interpretations of TN can be complicated by the effects of diagenesis and the multi-step reactions of the biological nitrogen cycle. TN includes organic material and inorganic N compounds, such as ammonium. When paired with

with TOC, the C/N ratio has been used as a proxy for determining the source of the organic matter in modern settings. Sources may include algal or vascular plants. Pelagic algae have higher protein and nucleic acid content (nitrogen-rich) than terrestrial marsh plants, and thus have correspondingly lower C/N ratios (Meyers, 1994). Organic matter deposited in nearshore environments tends to contain more vascular plants (carbon-rich), and therefore higher C/N ratios (Meyers, 1994; Hassan, 1997). Provided that nitrogen has not been preferentially mobilized during diagenesis, the C/N ratios for the coal, black shale, and grey mudrock within all four cores should shed light on determining nearshore versus offshore sedimentation.

2.4.2 Paleoredox Proxies

Redox-sensitive metal concentrations have been used as proxies to interpret both modern and ancient water column redox conditions whether oxic (fully oxygenated), dysoxic (generally 1-30% dissolved oxygen in the water column), anoxic (no dissolved oxygen), and euxinic (anoxic and containing dissolved H_2S) conditions. Among these elements Mo, V, Ni, Fe_{tot}, Th, and U were used for this study.

2.4.2.1 Molybdenum

Molybdenum (Mo) has been demonstrated to concentrate in anoxic sediments. Mo concentrations higher than the crustal average (2ppm) correlate with low redox potential of the water column at the time of shale deposition, and concentrations above 100ppm suggest euxinic conditions (Scott and Lyons, 2012; Schultz, 2004; Rimmer et al., 2004; Algeo, et al., 2007; Murphy, et al., 2000; Algeo, et al., 2004; Algeo and Lyons, 2006). Anoxic conditions also favor a high preservation potential for organic matter, thus a strong correlation between Mo and TOC is observed, particularly in black shales (Algeo

and Lyons, 2006; Scott and Lyons, 2012). The main source for Mo in sediments is derived from marine waters while Mo input from terrestrial sources (continental averages <2 ppm; Scott and Lyons, 2012) is minimal. Thus, Mo concentrations can also serve as proxies for seawater renewal, i.e. to determine when waters had adequate resupply of trace metal-rich seawater or whether waters were restricted.

Molybdenum is removed from the water column by two primary pathways; either by absorption of molybdate (MoO_4^{2-}) onto Mn-oxides, or as thiomolybdate ($MoS_{4\_x}O_x^{2-}$) in the presence of sulfide dissolved in pore water or bottom waters overlying sediment (Scott and Lyons, 2012). The Mn-oxides form a 'manganous zone' where Mo is sequestered temporarily but over time dissolves back into the water column and thus Mo is not retained onto Mn-oxides in ancient sediments (Scott and Lyons, 2012). Mo concentrations > 100 ppm in ancient sediments indicate that Mo-sulfides were likely present in the water column and conditions could be deemed as having sustained euxinia (Scott and Lyons, 2012). Mo concentrations that range between 25 to 100 ppm reflect euxinia but with a combination of other complicating factors, such as intermittent euxinia, dilution of Mo enrichments due to extremely high sedimentation rates, depletion of dissolved Mo from the water column, or the effect of sulfide on Mo-speciation (Scott and Lyons, 2012).

Mo/TOC cross-plots of modern euxinic analogues such as the Black Sea and the Cariaco Basin provide much-needed context for interpreting redox conditions and renewal rates for the eastern LPMS (Fig. 4). These ratios can fluctuate as changing sea level effectively isolates basins from open ocean circulation. Shallow sills prevent supply of nutrient-rich marine water to the modern euxinic basins of the Black Sea and Cariaco Basin during lowstand. The Mo inventories in these basins are then replenished during periods of highstand (Algeo and Lyons, 2006). Thus the rise and fall of Mo concentrations in LPMS waters has been suggested to be a result of a lack of nutrient-rich oxygenated marine water renewal (Algeo and Lyons, 2006; Algeo, et al., 2008). Although there is no structural evidence for a silled basin in the LPMS, the Illinois basin is located far (>2000 km) from the open waters of the Panthalassic. The paleogeographic position of the basin suggests that Mo replenishment could be restricted during times of lowstand.

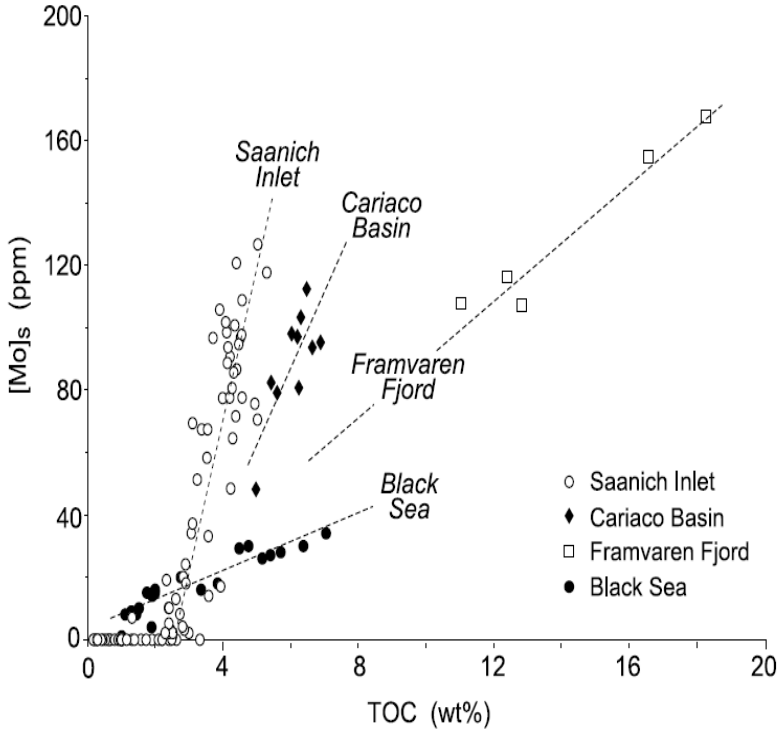

Figure 4: Mo/TOC (ppm/wt%) for modern anoxic silled basins, i.e. basins with some restriction on replenishment of Mo-rich seawater. Taken from Algeo and Lyons, 2006.

2.4.2.2 Vanadium

Vanadium (V) concentrations normalized to Al to control for detrital mineral phases are considered an excellent proxy for the evaluation of redox conditions. In oxic waters, V exists in vanadate ionic species such as HVO_4^{2-} and $H_2VO_4^-$. Under reducing conditions vanadate ions covert to the vanadyl ion (VO^{2+}) and forms related hydroxyl species $VO(OH)_3^-$ or an insoluble hydroxide such as $VO(OH)_2$ (Tribovillard, et al., 2006). In euxinic conditions the presence of H_2S causes reduction and V can be taken up by geoporphyrins or precipitated as solid oxide (V_2O_3) or hydroxide ($V(OH)_3$) phases. This two-tiered reduction process contingent upon the presence of sulfide in the water make V/Al not only a good indication of LPMS anoxic water conditions but also very important in establishing whether LPMS mudrocks were deposited in a sulfidic system (Algeo and Maynard, 2004; Tribovillard, 2006).

2.4.2.3 Thorium and Uranium

The trace elements thorium (Th) and uranium (U) and the calculated Th/U ratio have been used as a measure for redox conditions in the depositional environment (Dypvik and Harris, 2001; Doveton and Merriam, 2004). The Th^{4+} and U^{4+} ions have similar size and charge and display related geochemical behavior; however, U has an additional +2 and +6 charge making it subject to reduction and adhesion on both clay particles and organic matter (Dypvik and Harris, 2001). Under reducing conditions, the uranyl ion (UO_2^{2+}) will be reduced and precipitated or adsorbed on or with organic matter. In addition U is commonly associated with organic carbon and if used in conjunction with other redox proxies mentioned above provides further evidence for redox conditions of the LPMS. Th/U ratios with values >7 indicate an oxic water column.

Values between 2 and 7 suggest less oxic to dysoxic systems, while values <2 are interpreted as anoxic systems (Jones and Manning, 1994; Dypvik and Harris, 2001).

2.4.2.4 Iron

The concentration of total iron (Fe_{tot}) present in each sample throughout all cores was normalized to Al in order to isolate the reactive Fe from detrital components and then used as a paleoredox indicator. There was no speciation determination of Fe, and thus no indication of amount of iron locked in sulfides, sulfates, carbonates, etc. is known at this time. In addition, no determination of the degree of pyritization (DOP) was calculated, a proxy linking the production of reactive Fe to the availability of sulfides. However, recent work by Lyons and Severmann (2006) shows that Fe_{tot} can be used as an excellent paleoredox proxy especially when examined in conjunction with other pertinent trace metal proxies. In fact iron enrichments in ancient sediments (Fe_{tot}/Al >0.5) almost certainly indicate euxinic conditions (Lyons and Severmann, 2006) that result from the export of remobilized iron from the oxic shelf, which is then scavenged from the sulfide-rich water column during syngenetic (non-biogenic) pyrite formation in sediments. This pyritization however, can only indicate that the paleoredox conditions were both anoxic and sulfidic, which is a common state below the sediment-water interface. Whether this anoxic and sulfidic state occurs *above* this sediment-water interface (euxinia) is not illumined by Fe enrichments; only that it *did* occur.

2.4.3 Isotopes and Basin Parameters

2.4.3.1 $\delta^{13}C_{org}$

The stable isotope composition of organic carbon ($\delta^{13}C_{org}$) can be used to differentiate between terrestrial or marine derived organic carbon and have been used

with success in both ancient and modern sediments to determine the source of the organic delivered from overlying waters. Cyclothemic strata containing strata deposited during times of both terrestrial and marine depositional episodes contain a mixture of both terrestrial and marine organic matter. Pennsylvanian coals were originally composed of peat, which was dominated by low-lying or near coastal lycopsid vegetation (Mastalerz, 2010; Falcon-Lang, 2012) and represent the terrestrial endmember for organic carbon. In contrast, planktonic marine algae represent the other endmember for marine organic carbon. During the Pennsylvanian, terrestrial organic matter $\delta^{13}C_{org}$ values (-23‰ to -24‰) were slightly higher than those of Pennsylvanian algal-dominated deep marine organic matter (-28‰) (Lewan, 1986; Peters-Kottig et al., 2006, Davies et al., 2012). It is important to note these values are counter to those observed in modern $\delta^{13}C_{org}$ values for terrestrial (-27‰) and marine organics (-22‰). This reversal in endmember $\delta^{13}C_{org}$ values has been observed in sedimentary rock from the Cretaceous to the present (Arthur et al., 1985).

2.4.3.2 Zirconium

Zirconium (Zr) concentrations can be used in the absence of sand, silt, and clay distribution data (particle size analysis) as an indication of detrital silt input (Taylor, 1965). Zr is commonly associated with the relatively coarse-grained siliciclastic sediments with the highest concentrations generally found in sandstone (Dypvik and Harris, 2001). Specifically, higher Zr concentrations correspond to higher amounts of coarser grained sediments, specifically the presence of silt grains when comparing sediments from the same depositional basin/provenance area (Taylor, 1965; Dypvik and Harris, 2001, Davies, et al., 2012). During times of high deltaic or riverine influx (higher

detrital silt influx than marine siliciclastic deposition), Zr concentrations should show trends towards fluvial dominated systems while further offshore, Zr concentrations should decrease as sedimentation becomes less riverine, more marine and finer-grained.

3. HYPOTHESES

H1. Mudrocks and shales above the coal in Core 2 and Core 3, if deposited in a marine system as the lithology suggests, will have isotope values consistent with Pennsylvanian marine organic matter ($\delta^{13}C_{org} \approx$ -28‰) while the muds in Core 4 and Core 5, if deposited in a near terrestrial setting, will have more enriched $\delta^{13}C_{org}$ consistent with Pennsylvanian terrestrial organic matter, ($\delta^{13}C_{org} \approx$ -24‰) (Maynard, 1981; Arthur, et al., 1985; Meyers, 1993; Calvert, et al., 1996; Caplan and Bustin, 1998; Murphy, et al., 2005; Peters-Kottig, et al., 2006; Davies, et al., 2012).

H2. Shale and mudstone Mo values >100 ppm will indicate deposition during times of euxinia while Th/U ratios <2 and Fe_{tot}/Al values > 0.5 will indicate times of deposition during anoxic conditions (Lewan and Maynard, 1982; Lewan, 1984; Coveney and Glascock, 1989; Hatch and Levanthal, 1992; Schultz and Coveney, 1992; Algeo, et al., 2004; Rimmer, et al., 2004; Schultz, 2004; Lyons and Severmann, 2006; Scott and Lyons, 2012).

H3. Sulfur concentration >2.5% at the top of coal seams will indicate marine inundation of low-lying peat mires of southern Indiana (Gluskoter and Simon, 1968; Treworgy and Jacobson, 1979; Affolter and Hatch, 2002; Mastalerz, 2010).

4. METHODS

4.1 Core collection – Drilling and Core Extraction

The four study cores were drilled in July 2009 by Magnum Drilling Services for the University of Southern Indiana (USI) as part of an exploratory coal-bed methane project. Well USI 1-32 was drilled at 37°57'2.63"N, 87°40'12.24"W, on grounds owned by USI. Each core from USI 1-32 is approximately 20 ft. in length. All cores were stored in standard cardboard core boxes at ambient room temperature in the Paleontology lab at USI.

4.2 Lithostratigraphic and Paleontologic Methods

Visual sedimentological, lithological, and paleontological description was conducted at 0.1 ft. intervals (Broach and Elliott, 2011. The presence of carbonates within core sections was determined by reaction with dilute HCl and noted where present. Where possible, the mineralogy was noted at the same resolution and logged for possible future investigation. Sedimentary structures such as bioturbation and clear sediment mixing were noted where visible. Overall color and structure of the lithofacies was documented, e.g., where mudrock layers transitioned from a blocky texture (mudstone) to a fissile texture (shale), or where pseudo-slickenslides were prevalent in clay-rich zones. All fossiliferous sections of all cores were identified and samples were collected and photographed using simple light microscopy. Shale and mudstone classification was based on the mudrock classification scheme utilized by Blatt, Middleton, and Murray (1980). All lithology that displayed siliciclastic sedimentation (>50% silt and clay size particles) was deemed ‘mudrock’. Mudrock was deemed *shale* if clear fissility was observed and a *mudstone* if the texture was blocky (Blatt, Middleton, and Murray, 1980).

4.3 Thin Section Preparation and Procedures

In order to examine more closely the mineralogy and sedimentology associated with the mudrock common both before and after coal formation, thin section samples were taken both directly below and above the coal seams in Cores 2-5 in order to bracket the transitions in paleoenvironmental conditions. Samples were also taken at particularly fossiliferous sections of the core, regardless of the lithology, in order to investigate the presence of microfossils and examine sedimentary microstructures. In total, 13 samples were taken from Cores 2, 3, 4, and 5 (See Broach and Elliott, 2011 for complete thin section methodology).

An Olympus petrographic digital microscope 10XR37 was used to examine and take digital images of the thin sections. Various microfossils, minerals, sedimentary structures, and bedding features within the mudrocks and sandstones were identified. Photomicrographs of several of the thin sections were taken, labeled and documented appropriately.

4.4 Geochemical Methods

Sample splits were collected in May 2012 for geochemical analysis from the cores archived at USI. Ninety-three (93) core samples were identified from Cores 2-5 from well USI 1-32 at approximately 10”-12” intervals, to sample each facies change within this sampling resolution. Total core diameter was 3” and all sections were cut in-half vertically with rock saws. An archived half-round was stored with the core in each box and the interval tagged with red chemical tape. All sample half-rounds were approximately 150 g. Each sample half-round was broken either by hand or with a rock hammer parallel to bedding. The outer sections of each core interval were then cut using

rock saws, without water lubrication, to remove potential contaminants such as drilling mud and groundwater exposure during core extraction. The core sample piece was on average approximately 4 cm long. The rock saws and the crusher were cleaned and vacuumed to eliminate contamination between samples. In addition to the core samples, each bag of the drill site cuttings was homogenized and sub-sampled. In December of 2012, four additional samples (C2-21, C4-23, C4-24, C5-22) were collected from the shale intervals above the coals in Core 2, Core 4 and Core 5. The above procedure was duplicated for these four samples. In total, 93 samples from the cores of USI 1-32 (22 from Core 2, 25 from Core 3, 24 from Core 4, and 22 from Core 5) were taken for geochemical analysis and 26 samples from the cuttings. Core samples are labeled first by the core from which they came (e.g. Core 2 samples are all labeled C2) and then numbered sequentially from the top of the core down.

4.5 Metal Geochemistry

All 93 samples were sent to Activation Laboratories, Inc. (Ottawa, Canada) for elemental analysis. All samples were pulverized to a 60-mesh powder and then analyzed for total elemental analysis by a combination of Inductively Coupled Plasma Mass Spectrometry (ICP-MS), Fusion ICP, and Instrumental Neutron Activation Analysis (INAA). Initially all samples were fused, diluted and then analyzed with a Perkin Elmer Sciex ELAN 6000, 6100 or 9000 ICP-MS. Three blanks and five controls were analyzed per group of samples. Duplicates were fused and analyzed every 15 samples and the instrument recalibrated every 40 samples. Samples with high Mo concentrations were reanalyzed by Fusion ICP. For the major elements portion a 0.2 g sample was combined with a mixture of lithium metaborate/lithium tetraborate and fused in a graphite crucible.

The molten mixture was poured into a 5% nitric acid solution and shaken until dissolved (~ 30 minutes). The samples were run for major oxides and selected trace elements on a combination simultaneous/sequential Thermo Jarrell-Ash Enviro II ICP. Calibration was achieved using a variety of international reference materials. Independent control standards were also analyzed.

For INAA analyses, a 1 g aliquot of sample was encapsulated in a polyethylene vial and irradiated with flux wires and an internal standard (1 for 11 samples) at a thermal neutron flux of 7×10^{12} n cm^{-2} s^{-1} (Hoffman, 1992). After a 7-day period to allow ^{24}Na to decay, the samples were counted on a high purity Ge detector with resolution of better than 1.7 KeV for the 1332 KeV Co-60 photopeak. Using the flux wires, the decay-corrected activities were compared to a calibration developed from multiple certified international reference materials. The elemental composition of a subset of samples (10-30%) was rechecked by re-measurement. One standard was run for every 11 samples.

For base metals and selected trace elements, a 0.25 g sample was digested with four acids beginning with hydrofluoric, followed by a mixture of nitric and perchloric acids, heated using precise programmer controlled heating in several ramping and holding cycles which takes the samples to dryness. After dryness was attained, samples were brought back into solution using hydrochloric acid. An in-lab standard (traceable to certified reference materials or certified reference materials) was used for quality control. Samples were analyzed using a Varian Vista.

For Hg concentrations, a 0.5 g sample was digested with aqua regia at 90ºC. The Hg in the resulting solution was oxidized to the stable divalent form. Since the concentration of Hg is determined via the absorption of light at 253.7 nm by Hg vapor,

Hg (II) was reduced to the volatile free atomic state using stannous chloride. Argon was bubbled through the mixture of sample and reductant solutions to liberate and to transport the Hg atoms into an absorption cell. The cell was placed in the light path of an Atomic Absorption Spectrophotometer. The maximum amount absorbed (peak height) is directly proportional to the concentration of mercury atoms in the light path. Hg analysis was performed on a Perkin Elmer FIMS 100 cold vapor Hg analyzer at Actlabs.

All coal samples, due to their high organic matter content and the associated complications with traditional ICP and INAA analysis, were analyzed for full elemental composition by a lab specializing in high-resolution elemental coal analysis, CONSOL R&D, Inc (Pittsburgh, PA). These results were then compared to the ActLabs results for consistency but in all cases the geochemical coal metal data is taken from the CONSOL R&D results. For moisture content and ash Loss on Ignition (LOI) all samples were weighed into a crucible, placed in a Thermogravimetric Analyzer, heated to 105 °C until reaching a constant weight, and the weight lost was the moisture. For the LOI, the same sample was heated to 750°C in air to burn off all the coal and combustibles. The residual weight was the ash. For mercury concentrations in coal, the samples were combusted in an oxygen atmosphere and all mercury was reduced to the elemental species and captured on a gold amalgamator. The amalgamator was heated quickly to drive off the mercury, and detected by atomic absorbance. The signal for each sample was compared to a calibration from coal standards with known mercury concentrations. For major elements the coal sample was ashed at 750°C to a constant weight. The ash was digested with mixed acids in a closed vessel. The dissolved sample was then analyzed by Inductively Coupled Plasma Atomic Emission Spectrometry and calibrated against

solutions of known elemental composition. By convention in the coal industry, results for the elements were converted to the oxide state and reported as oxides in the ash. For trace elements in coals the samples were ashed at 500°C to a constant weight. The ash was digested in mixed acids, then analyzed by ICP-MS. Calibration was done with solutions of known elemental composition. The ash oxides results were back-calculated to the elements in coal based on the weight loss at 500°C.

All metal data was normalized to mole % where necessary for proxy utilization. When appropriate, and in order to isolate water column metal abundances against detrital metal input, molar concentrations were also normalized against Al mol %.

4.6 Sedimentary carbon and nitrogen

In order to determine Total Carbon (TC), Total Nitrogen (TN), Total Organic Carbon (TOC) and Total Inorganic Carbon (TIC) several procedures were utilized. Total carbon and TN was determined by combustion with an elemental analyzer. TIC was measured by acidification with a UIC 5130 Acidification Module coupled to a UIC5012 CO_2 Coulometer. Coulometry provides a highly accurate means of measuring the CO_2 released from the sample by acidification. TOC was calculated as the difference between total carbon and TIC, where TC (Costech EA) – TIC (Coulometer) = TOC. Details of each analytical technique (combustion and acidification) are presented below.

4.6.1 TIC Procedures

Approximately 10 g of pulverized sample (60 mesh) were placed in a heated vial and acidified with 6 mL of 2N HCl in a closed system purged with pure O_2 as a carrier gas (settings, Table 1). All gas evolved was transferred through a trap of $AgNO_3$ to

remove SO_2, and the purified sample gas was introduced to the coulometer. The coulometer uses electrolysis to measure the mass of carbon in the gas stream. The sample gas stream is transferred through a cell containing a UIC proprietary solution containing monoethanolamine and colorimetric pH solution, a platinum cathode and a silver anode. The cell is placed between a light source and a photodetector. As the CO_2 gas stream passes into the cell, the CO_2 is quantitatively absorbed, reacting with the monoethanolamine to form a titratable acid. This acid causes the color indicator to fade. Photodetection monitors the change in the color of the solution as a percent transmittance (%T). As transmittance increases, the titration current is automatically activated to electrochemically generate base at a rate proportional to the %T (approximately 1500 μg carbon/minute). When the solution returns to its original color (original %T), the current stops. Faraday's Law states that one faraday of electricity will result in the alteration of 1 GEW (gram equivalent weight) of a substance during electrolysis. In the coulometer, each faraday of electricity expended is equivalent to 1 GEW of CO_2 titrated. This is then converted into μg of C and then divided against the original mass of C in the sample to reach a very precise measure of TIC in the sample.

Table 1. Coulometer Settings	
Heat	5-6
Flow Rate	90 ml/min
Acid Volume (2N HCl)	6 mL
Minimum purge time between each run	15-30 seconds
Run Time	8 min (average) for full titration

A $CaCO_3$ standard was run at the beginning of each sample run and a consistent recovery on three consecutive samples (99-100%) was achieved before samples were analyzed. Each vial was cleaned with DI water, dilute HCl, rinsed again with DI water and then dried in an oven at 50°C prior to sample addition.

4.6.2 Total Carbon and Total Nitrogen Procedures

TC and TN were measured simultaneously on unacidified samples by combustion in an elemental analyzer (Costech Analytical ECS 4010). Elemental combustion analysis is based on transformation of the solid sediment to the gas phase by extremely rapid and complete flash combustion of the sediment. Sediments were weighed into tin capsules and placed in a Zero Blank autosampler (Costech Analytical). The autosampler dropped each sample into the top of a quartz combustion tube under in a closed system purged with helium. A pulse of oxygen was supplied and the resulting thermal energy from the combustion of the tin and sample material resulted in an instantaneous temperature of as much as 1700°C at the moment of flash combustion. All carbon was then converted into CO_2 and all nitrogen into N_2 gas. Water produced during combustion was removed with a magnesium perchlorate trap and SO_2 was not analyzed. The sample gases were separated on a gas chromatographic (GC) column, which was kept at a constant temperature (55°C). As the gases pass through the GC column they were detected sequentially by the Thermal Conductivity Detector (TCD), which generated a signal proportional to the amount of gas evolved from the sample. Elemental concentrations are determined from regression analysis of standard reference materials.

4.7 Stable Isotopes

An acidification process was utilized to remove carbonates in the sample in order to isolate TOC for $\delta^{13}C_{org}$ analysis. All samples were wetted with 18 MΩ deionized water, acidified with 2N HCl, and reacted for 24 hours to thoroughly effervesce any carbonates. Samples were spun in a centrifuge, the supernatant (acid) was pipetted off, and the sediment pellet was sequentially rinsed (4-6 times) with 18 MΩ deionized water. Because chloride can damage and interfere with mass spectrometry, the supernatant from each sample was tested after the rinsing procedure for the presence of Cl^- ions introduced during acidification by reaction with a 3% $AgNO_3$. This test will produce a white precipitate of AgCl(s) if chloride remained in solution. Once a negative result was obtained, samples were frozen and then freeze dried for approximately 24 hours.

All stable isotope analyses were measured on a Thermo Delta V Plus stable isotope ratio mass spectrometer (IRMS) coupled under continuous flow with a Costech Analytical ECS 4010 elemental analyzer (EA). Carbon isotopes ($\delta^{13}C$) and nitrogen isotopes ($\delta^{15}N$) were calculated according to the equation: $\delta^{x}E = (R_{sample} / R_{standard} - 1) \times 1000$; where ^{x}E is the particular isotope (^{13}C or ^{15}N) and R is the isotope ratio ($^{13}C/^{12}C$ or $^{15}N/^{14}N$). All sample values were normalized to multi-point regressions of standard reference materials USGS 40 ($\delta^{15}N$ = -4.52‰; $\delta^{13}C$ = -26.39‰), RM 8704 Buffalo River Sediment ($\delta^{15}N$ = 4.01‰; $\delta^{13}C$ = -19.75‰), NBS-19 ($\delta^{13}C$ = 1.95‰), and IAEA N1 ($\delta^{15}N$ = 0.4‰). Analytical precision was within 0.1‰ for both $\delta^{15}N$ and $\delta^{13}C_{org}$.

4.8 Statistical Analyses

All statistical analyses were completed using PAST: Paleontological Statistics software package for educational and data analysis version 3.01 (Hammer, 2001). ‘N’ is equal to the number of samples in the sample. ‘s’ is equal to the standard deviation of the of the sample set. R^2 is equal to the correlation coefficient between any two variables.

5. RESULTS

5.1 Core 5

5.1.1 Lithology and Paleontology

Core 5 consists of a portion of the Staunton Formation and in depositional order the core is comprised of a blocky poorly indurated mudstone from 675.0’ to 668.2’, which is overlain by 4.1’ of the Seelyville Coal. Overlying the coal seam is a fissile clay-rich grey shale, which continues to the top of the core (663.9’-655.0’). Core 5 does not contain black shale and there is no evidence for marine macrofossils (Fig. 5).

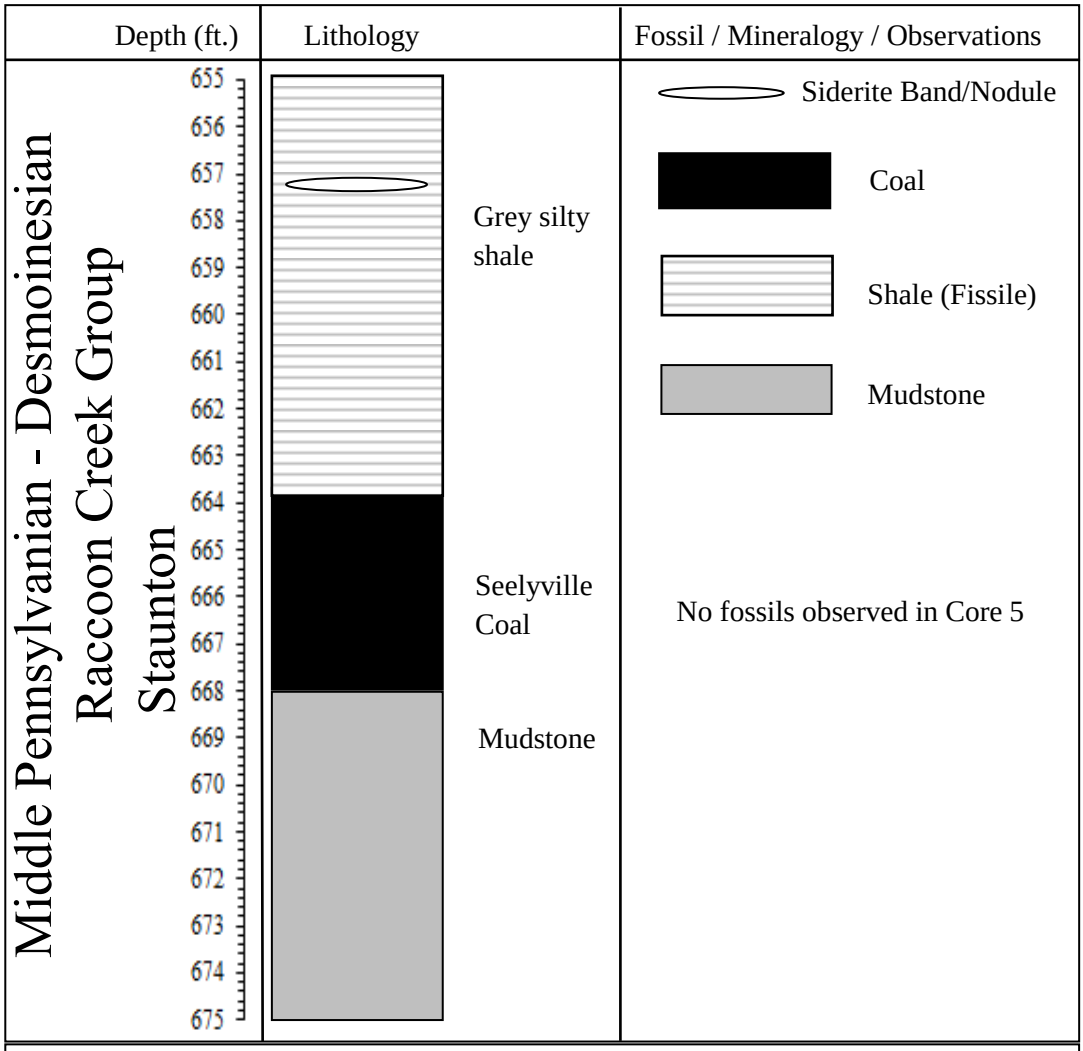

Figure 5: Core 5 description with depth in feet, lithology, fossil presence, and mineralogy.

5.1.2 Carbon, Nitrogen, and Sulfur

TOC% values for Core 5 were low (<1%) with the only values larger than this found in the coal seam (Fig. 6). The Seelyville coal seam averaged 61% TOC. The mudrock sections below and above the coal seam averaged <1% TOC. Average TIC% values were 0.34% and showed very little variation upsection of the Seelyville. TS concentrations were highest in the Seelyville coal. Concentrations increased from the base of coal (7.6% TS) to the top of the coal (17.8% TS). Below and above the coal TS% concentrations were low and averaged 0.9%. TN % values for Core 5 covaried with TOC and averaged 1.3% in the Seelyville coal and near zero throughout all overlying shale (avg. 0.08%).

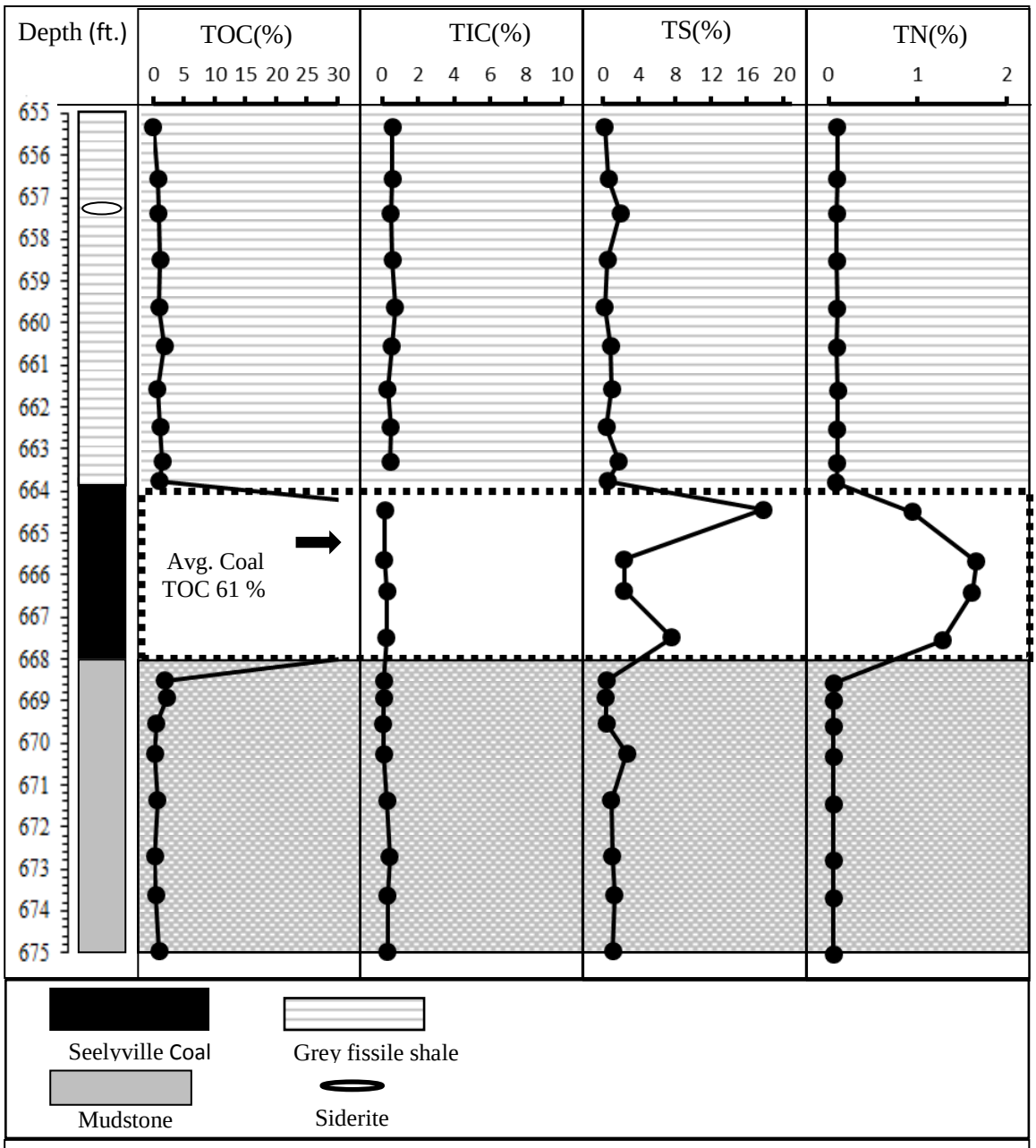

Figure 6: Core 5 Carbon, Nitrogen, and Sulfur

5.1.3 Paleoredox

Mo/Al ratios were near zero except at the top of the Seelyville coal with a value near 0.2 ([Mo] = 37 ppm; Fig. 7). V/Al values were near zero for the entirety of Core 5 but did decrease from 0.08 to 0.06 from the base of the grey shale to the top of the core.

Th/U ratios for Core 5 remain around 3 for the majority of the Seelyville coal. The Th/U ratio decreases to <1 (0.48) at the very top of the core and then decreases to values around 4 throughout the entirely of the grey shale/mudstone upsection.

Fe_{tot}/Al values are near zero throughout the core with the exception of one large enrichment (5.7) at the top of the coal at 664.5' coincident with a small band of pyrite present in the coal. It was noted that Fe_{tot}/Al trends very closely track the TS% in the Seelyville coal, both mirroring increases in concentrations throughout the coal seam.

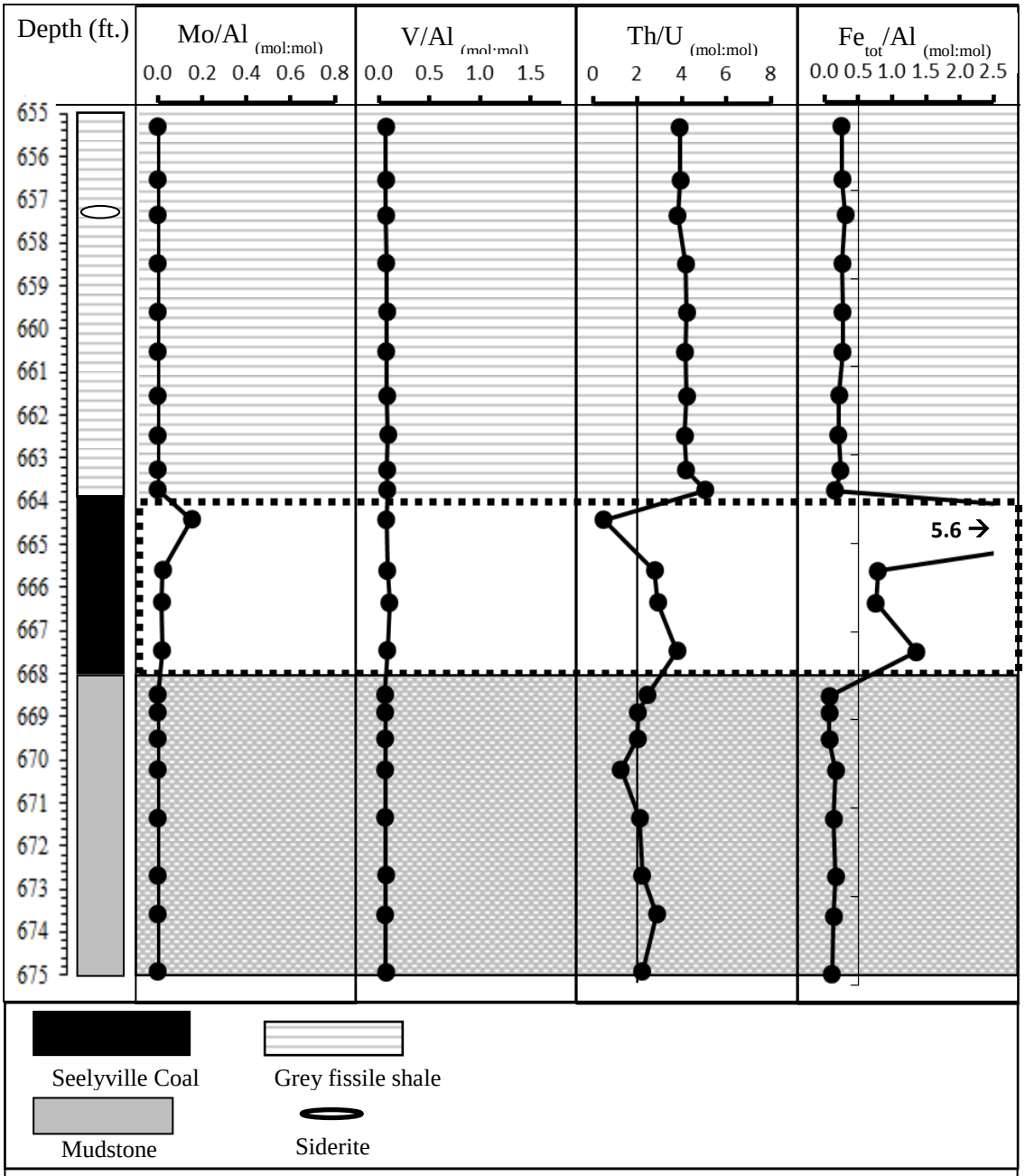

Figure 7: Core 5 Paleoredox

5.1.4. Isotopes and Basin Parameters

$\delta^{13}C_{org}$ values for Core 5 show very little variation (Avg. = -24.0‰, s = 0.33‰,N = 22) throughout the entire core (Fig. 8). Average $\delta^{13}C$ values in the coal section are -

24.5‰ and all values above coal in the grey shale are isotopically similar, ($\delta^{13}C \approx$ -24.0‰)

Zr concentrations are somewhat variable in the mudrock above the coal (average 132, s = 43, N = 10). Values below the coal are very high averaging around 250 ppm. Concentrations decrease in the coal to near zero values (avg. 15 ppm) and then immediately increase to around 100 ppm and gradually increase to 167 ppm at the top of the core.

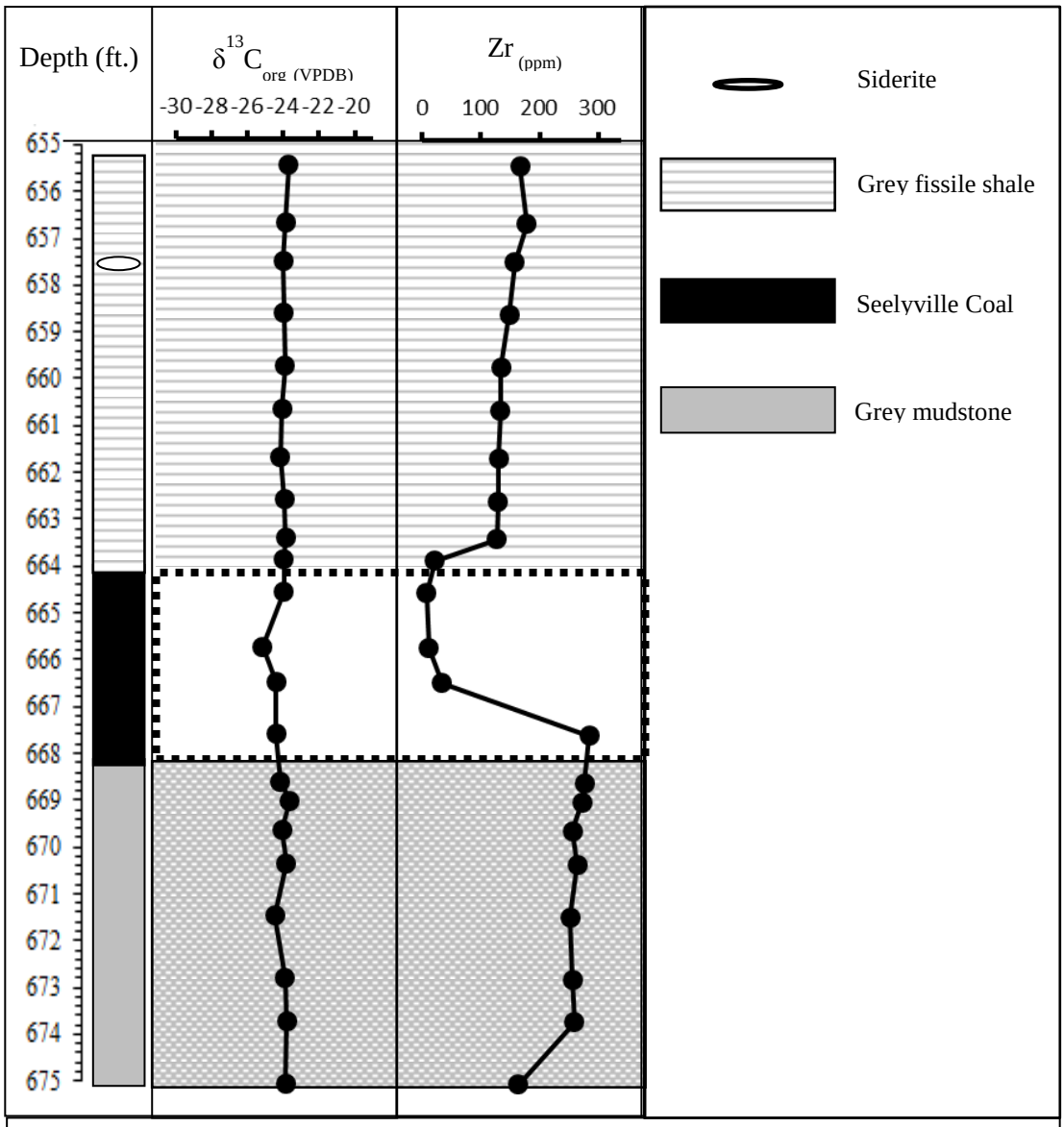

Figure 8: Core 5 Isotopes and Basin Parameters

5.2 Core 4

5.2.1 Lithology and Paleontology

Core 4 comprises a portion of the Linton Formation and in depositional order consists of 1.2’ of muddy sandstone with a thin (1cm) strip of coal at 559.4’ (Fig. 9). The lithology transitions into an organic shale/underclay from 558.7’-558.0’. The underclay

is overlain by 2.1' of the Survant Coal. Grey shale and mudstone are above the Survant Coal seam. From 558.8' to approximately 548.0 the rock is fissile and not well indurated. Fissility in the grey shale transitions to a hard blocky texture from 548.0' to 541.3' and then becomes more fissile from 541.3' up to the top of the core. Several siderite band and nodules occur in the grey shale and mudstone overlying the Survant Coal. Core 4 does not contain black shale, and there is no evidence for marine body fossils or microfossils.

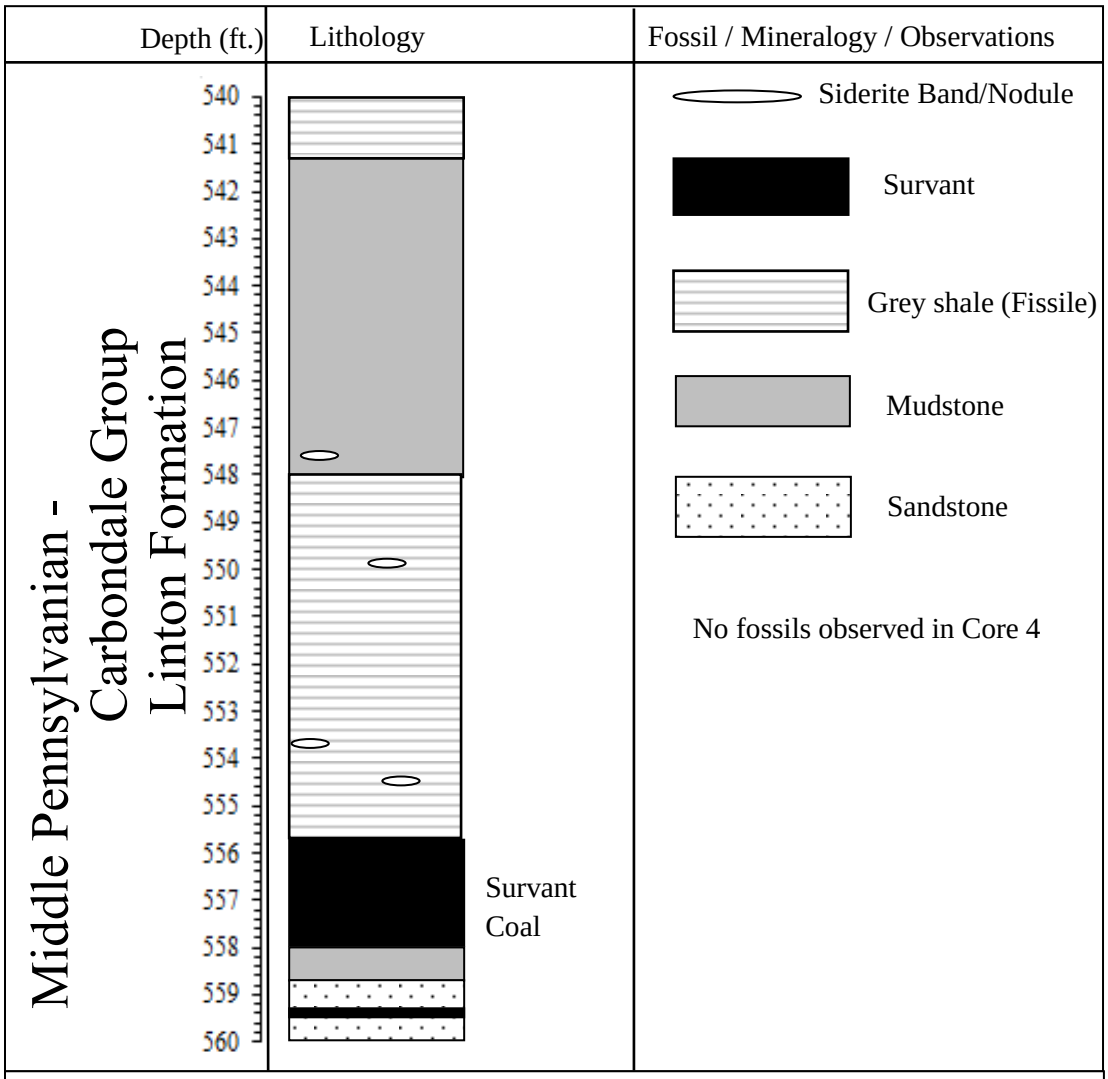

Figure 9: Core 4 description with depth in feet, lithology, fossil presence, and mineralogy.

5.2.2 Carbon, Nitrogen, and Sulfur

TOC concentrations in the Survant Coal in Core 4 averaged 72% (Fig 10). TOC concentrations were low (≤ 1%) outside of the coal seam. TIC values were near zero throughout the entirely of Core 4, and all values averaged 0.3%.

The highest sulfur concentrations are in the coal seam with an average of 3.8% TS. The superjacent strata above the coal seam also contained high TS concentrations (5%) but upsection values approached zero and averaged 0.2%. TN content covaried with TOC and was near zero for all strata outside the coal seam. Coal averaged 1.7% TN while all non-coal values averaged 0.09%.

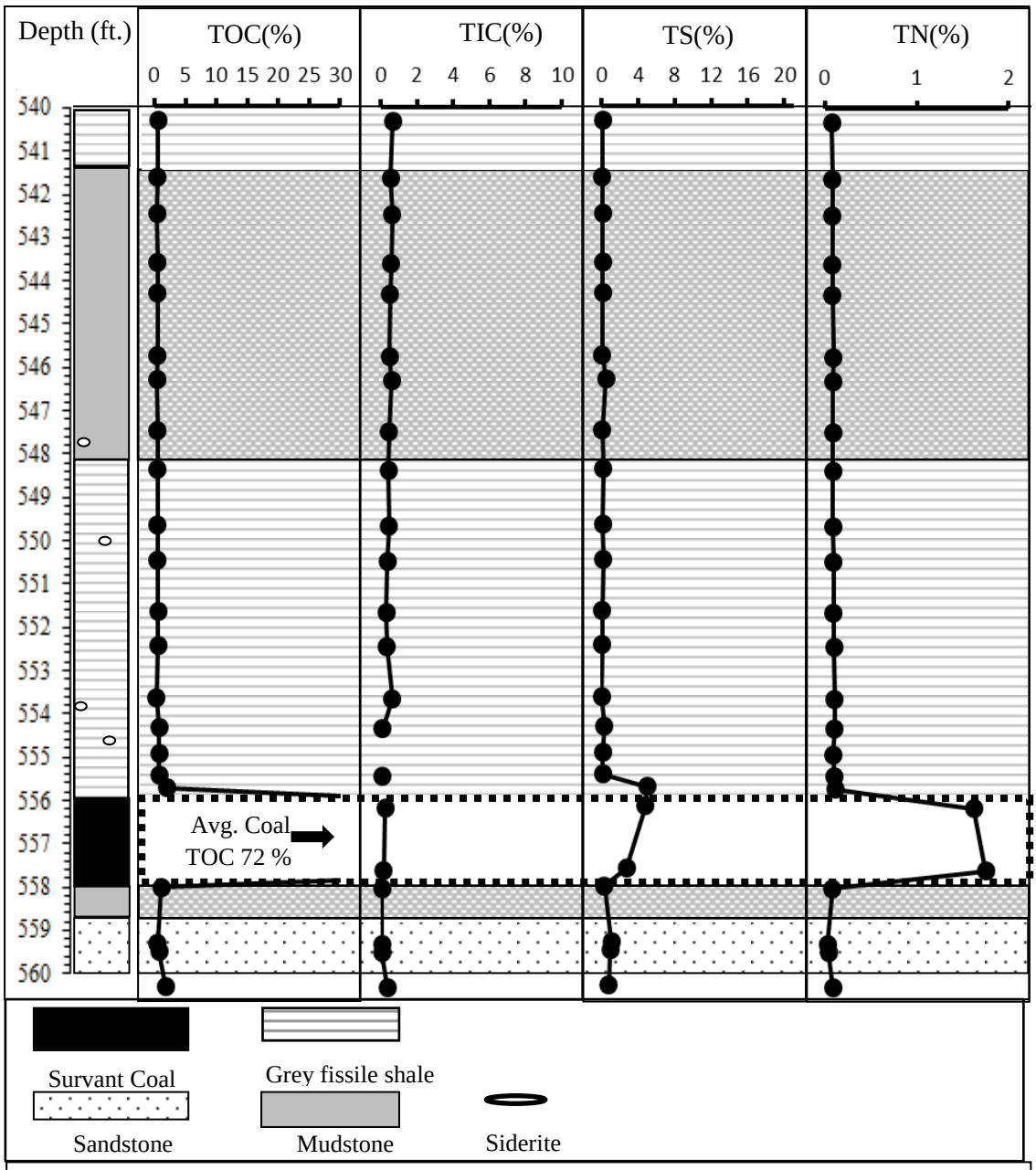

Figure 10: Core 4 Carbon, Sulfur, and Nitrogen

5.2.3 Paleoredox

There are no enrichments in Mo/Al or V/Al in Core 4 (Fig. 11). Mo concentrations are near zero (<2 ppm) throughout the core and V concentrations are highest (163 ppm) at the base of the grey shale (directly above the coal) and gradually

decrease upsection to 110 ppm. Average V/Al ratios are 0.07. Th/U ratios exhibit an excursion toward lower values at 555.6', where Th/U decreases to approximately 2. Above this excursion, Th/U increases to a baseline value of 4, and remains constant throughout the section to the top.

Fe_{tot}/Al values were also near zero for the shale and mudstone upsection of the coal, but highly elevated in the coal with values averaging 1.5.

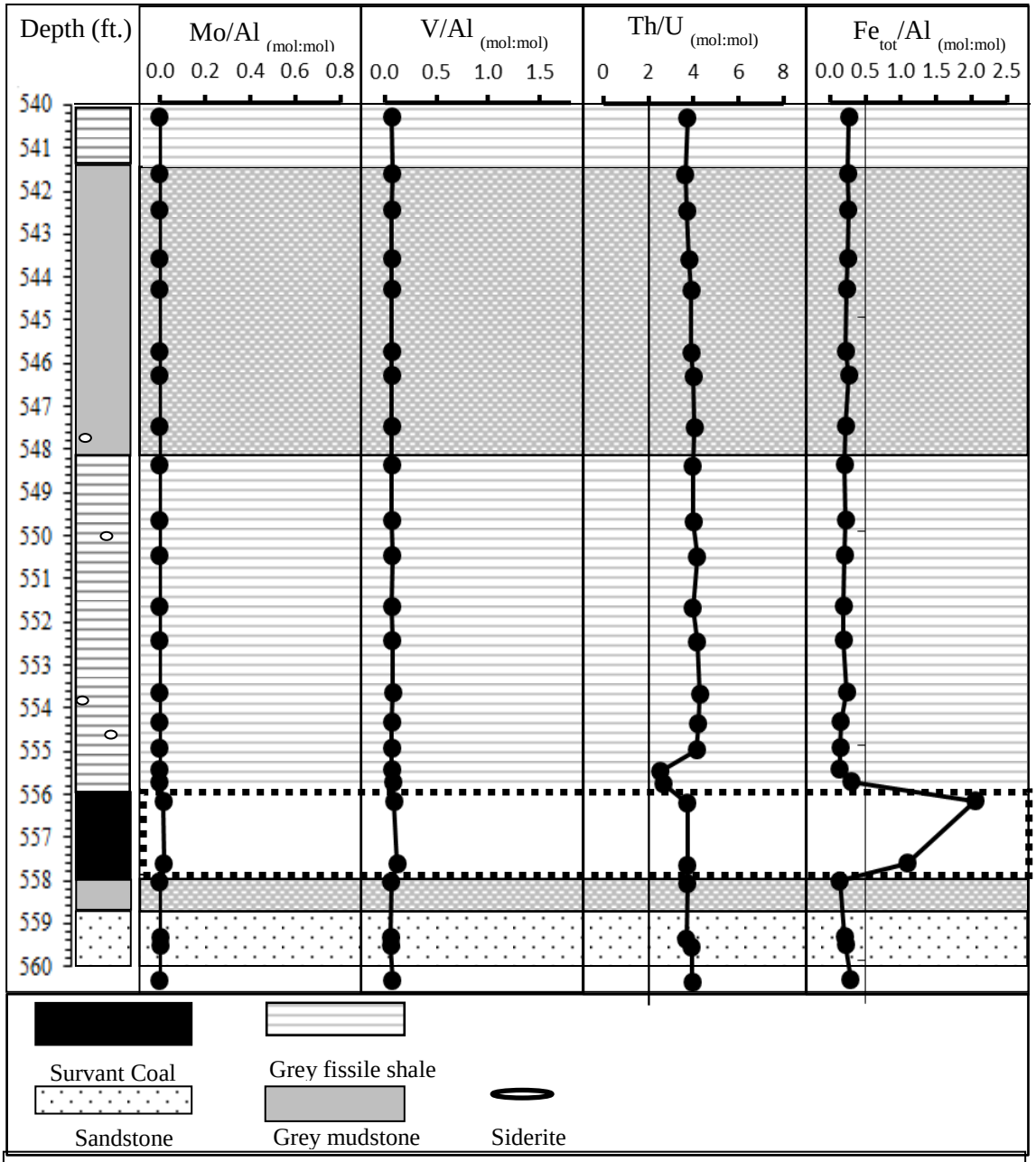

Figure 11: Core 4 Paleoredox

5.2.4 Isotopes and Basin Parameters

$\delta^{13}C_{org}$ values are fairly uniform throughout Core 4 (N = 24; s = 0.31‰; Fig. 12). The $\delta^{13}C_{org}$ of the two samples collected from the Survant coal seam average -24.4‰.

The carbon isotopic composition of organic matter in the grey shale was invariant upsection, averaging ($\delta^{13}C_{org}$ = -24.2‰).

Zr concentrations approach near zero in the coal seam and then steadily increase upsection to a maximum of 245 ppm at the top of the core.

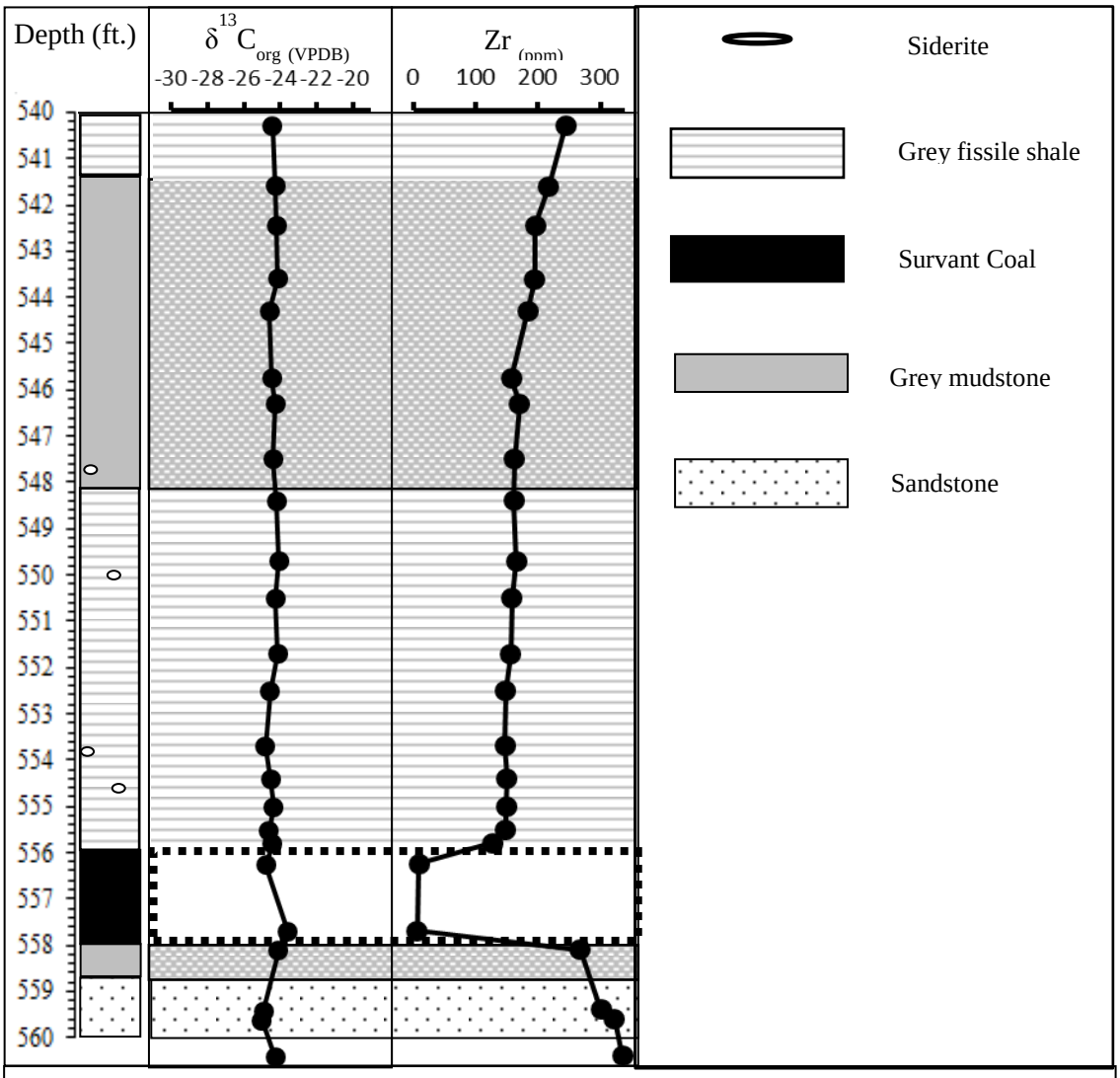

Figure 12: Core 4 Isotopes and Basin Parameters

5.3 Core 3

5.3.1 Lithology and Paleontology

Core 3, a portion of the Petersburg Formation, exhibits the most distinct and easily observable facies changes of any of the four cores studied (Fig. 15). In depositional order, the core consists of siltstone with several calcareous sections above it. Overlying the calcareous section is well-sorted cross-bedded to flaser-bedded fine-grained sandstone transitioning into a clay-rich mudstone/underclay. The Houchin Creek Coal (1.3' thick) is above the underclay section. Immediately overlying the coal seam is an approximately 6-8" pyritic black shale (Excello Shale) at 505.8' (Fig. 13, 15). The pyrite is dissiminated throughout the black shale matrix. Overlying the pyritic black shale is 5.2' of organic-rich mostly fissile black shale. A 6" section around 503.0' is blocky and lacks all fissility. Immediately overlying the Excello Shale at approximately 500.0' is a fossiliferous grey shale and mudstone (Fig. 15). A distinct calcareous section is also present at 500.6'. A small (1 cm diameter) fully intact rugose coral was found at this interval, identified as *Siphonophyllia cylindrica* (Fig. 14 C). In addition to the macrofossil evidence of marine conditions, several thin section photomicrographs revealed foraminifera tests, possibly of the genus *Nonionella* (Fig. 14 A and B). The grey shale continues to the top of Core 3 with the occasional siderite band and a small section of calcareous shale at 496.0'.

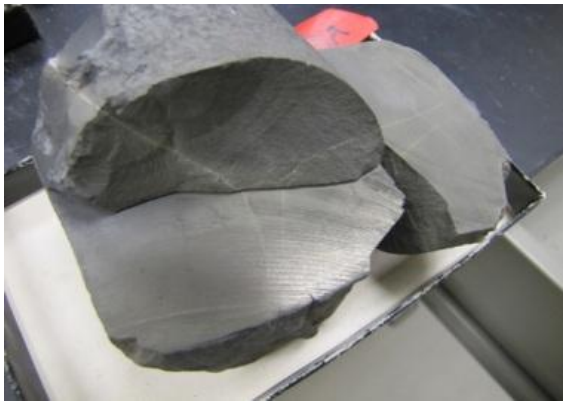

Figure 13. Pyritic section of black shale at base of the Excello, 505.8'.

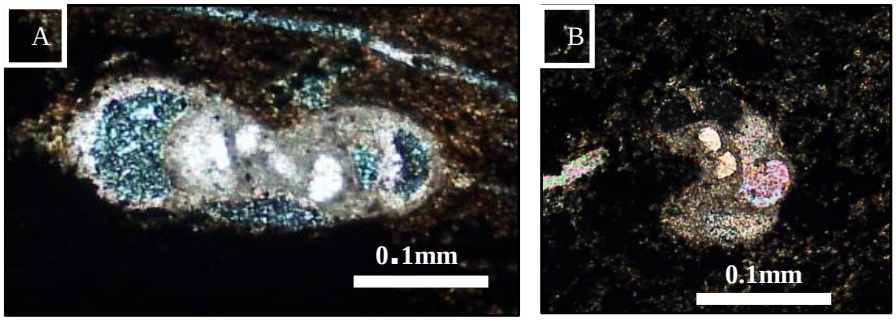

Figure 14: A, B) Foraminifera tests in laminated grey shale *Nonionella sp (?)* (Broach, 2011); C) Cross section of rugose coral *Siphonophyllia cylindrica* in laminated grey shale (Broach, 2011)

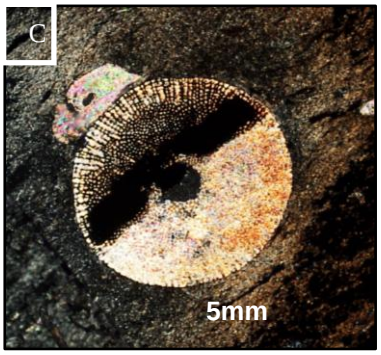

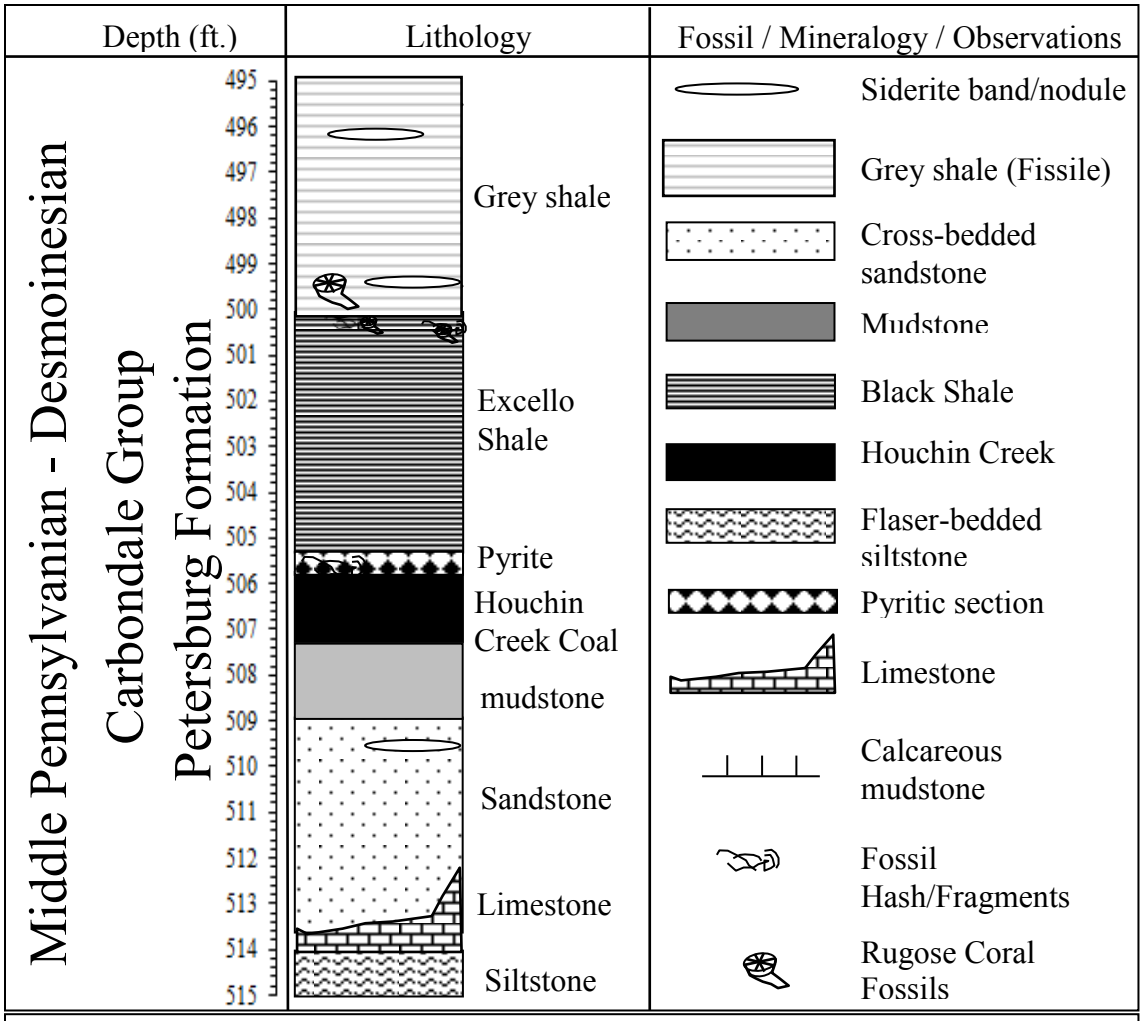

Figure 15: Core 3 description with depth in feet, lithology, fossil presence, and mineralogy.

5.3.2. Carbon, Sulfur, and Nitrogen

TOC concentrations in Core 3 varied from 0-72%. The highest values were found in the coal seam and averaged 69% TOC (Fig. 16). The transition above the coal seam from black shale to grey shale varied widely, ranging from <1% at the base of the black shale (pyritic section) to almost 28% TOC at 502.3' at the top of the black shale. The

Excello shale values averaged 11.8% and the overlying grey shale values averaged 1.2% TOC.

TIC values were low (<1%) for most of the core with the exception of two intervals. The first TIC value of 5.5% was located in the calcareous sandstone well below the coal seam and the second (~10%) was located just above the pyritic section of the black shale at 505.3'.

The Houchin Creek coal had high sulfur concentrations averaging 3.4%. The pyritic section of the Excello has the highest TS value of ~20%. As a whole, the Excello shale averaged 5.2% TS. The grey shale had low amounts of sulfur (<1%).

TN values were exceptionally low (~0.1%) with the exception of the Excello Shale above the pyritic section and the coal seam. Excello Shale TN values above the pyritic section averaged 0.6% and coal values averaged 1.5%. TN covaried with TOC throughout Core 3 in both the coal and the overlying shale and mudstone. The C/N for the coals was slightly higher than that of the rest of the shale.

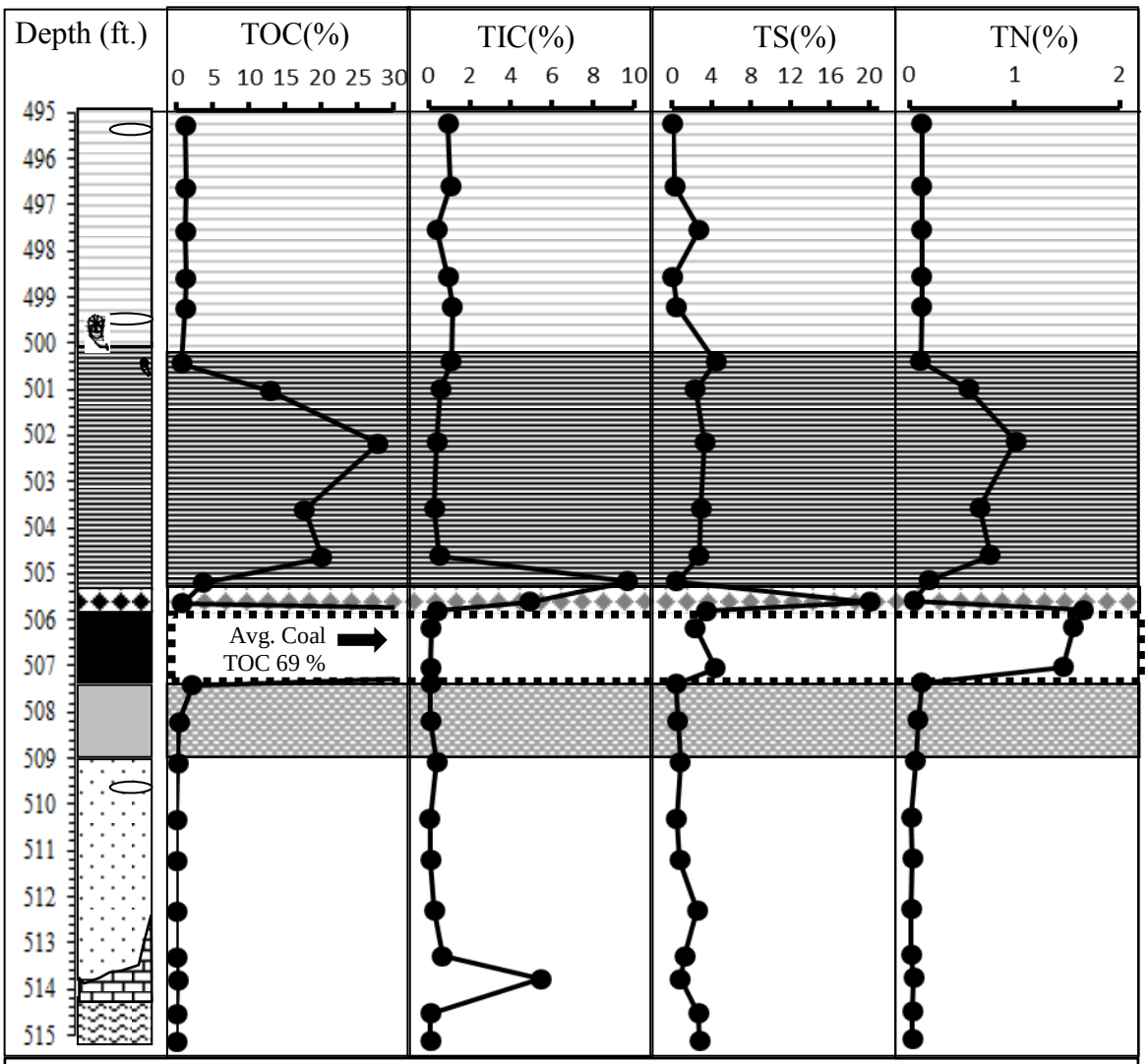

Figure 16: Core 3 Carbon, Nitrogen, and Sulfur

5.3.3 Paleoredox

Mo/Al ratios in Core 3 are high within the Excello shale (Fig. 17), at 505.35' and 502.3' and at least at four other datum (503.5'-506.3') from the top of the Houchin Creek

coal through at least the first four feet of Excello shale deposition. All values above the Excello are near zero and contained less than the crustal average of Mo (2 ppm).

V/Al values are highest at the top of the pyritic section of the Excello (V/Al = 1.72), and these values are elevated throughout the black shale relative to the other facies. The grey shale values are near zero.

Th/U values decrease under the 2 threshold gradually throughout the Houchin Creek coal seam, and remain <2 for the Excello Shale until gradually increasing to higher values (>2) within the transition from black to the grey shale. The grey shale values (average 4.9) are substantially higher than the black shale Th/U values (average 0.67).

Fe_{tot}/Al values exceeding the 0.5 ratio for normal marine occur in three distinct intervals. The first is observed in the limestone section well below the coal seam. The second and third are observed at the base of the Houchin Creek Coal and at the base of the Excello Shale within the pyritic section (505.8') with a value of almost 12.

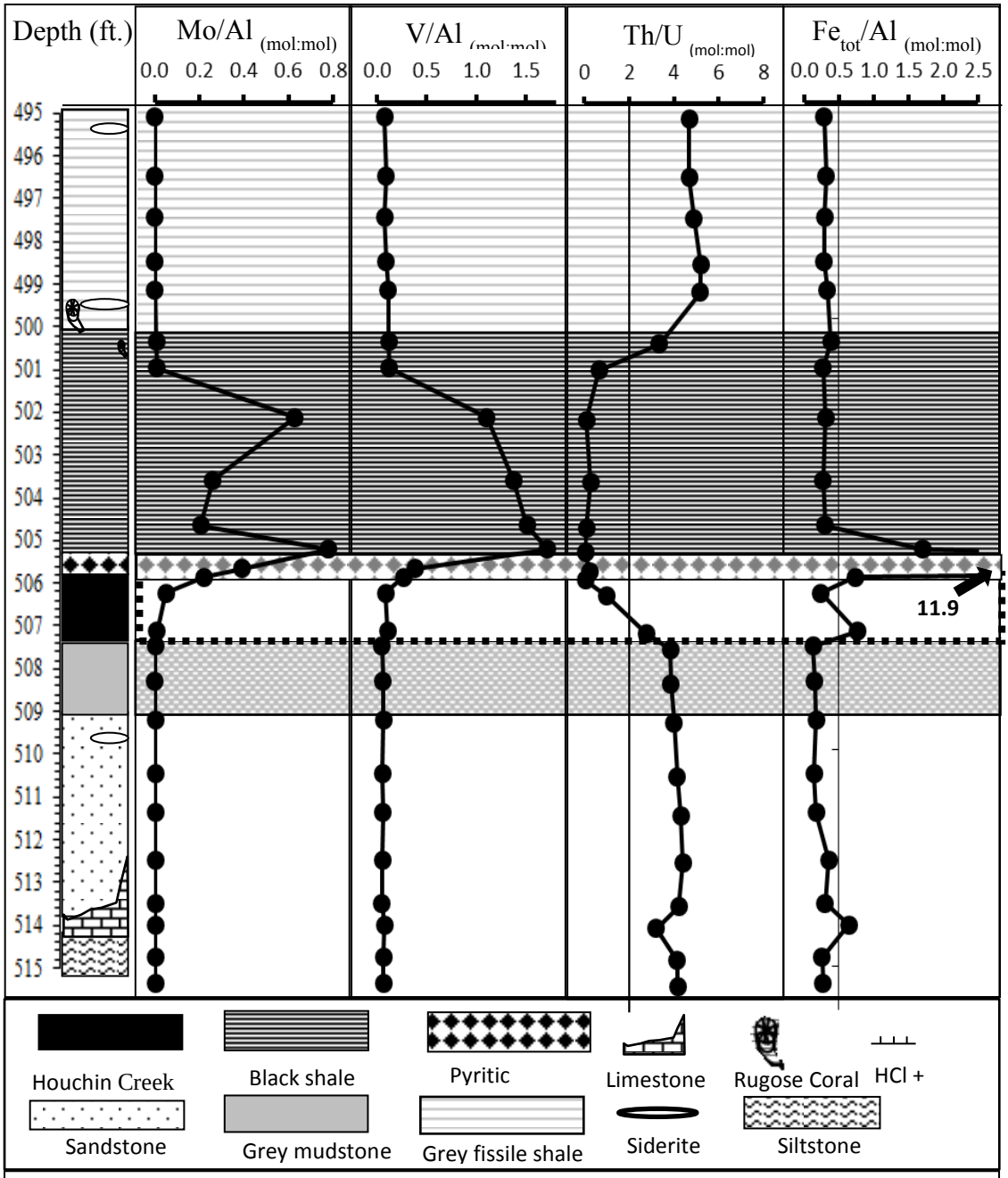

Figure 17: Core 3 Paleoredox

5.3.4 Isotopes and Basin Parameters

The carbon isotope composition of Core 3 organic matter is consistent with algal inputs (low $\delta^{13}C_{org}$) at the base of the black shale (-26.3‰ at 505.8'; Fig. 18). $\delta^{13}C_{org}$ gradually becomes more ^{13}C-enriched upsection to values more consistent with the end-

member composition of terrestrial organic matter ($\delta^{13}C \approx -24‰$). However, in the pyritic section (505.3'), there is an extremely high $\delta^{13}C_{org}$ value of -19.0‰ near the base of the black shale. If we exclude this outlier value, the black shale values average -26.0‰, and the overlying grey shale values average -23.9‰.

Zr concentrations in Core 3 closely track the changes in lithofacies from below the coal to the top of the core. The silty underclay and sandstone below the coal have high Zr concentrations and averages 277 ppm. Zr concentrations decrease dramatically at the base of the coal and remain low in the black shale (100 ppm). Grey shale values increase immediately after facies change to an average of 120 ppm.

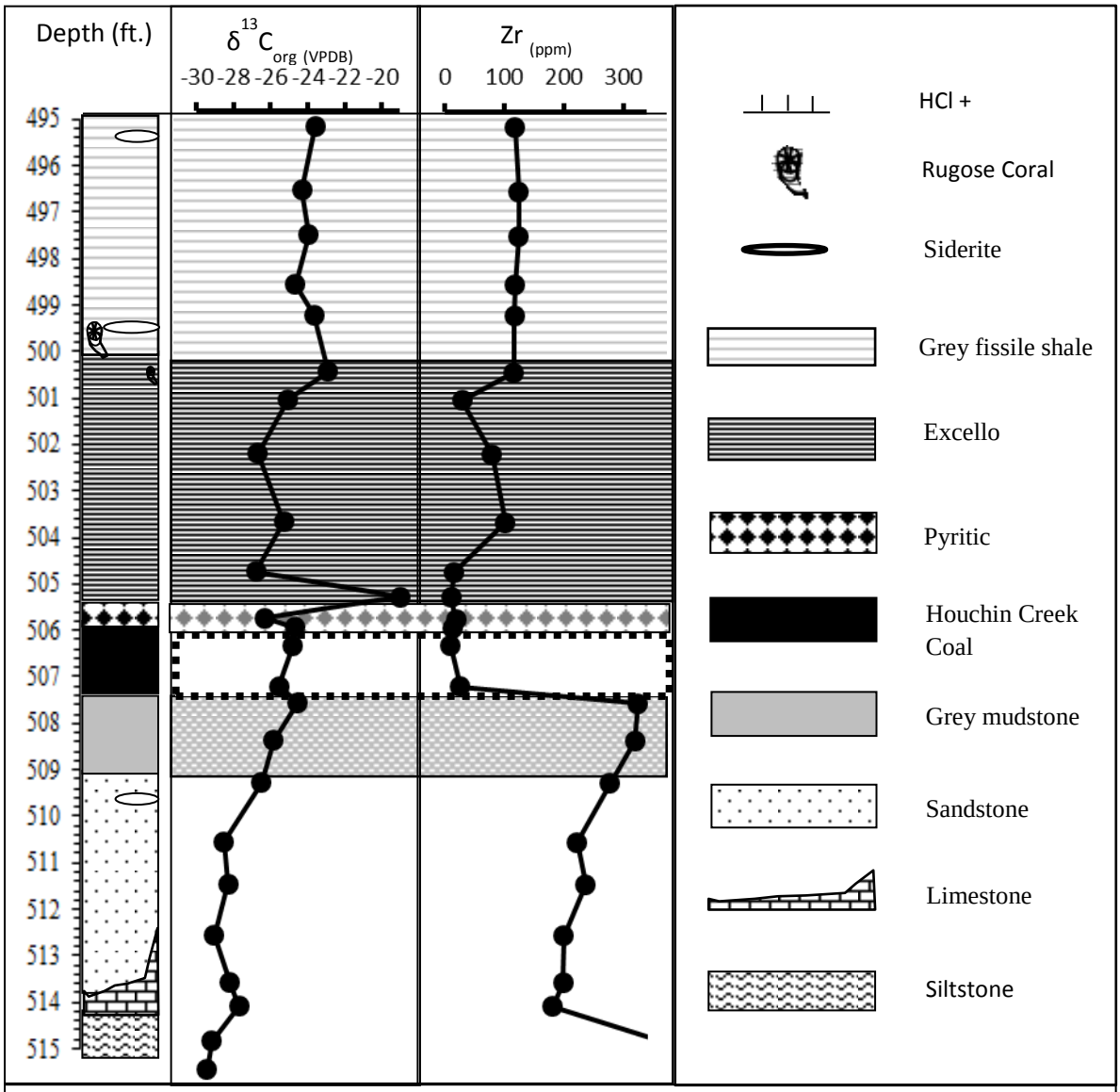

Figure 18: Core 3 Isotopes and Basin Parameters

5.4 Core 2

5.4.1 Lithology and Paleontology

Core 2 was recovered from 415.0 – 395.0 feet in depth (Fig. 21). In depositional order, the core consists of a mudstone/underclay section at 415.0'-414.2', overlain by more than four feet of the Springfield coal (414.2'-409.9'). Elemental sulfur and secondary calcite in vertical cleats was observed throughout the Springfield coal section. Overlying the Springfield is 1.6' of finely (1 mm thick) laminated black shale (409.9-408.3), which gradually transitions into a fossiliferous grey mudstone at 408.3'. The core becomes more fissile upsection and fossil abundance is sporadic but continuous up to 398.4' where grey shale gradually becomes darker to the top of the core at 395.0'. Siderite bands and nodules are present throughout the grey mudstone and shale above the black shale (Fig. 19, 22). While most

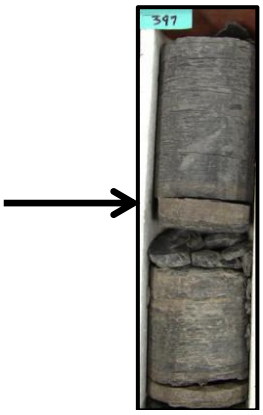

Figure 19: Siderite band in middle of core at ~397.5'.

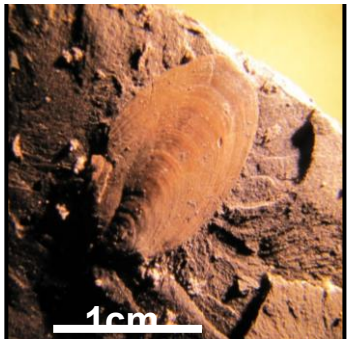

Figure 20: *Barroisella campbelli*
Family*: Lingulidae*
Phylum: Brachiopoda (Broach, 2011)

Figure 21: Expanded section at 414.2' depth. Note whitish yellow powdered mineral.

fossils were found disarticulated, an abundant section of intact lingulid brachiopod fossils with original aragonite shells, identified as *Barroisella campbelli,* were present at 398.7' (Fig. 20, 22). Several sections of Core 2 tested positive for the presence of calcite with a dilute HCl acid test including the entirety of the mudstone/shale from 401.0-405.0 (Fig. 22). The underclay directly beneath the coal seam (414.2'), after borehole extraction volumetrically expanded approximately 100% and was composed of a whitish-yellow powdered mineral speckled with a yellow mineral (Fig. 21). Two other segments also displayed the same type of expansion but much less so, in the range of 10-30%, directly above the coal at 409.8'and in the grey shale ~8 inches above the black to grey transition at 407.8' (Fig. 6.).

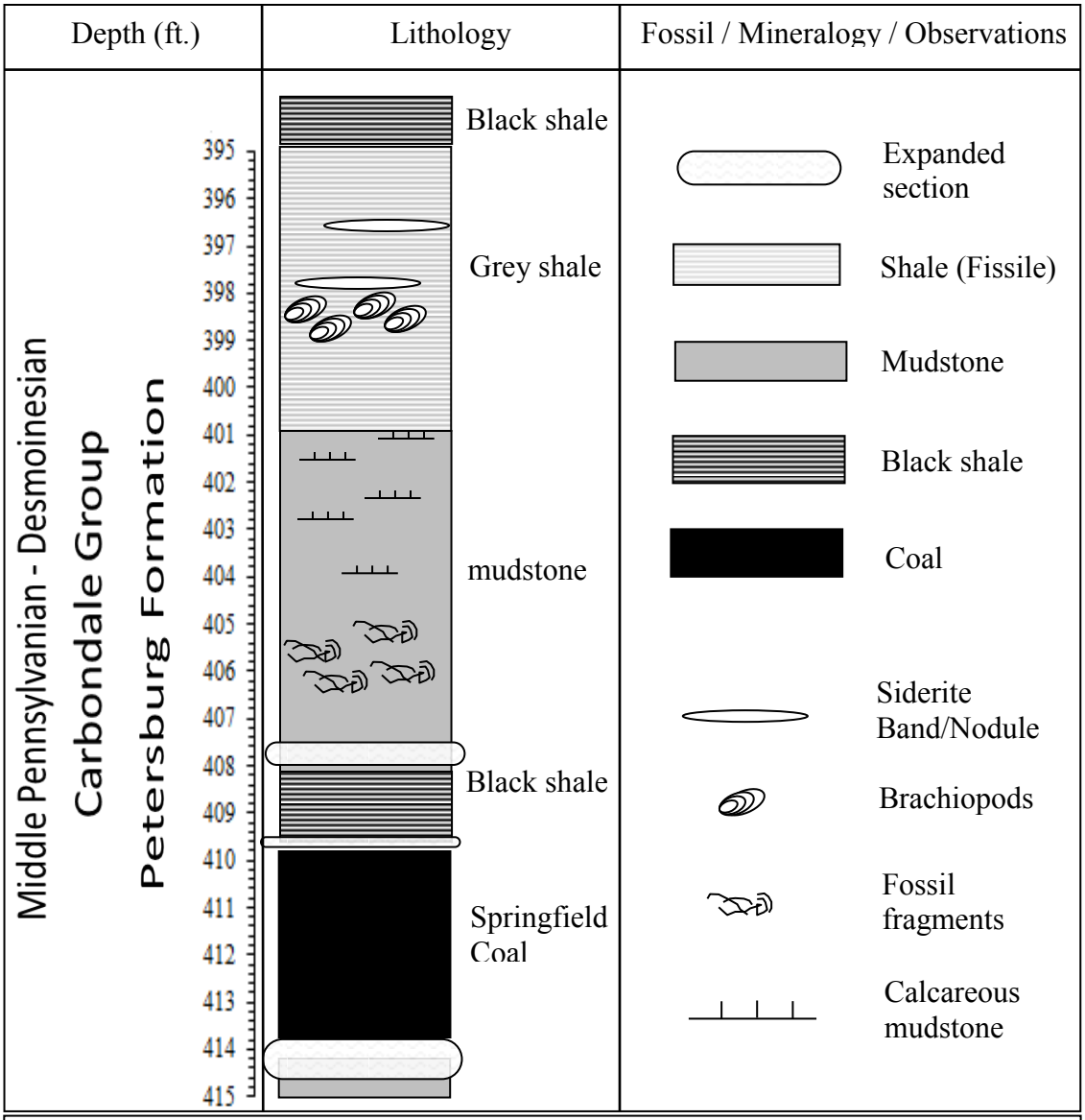

Figure 22: Core 2 description with depth in feet, lithology, fossil presence, and mineralogy. Wireline geophysical logs and cutting data (not shown) indicate the presence of a black shale directly above Core 2, ~394.0' depth.

5.4.2 Carbon, Sulfur, and Nitrogen

TOC concentrations in Core 2 ranged widely, from a high of ~68% in the Springfield coal down to 0.35% in the shale (Fig. 23). The average TOC concentration of the shale above the coal seam was 4.1% with two maxima, the first in the black shale superjacent to the Springfield (12.8%) and the second at the very top of the core (395.6')

in the grey shale (15.4%). TIC values were minimal and averaged <1% throughout the core with a maximum of 3.1% in the fossiliferous section of the grey shale.

TS concentrations were very high (20%) in the underclay section below the coal seam. The maximum in TS corresponds to the mineral szomolnokite (details in Appendix A) detected in at this depth. Sulfur concentrations throughout the Springfield coal averaged 2.7% with the highest value at the transition between the coal seam and the black shale. The black shale superjacent to the coal seam contains 4.5% TS. A high TS concentration of 5% was observed at the facies change from black to grey shale with very low values (<1%) to the top of the grey shale.

TN values were overall very low above the coal (0.1 – 0.3%), and averaged 0.4% throughout the core. The coal seam had the highest amount of sedimentary nitrogen (2%). It was observed that TN covaried with TOC throughout the entirety of Core 2, i.e. when TOC increased so too did TN. C/N ratios are slighter higher in coal than in either the black or grey shales.

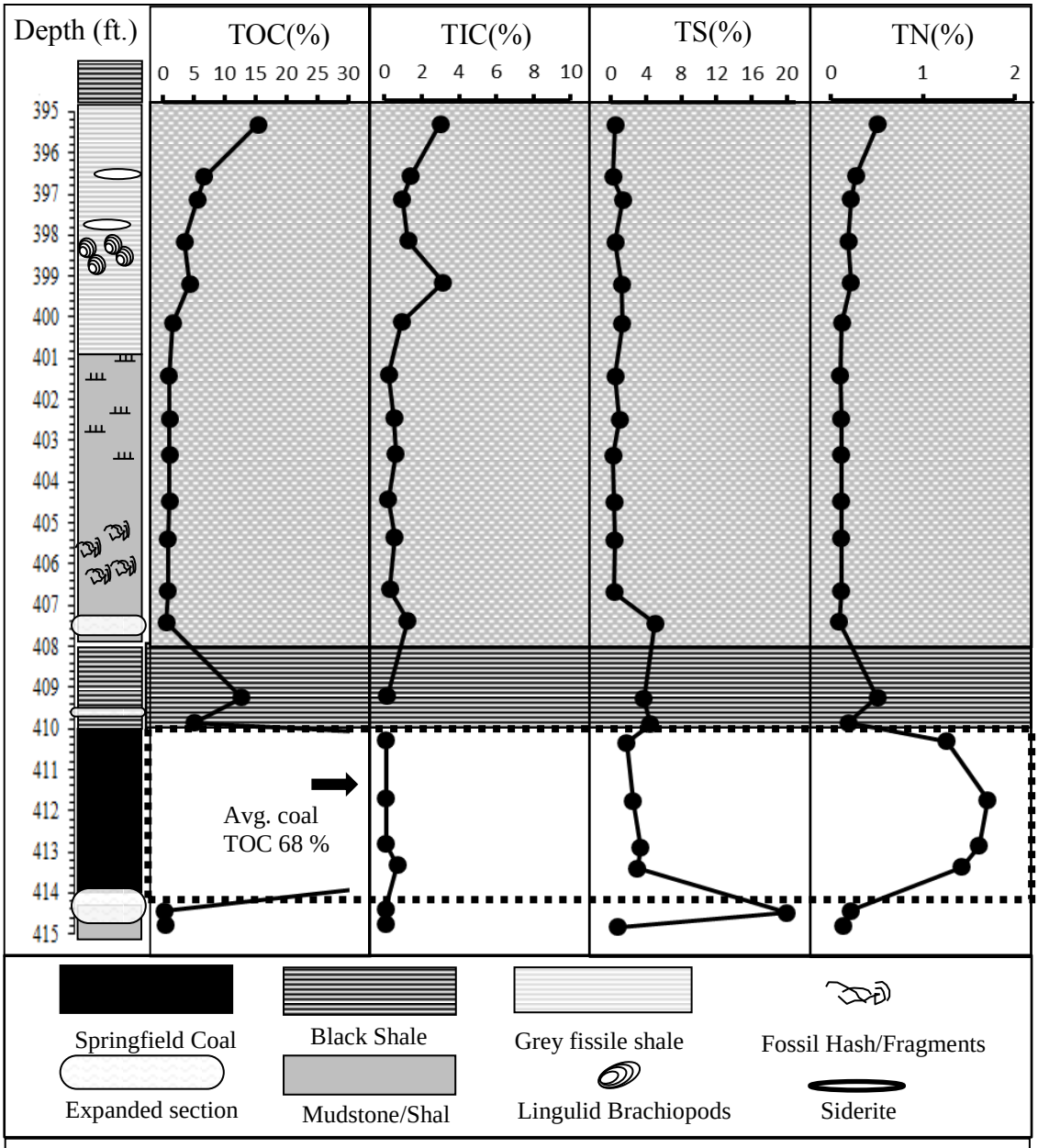

Figure 23: Core 2 Carbon, Nitrogen, and Sulfur

5.4.3 Paleoredox

Mo/Al $_{(mol:mol)}$ ratios in Core 2 coal and grey shale had Mo ppm values less than crustal ranges (<0.2 ppm; Fig. 24). However, higher than crustal values for Mo were observed in the black shale with one very high value (196 ppm) which resulted in a

significant Mo/Al ratio of 0.13 at 409.25’ at the base of the black shale just superjacent to the coal seam. All other ratios were near zero (Fig. 24).

Vanadium concentrations normalized to Al were also high (0.53) at 409.25’ at the base of the thinly laminated black shale. All other V/Al ratios throughout Core 2 were near zero.

Th/U ratios are <2 within the black shale. The sections above and below the black shale have an average Th/U of 3.9, which is in the range for the marine/terrestrial mixture parameters between 2 and 7. High ratios (Th/U >7) were not observed in the core overlying the coal seam.

Fe_{tot}/Al ratios for Core 2 are above the normal marine threshold of 0.5 at three depths in Core 2. The first is a very high Fe_{tot}/Al ratio of 12.2 within the expanded section below the Springfield coal. The second is in the fossiliferous shale section (399.4’) and the third is near the top of the core where fissility increases directly subjacent to another black shale above the core (not cored; Fig. 24)

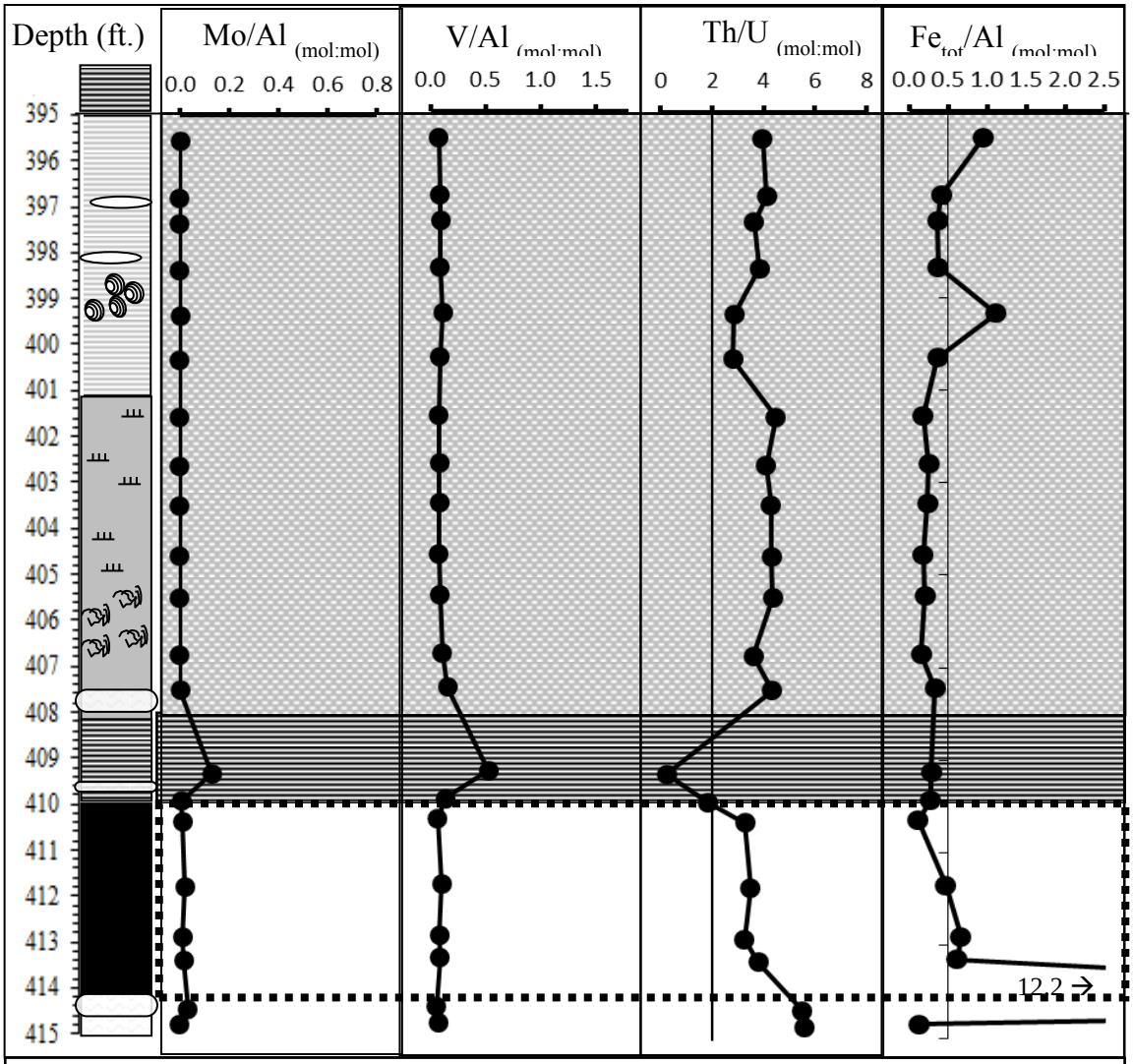

Figure 24: Core 2 Paleoredox

5.4.4 Isotopes and Basin Parameters

$\delta^{13}C_{org}$ in Core 2 exhibits distinct trends across black shale, mudstone and fissile grey shale (Fig. 25). Black shale $\delta^{13}C_{org}$ averages -26.7‰. Upsection, the isotopic composition of organic matter becomes more ^{13}C-enriched in the blocky grey mudstone

(-23.6‰) and then ^{13}C-depleted as the section becomes more fissile and transitions to an overlying black shale above the core (not sampled).

Zr (ppm) values in the black shale average 102 while those of the grey shale average 120 ppm. However, a clear trend exists in the data, with values highest in the center of the grey section (400.0'-402.0'), which then decrease to ~100 ppm as fissility increases and lithology transitions to more organic-rich rock and the black shale overlying the core (not cored).

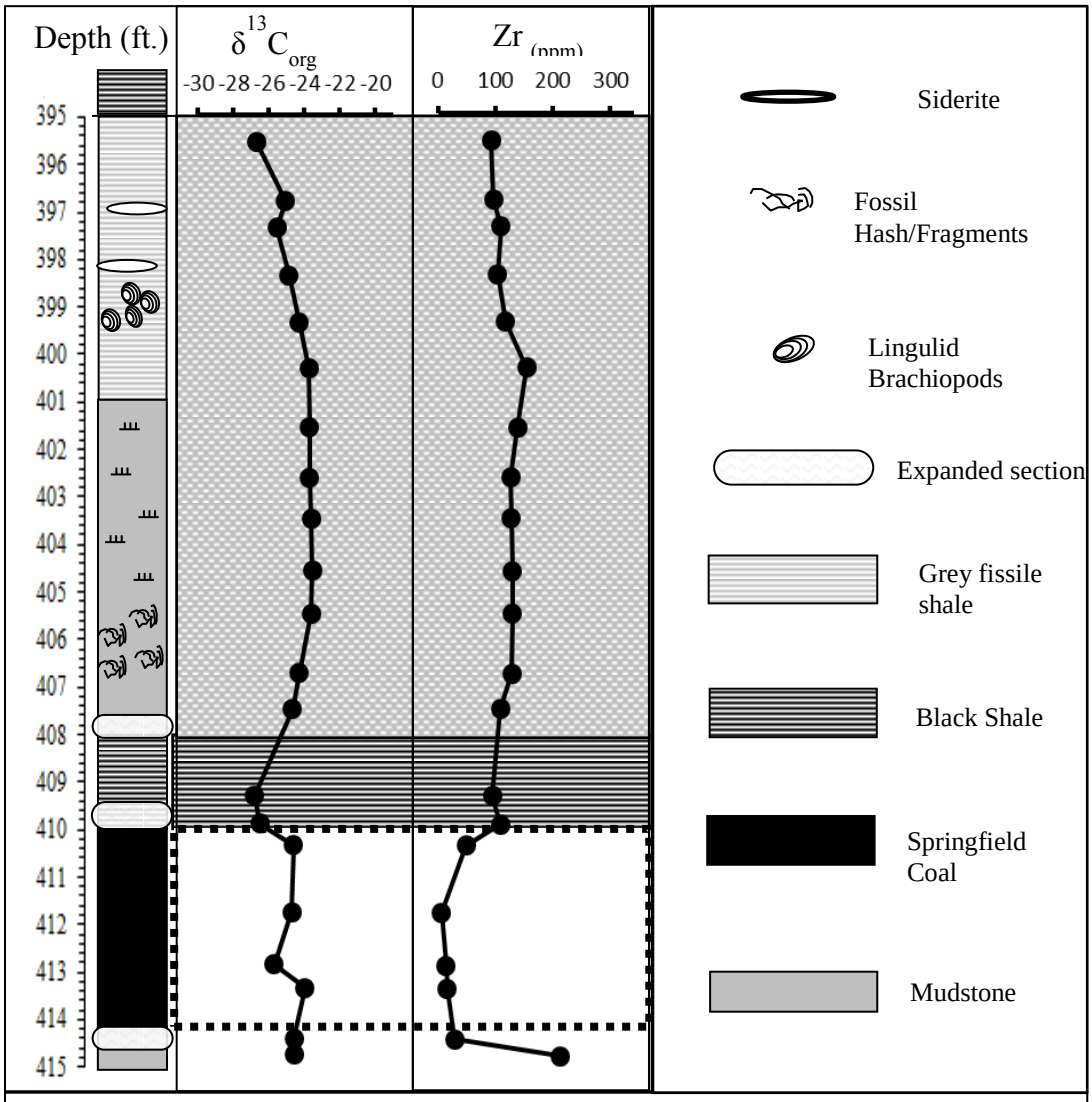

Figure 25: Core 2 Isotopes and Basin Parameters

6. DISCUSSION

6.1 Research Questions and Relevance

The purpose of this research was to use geochemical proxies in conjunction with observed lithological and paleontological data at a core level and precisely identify and characterize shales and mudstone superjacent to coals common in the Pennsylvanian bedrock of southern Indiana. This combined approach can help more accurately identify the mode of deposition and water chemistry during these coal-mudrock transgressive sequences. Geochemical proxies were used to better constrain the source of organic matter, redox chemistry and detrital inputs within each core. The environmental change associated with sea level rise (and fall) is best recognized in chemostratigraphic patterns recorded across facies changes, such as coal to shale. Each coal seam and overlying strata contain a unique geochemistry that when looked at in depositional context reveals information about the manner and magnitude of each transgressive flooding event. As such, the transition from coal to mudrock was the focus of comparing the chemostratigraphies of Cores 2-5 (e.g. Fig 26). The presence of black shale and marine fossils in Cores 2 and 3 and the lack of fossils in Cores 4 and 5 offered an ideal sample set to explore chemostratigraphic variations. These variations in solid phase chemistry and isotope composition reveal certain clues that can be used to reconstruct the origin of the shale and organics deposited above the coal seam. Only after the interplay of these factors is assessed can the depositional story of these four cores be determined.

6.2 TOC and Black Shale Deposition

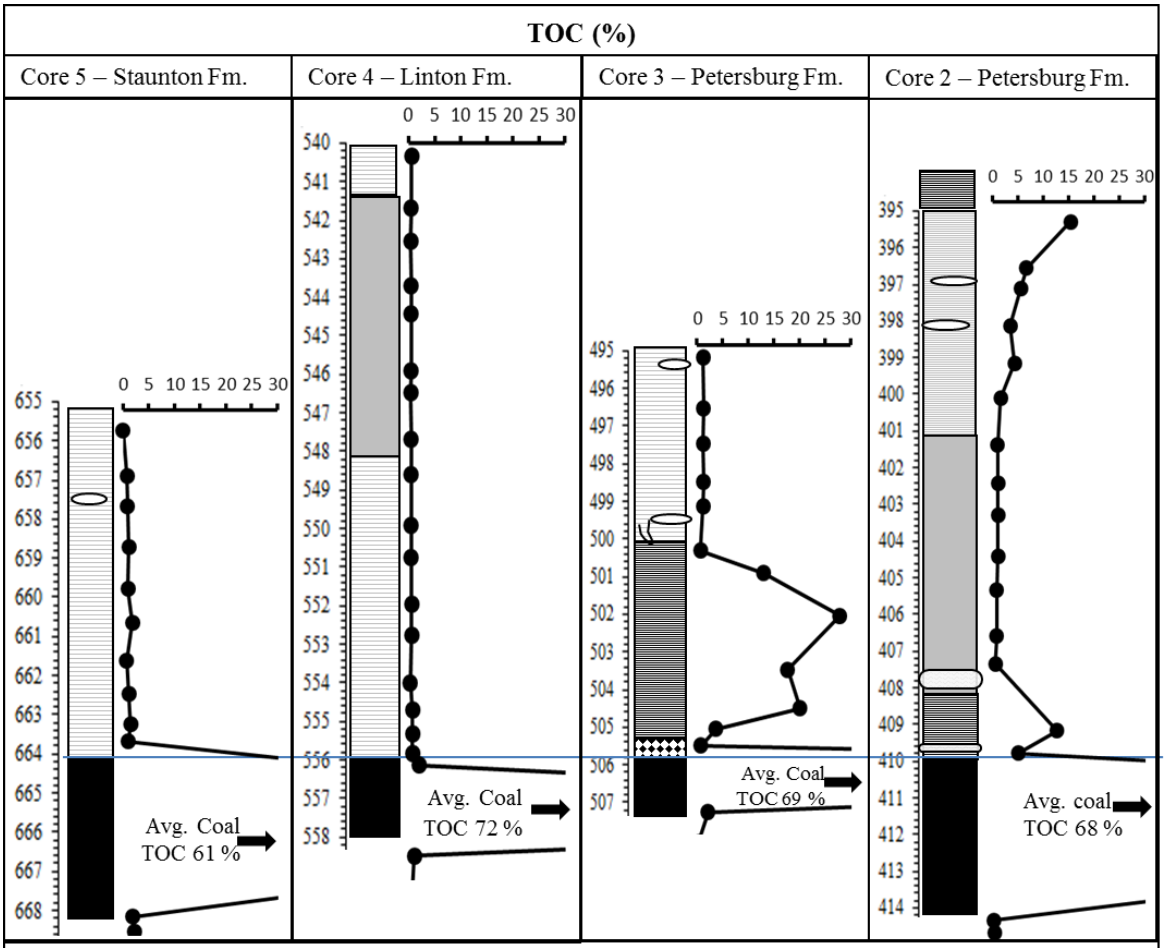

Figure 26: TOC Comparison between Cores 2-5 – Coal→Mudrock Only

Not surprisingly, the highest amount of TOC in all four cores occurs in the coal sections. Coal is lithified peat, or accumulated and compressed organic matter from paludal environments, mainly terrestrial plants and is comprised of generally 60-90% organic matter (Mastalerz, 2010). These TOC coal values are almost exclusively of terrestrial organic matter due to the fact that Pennsylvanian peat mires, while possibly near-coastal, were deposited subaerially and in a freshwater aquatic system. While seawater inundation of Pennsylvanian swamps certainly mixed a small amount of marine organic matter with that of the terrestrial and porous peat vegetation, the contribution to

overall TOC preserved in the coal is most likely orders of magnitude lower than the terrestrial biomass.

As opposed to the coal organic carbon, shale and mudstone are composed of variable amounts of organic matter that are a result of organic remains both generated in or brought into a water column and deposited into the predominantly siliciclastic sediment. For Core 2 and Core 3 TOC values remain high in the overlying black shale and grey shale. Cores 4 and 5 however, do not have black shale and the TOC concentrations are very low (<1%). Extremely high TOC (15%) in the black shale above the coal in Core 2 may indicate the lack of aerobic decomposition within anoxic bottom waters. Values then decrease to near zero and as the grey shale gradually becomes more fissile and transitions to another black shale directly above Core 2. The values at the top of the section increase to 15%, indicating a return to low-energy benthic conditions and possibly benthic anoxia or enhanced productivity. The TOC concentrations in the black shale of Core 3 are also high and likely the result of bottom water anoxia that enhanced preservation of the organic matter. Cores 4 and 5 however, contain virtually no organic matter above the coal seams. Thus either bottom waters were not anoxic with low TOC preservation potential, productivity in surface waters was extremely low with no organics to preserve, or dilution with clastics or other detrital input. The use of other redox-sensitive proxies and basin source indicators are therefore needed to provide a more robust interpretation of depositional conditions.

6.3 TIC

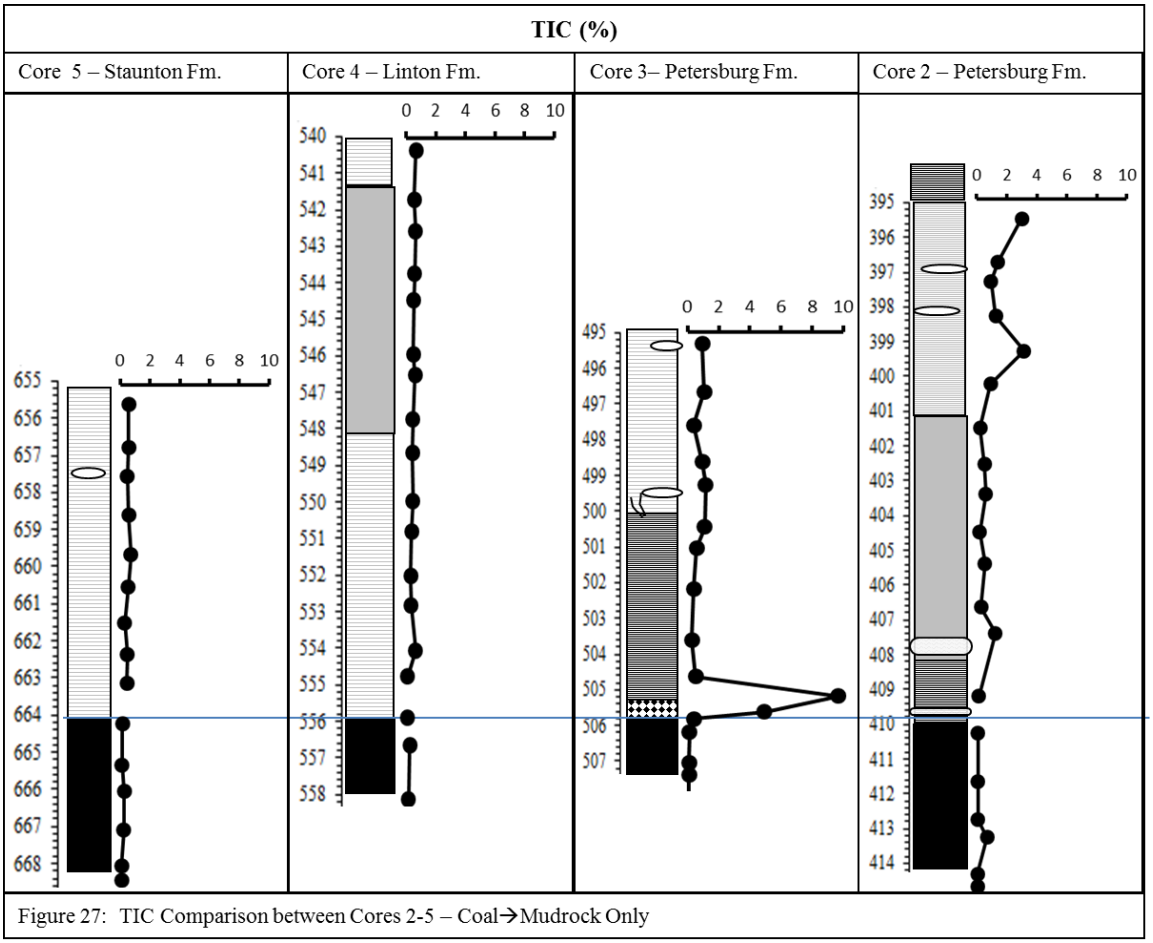

Figure 27: TIC Comparison between Cores 2-5 – Coal→Mudrock Only

In all four cores, there was minimal TIC (<1%) and no calcareous sections (>10%) were found. Indeed the 'deepwater' limestone facies associated with similar cyclothemic stratigraphy during this time was not observed in these cores (Heckel, 2008). All four cores show a lack of limestone development above their respective coal seams and suggest that the 'deepwater' or highstand facies of each was the black shale in Core 2, the black Excello Shale in Core 3 and the grey shale/mudstone just overlying the coals in Cores 4 and 5.

Only in Core 3, at the base of the Excello shale, directly above the large pyritic section was there an appreciable amount of carbonate, ~10% TIC (Fig. 14). This increase in carbonate is possibly indicative of beginning of regressive marine waters moving core

location closer nearshore (Heckel, 2008). However, this carbonate event was short-lived as all paleoredox proxies indicate prevalent benthic anoxia throughout the rest of the Core 3 black Excello Shale deposition. Near zero values for TIC in muds above Core 4 and 5 are interpreted as a nearshore marine but clastic-dominated system, fully oxic but mixed with siliciclastics which inhibited the production of carbonate in environments such as an estuarine or deltaic coast.

6.4 Total Sulfur

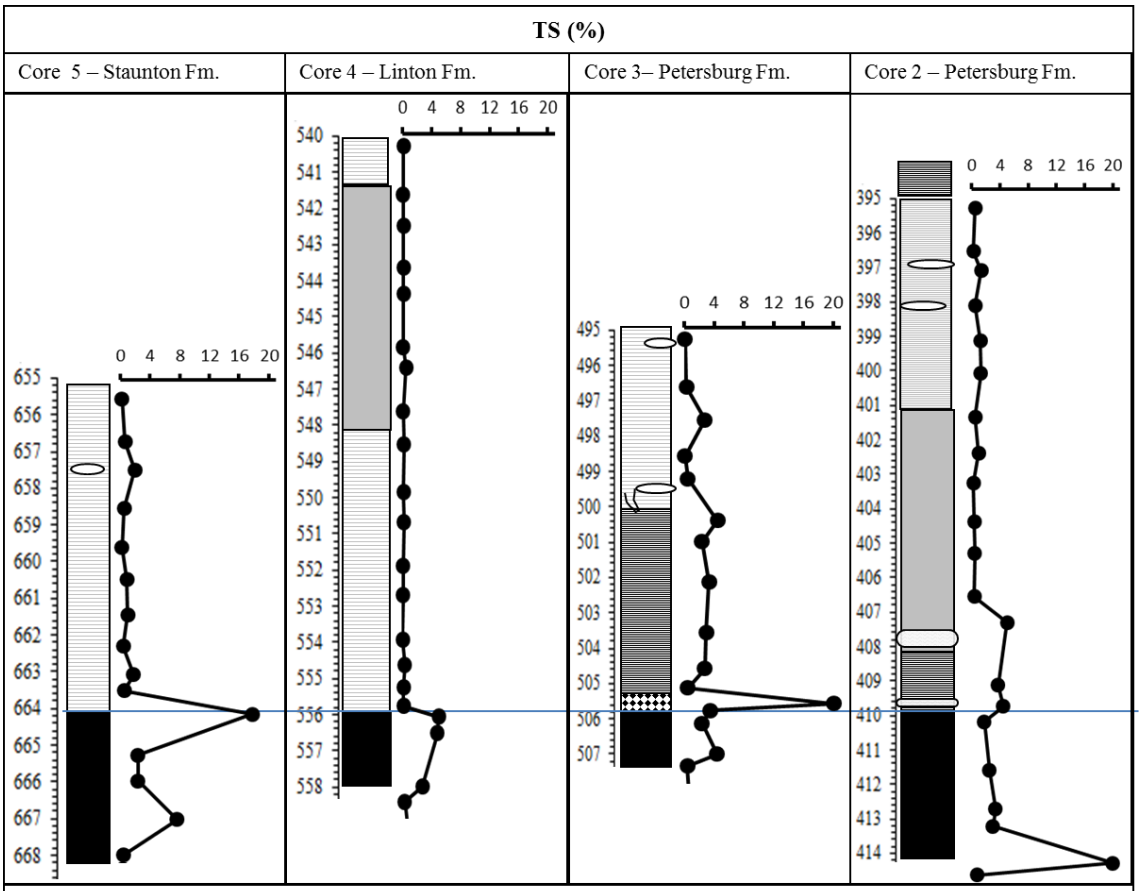

Figure 28: TS (%) Comparison between Cores 2-5 – Coal→Mudrock Only

TS values between for all coals averaged 4.5%. All black shale values averaged 4.9% and all grey shale and mudstone values averaged 0.7%. Having ruled out other possible sources of sulfur for these high concentrations (riverine, hydrothermal, volcanic

outgassing, peat organics) and bearing in mind that higher sulfur coals (TS > 2.5%) have long been associated with overlying marine strata (Gluskoter and Simon, 1968; Affolter and Hatch, 2002) one can assume that >2.5% TS indicates marine inundation. Given that each coal seam, irrespective of overlying lithology, contained on average greater than twice this amount it is reasonable to assume that marine waters inundated low-lying southern Indiana peat mires in all four cores. This sulfate then diffused down through the porous peat, was reduced to sulfide and combined with reactive iron when available to produce high pyrite concentrations visible in many of the cores.

Paleoredox assessments and overall C/S relationships are illustrated in the figure below (Fig. 29) adapted from Berner and Raiswell (1983). The ratio of organic carbon to total sulfur (C/S) is clearly different for Cores 2-5. Freshwater basins that contain less dissolved sulfate but generally high concentrations of organic carbon tend to plot along the x-axis (Fig. 29 B). Marine basins with high amounts of dissolved sulfate and less carbon tend to follow a consistent covariance between S and C for 'normal' (oxic) marine basins (dashed line, Fig. 29A and B). Euxinic marine systems have high amounts of dissolved sulfides and variable amounts of C and tend to intersect along the Y-axis.

The cores analyzed in this study, portions of the Petersburg, Linton, and Staunton Formations, show various relationships. The first is the distinct range for C/S ratios for the black shale of Core 2 and the Excello of Core 3. These cores are characterized by high sulfur (>2.5%) and variable carbon concentrations (near zero to near 30%; Fig. 29A, L-shaped box). The data outlier (20% TS and <1%TOC) was from the massive pyrite section at the base of the Excello Shale in Core 3. Grey shale values vary widely (Fig 29B). While many grey shales values plot close to the modern normal marine ratio of

C/S there is large amount of variance with a large portion (56%) of data that plot below the freshwater line (Berner, 1983) and many plotting well above it (44%). However, in every case the highest sulfur concentrations are reported at the transition from coal to grey shale. This fits with the estuarine model of deposition where marine flooding mixes with terrestrial freshwater and sulfur and carbon concentrations fluctuate as base level rises. There is one exception to this trend at the very base of Core 4, where the C/S value plots within the euxinic field (Fig. 29 A). This value in Core 4 suggests that sulfate-rich seawater flooded the Survant coal, and indicates sedimentation during this time period was marine and possibly even euxinic. Also noted was that Core 5 shows high sulfur relative to carbon indicating that waters were most likely marine but did not sequester appreciable amounts of carbon in the sediment. The TS% for suggests that *all* cores were inundated by marine waters with reduced sulfur dominating the C/S ratios with anoxic and often euxinic water columns present for black shale deposition. Detrital influx dilution into the water column thus impeding organic carbon sequestration in times of increasingly oxic conditions in the grey shales for all cores is a possible mechanism for the geochemical facies observed.

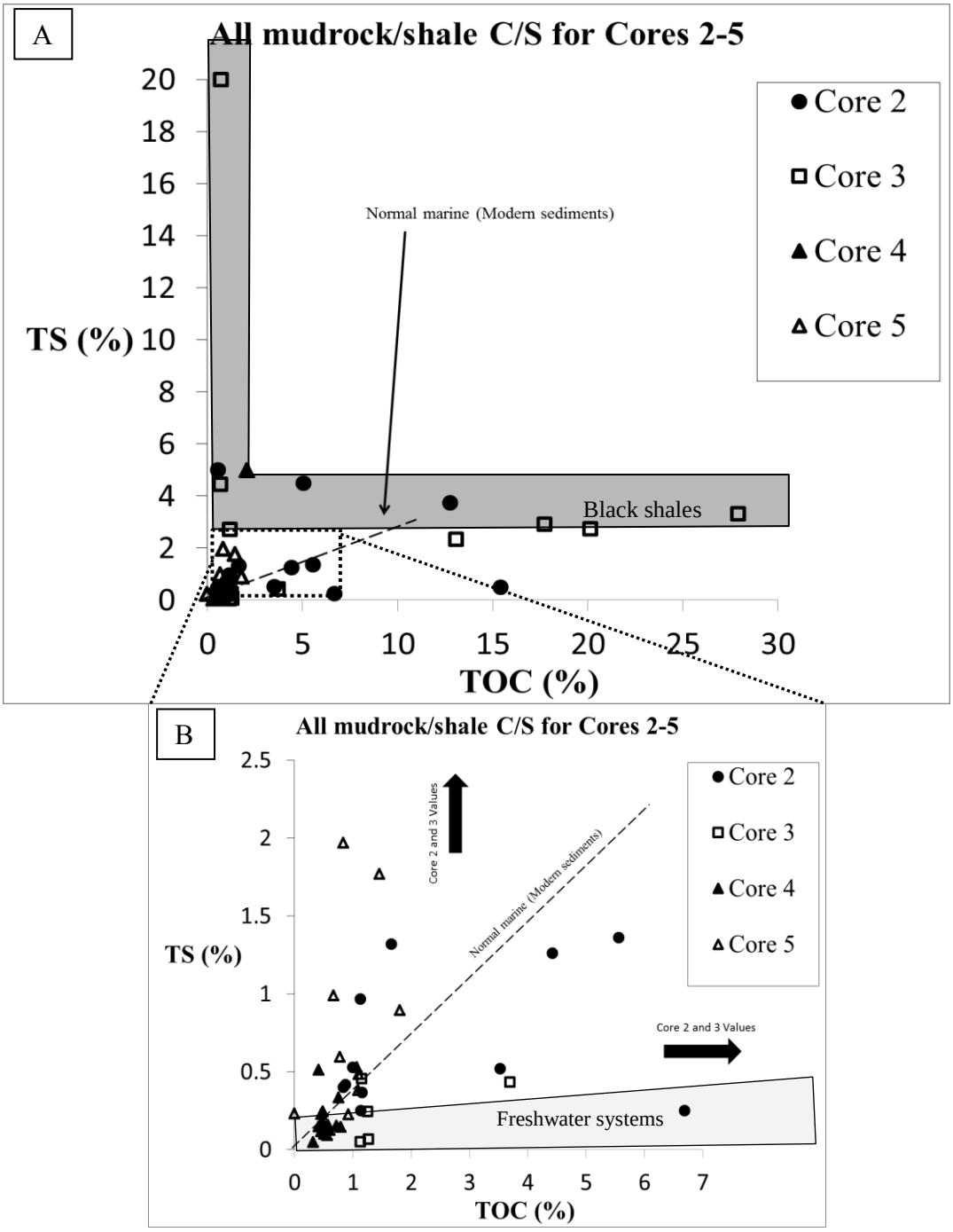

Figure 29: C/S plots for Cores 2-5. A) Full range of data. Black shales fall in 'L'-shaped box with dashed line indicating modern normal marine ratios. B) Zoomed in plot showing freshwater ranges from Berner and Raiswell (1983) compared to Core 2-5 mudrock. Note: All data within the inset (B) are grey shale/mudstone. Modified from Berner and Raiswell (1983).

The TS concentrations in Core 2 are highest at the base of the core in the expanded section below the coal (Figs. 23, 28). Based on the amount of expansion in

Core 2, likely the result of *in situ* sulfide oxidation and the formation of szomolnokite ($FeSO_4$-H_2O; Appendix A), which forms from the secondary alteration of sulfide minerals like pyrite (Pistorius, 1960), one can infer that a great deal of pyrite was present at the base of the coal at some point in time. However, at one of the two other sections of Core 2 that displayed slight expansion, pyrite was identified by XRD and szomolnokite was not detected. This section was not explored further with FE-SEM or EDS, but may represent the early stages of pyrite alteration to szomolnokite. See Appendix A for expanded section results, discussion and interpretations)

The sulfur story of all cores points to sulfate-rich marine inundation of low-lying peat bogs. Cores 2 and 3 further indicate a near-euxinic to euxinic water column forming and resulting in water column (syngenetic) pyrite formation. Cores 4 and 5 have evidence for marine transgression but are sulfur limited and have very little organic carbon sequestration indicating benthic oxic conditions throughout grey shale deposition and the possible dilution by detrital material.

6.5 Total Nitrogen

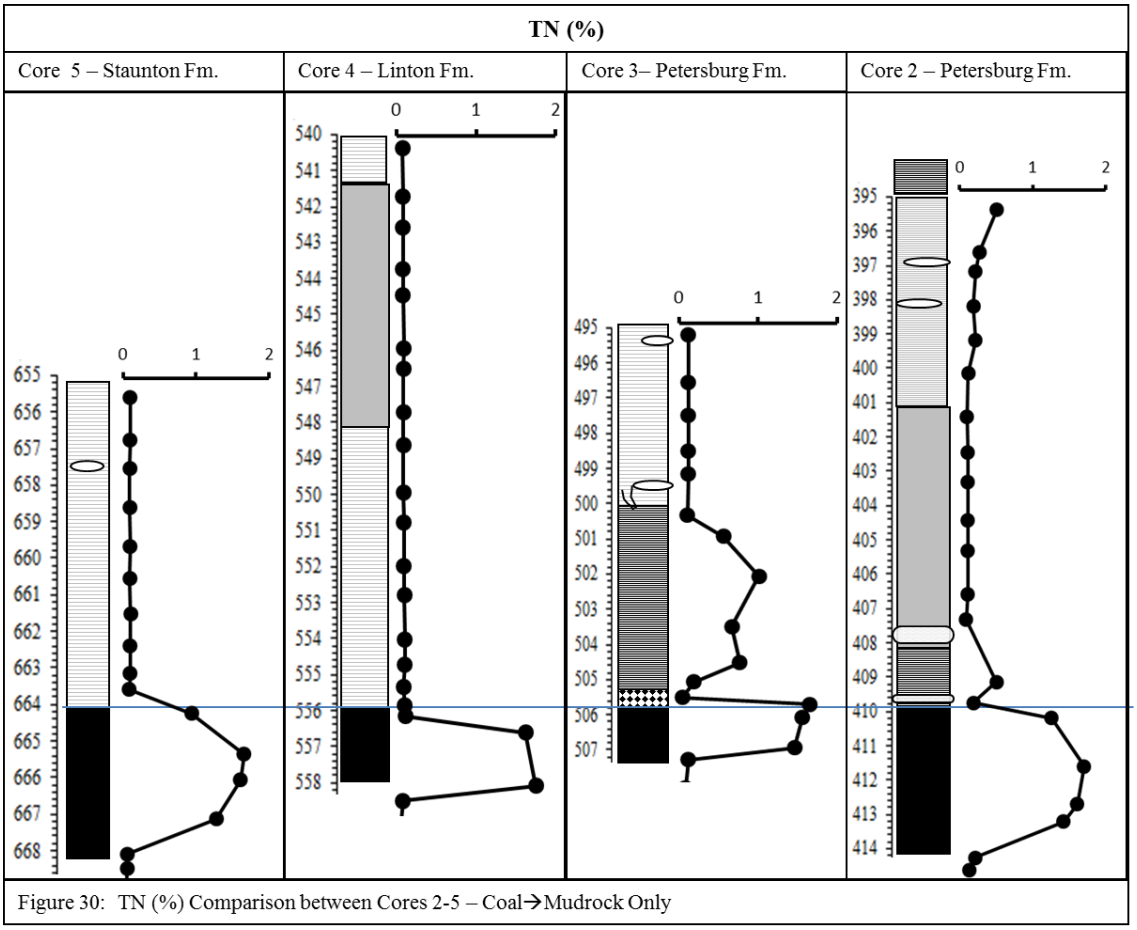

Figure 30: TN (%) Comparison between Cores 2-5 – Coal→Mudrock Only

In all four cores, TN is low (<2%) and covaries with TOC in all facies. Other observations were that the coals contained substantially more nitrogen than all other facies observed and two clear groupings are visible, coal C/N versus all mudrock C/N values (Fig. 31). The strong positive relationship between TN and TOC, suggests that TN for all lithofacies is composed primarily of organic nitrogen.

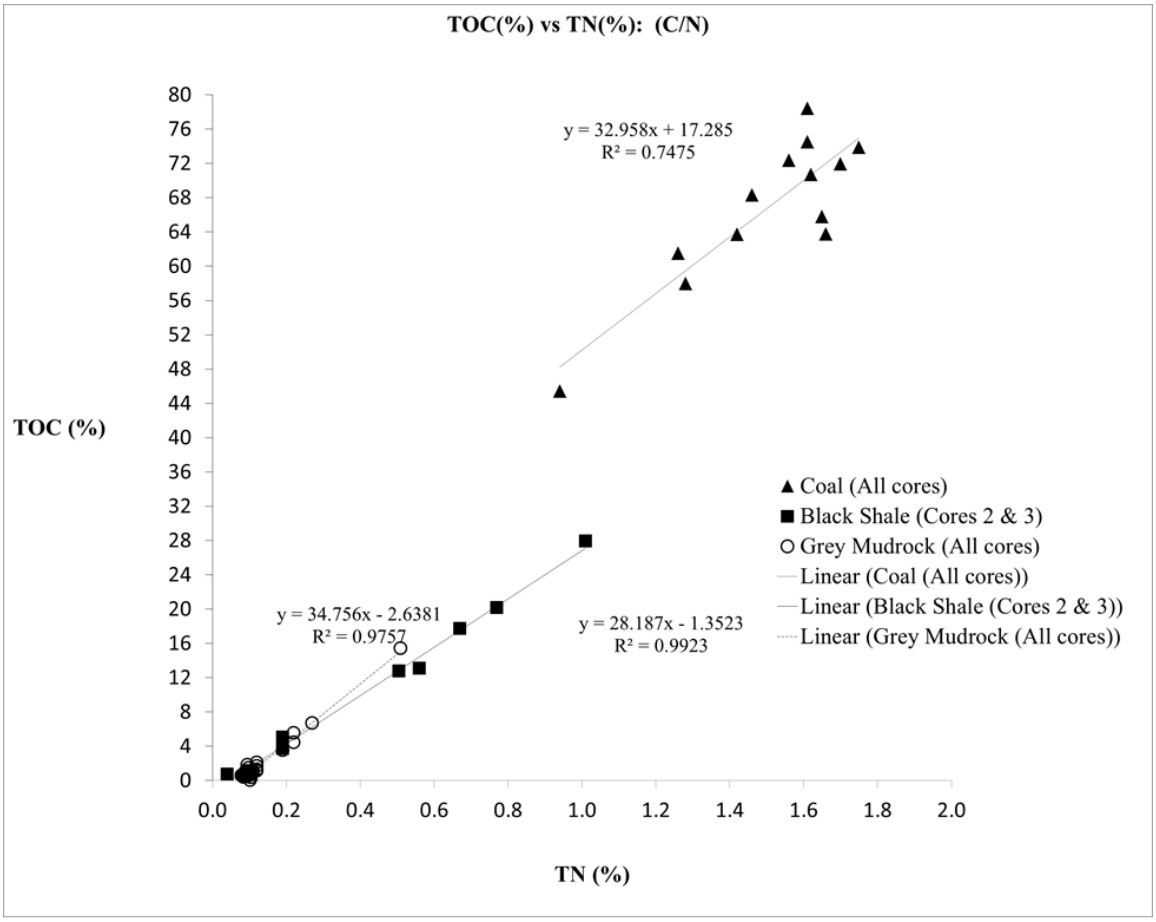

Figure 31: C/N ratios for all cores separated by lithology: Coal, Black shale, and Grey Mudrock.. Not e the slightly different ratios of C/N for black and grey mudrock.

Several observations are clear when examining the C/N data for all cores and the three distinct lithologies, i.e. coal, black and grey shale. The first is that coal values have higher absolute concentrations of both C and N (Fig. 31). Also that C/N values in the coal average 42 for all four cores which are are consistent with terrestrially derived organic matter (Meyers, 1994). However, in relative deeper-water facies (black shales) C/N values where one might expect to find a distinct lower C/N ratio associated with algal sources of organic matter (Meyers, 1994), C/N values average 22 and are *higher* than the grey shale and mudstone (average 10) that are interpreted as more nearshore facies. This discrepancy is possibly due to the effect of detrital dilution during grey shale

deposition, i.e. an increase in siliciclastic contributions from black to grey shale or possibly that the differences in values are a result of an algal influence (low C/N) affecting both nearshore *and* offshore organic matter contributions prior to organic matter deposition and sequestration.

6.6 Paleoredox: Molybdenum

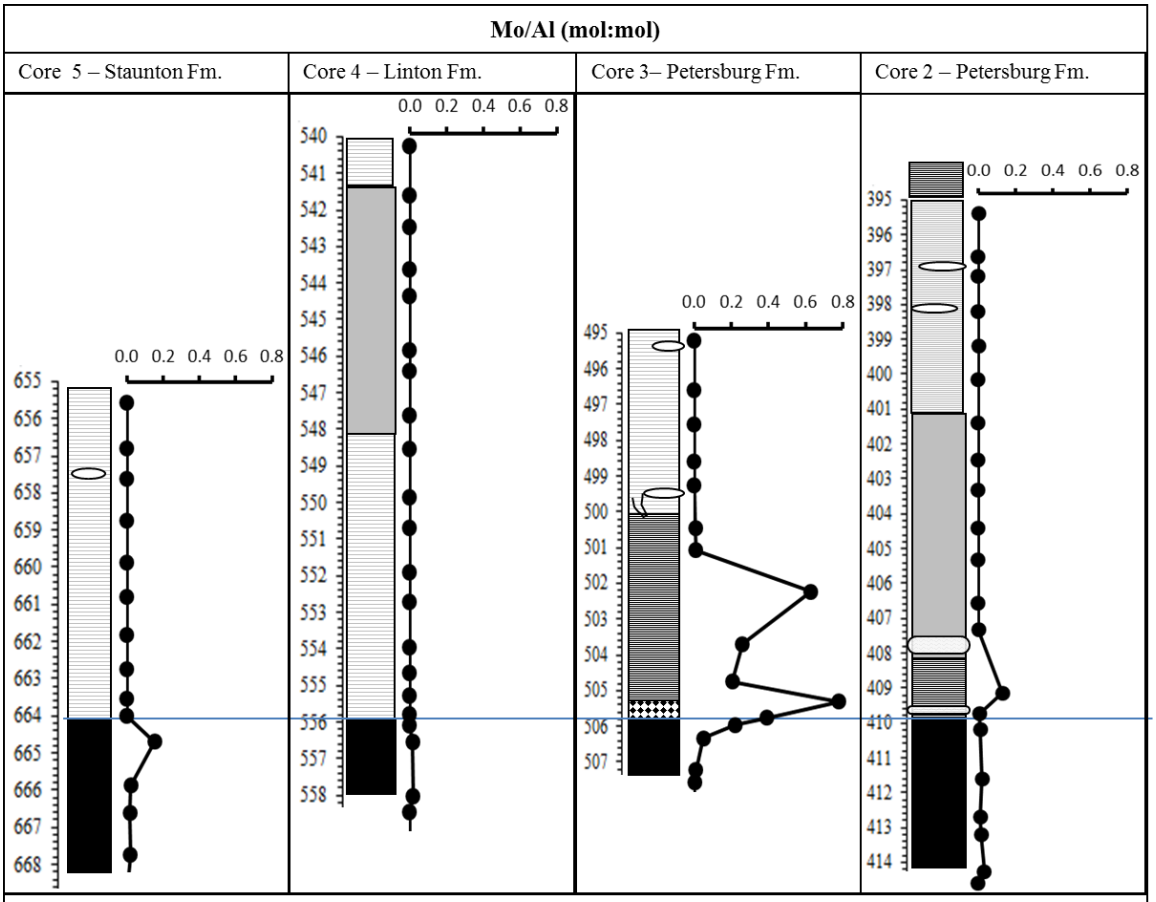

Figure 32: Mo/Al Comparison between Cores 2-5 – Coal→Mudrock Only

Mo concentrations were near zero (<2 ppm) for all grey shales and mudrock for all cores implying fully oxygenated conditions. The Excello Shale has the highest Mo concentrations for any facies studied, (average 208 ppm) and Core 2 has a high Mo (196 ppm) at the top of the black shale above the Springfield Coal. These values are above the euxinic threshold (> 100 ppm) as defined by by Scott and Lyons (2007), and from

observations in Figure 32 and 33, and corresponding C/S ratios, the black shales of Core 2 and 3 were deposited under euxinic bottom waters. Core 2 Mo values indicate at least intermittent euxinic conditions while it is reasonable to suggest that the Excello Shale had sustained euxinic conditions until transitioning to the overlying grey shale and an oxygenated water column. Core 4 and 5 have near-zero values throughout the mudrock indicating that the water entering these basins was: (1) predominantly nonmarine, (2) marine but the basin was cut off from marine resupply, or (3) 'normal' marine and fully oxygenated preventing thiomolybate reduction and Mo sequestration. To test which of these is more likely, a cross plot of Mo vs TOC is shown in Fig. 33. The Cariaco and the Black Sea each have restrictions, which impede Mo replenishment but are either intermittently euxinic (Cariaco) or sustained euxinic (Black Sea; Algeo and Lyons, 2006). Regression lines are shown for the Cariaco Basin and Black Sea data from data taken from a variety of publically available publications (See Algeo and Lyons, 2012 for complete list of sources). The regression line for Core 3 mudrock is shown for comparison (Fig. 33).

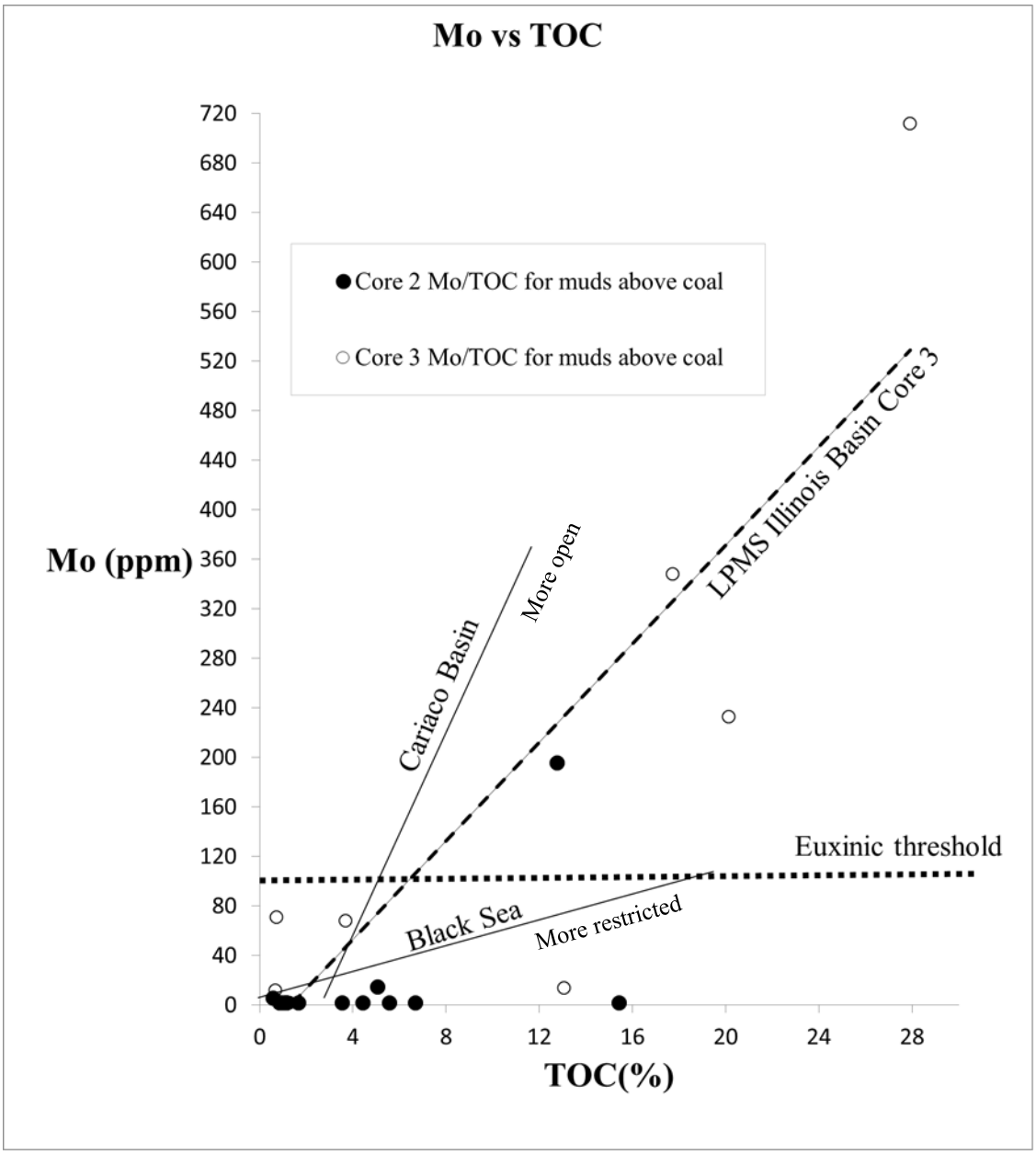

Figure 33: Mo (ppm) plotted against TOC(%) for mudrocks (black and grey) for Cores 2 and 3 (cores with mudrock that contained >2ppm Mo). Dashed line is regression line for Core 2 (Excello and overlying grey shale). Dotted line is euxinic threshold of 100ppm per Scott and Lyons, 2012. Figure adapted from Algeo and Lyons, 2007.

While both the Cariaco and Black Sea are euxinic and Mo is sequestered in these sediments, both basins lack complete Mo replenishment from the open ocean. This restricted scenario is suggested in the patterns of Mo/TOC for the Excello as well (Fig. 26) where replenishment rates (slope of regression) fall between that of the restricted

Black Sea and the lower-silled less-restricted Cariaco basin. The extremely high Mo values (Excello averages >200 for entire 5.2') suggest at least periodic but sustained marine Mo replenishment in times of highstand, i.e. black shale deposition. Although the Mo/TOC patterns in the Excello suggest restricted circulation, no sill is known to exist during LPMS sedimentation. A certain of degree of restriction is indicated by the paleogeography of the epeiric LPMS and especially for far eastern waters over southern Indiana during the Desmoinesian.

In summary, during both Core 2 and Core 3 black shale deposition (during times of highstand; at deepest facies deposition) Mo was sequestered in marine sediment and marine waters were most likely anoxic and at least intermittently euxinic to permanently euxinic. A persistent euxinic state may have occurred during Excello shale deposition in Core 3. For Cores 2 and 3, regressive waters and a shallowing of the water column indicated a return to more nearshore sedimentation with water columns increasingly oxygenated upsection (grey shale and mudstone).

6.7 Paleoredox: V/Al

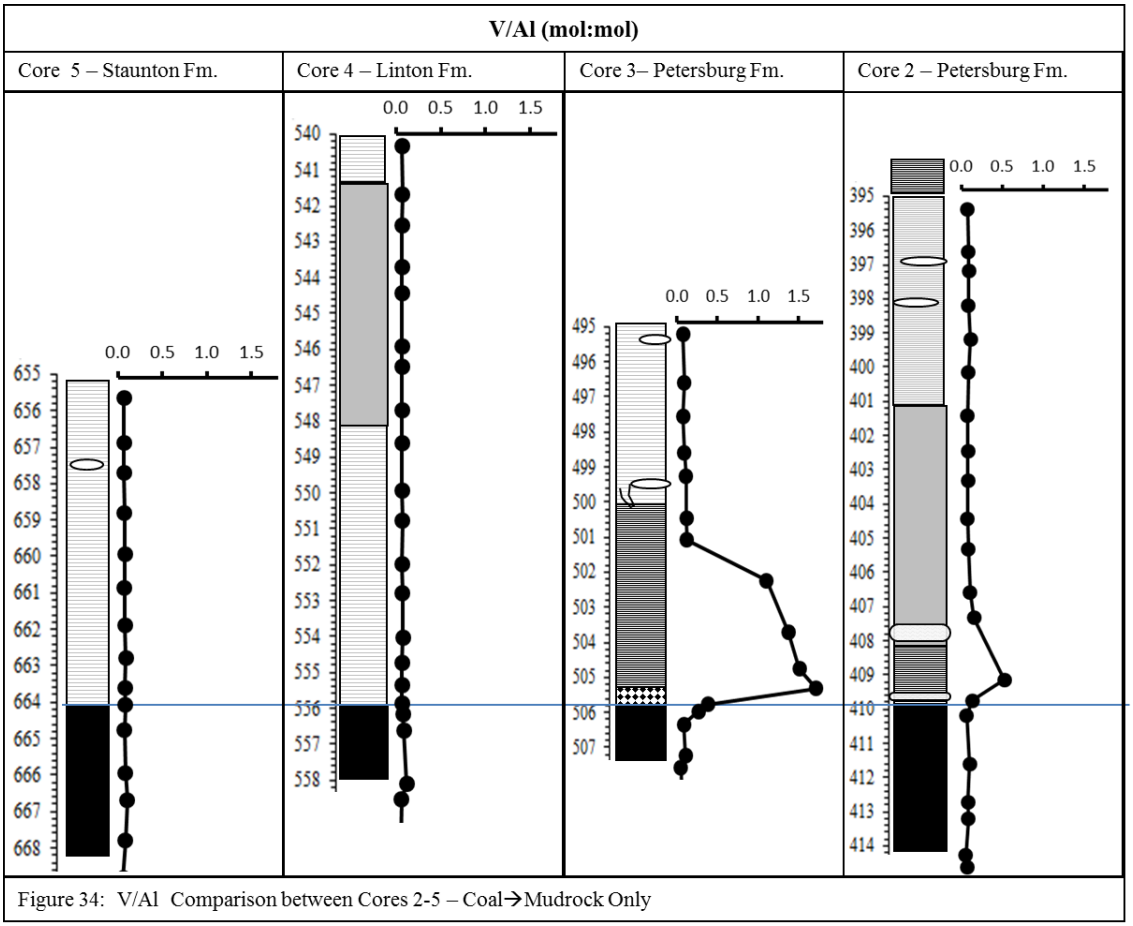

Figure 34: V/Al Comparison between Cores 2-5 – Coal→Mudrock Only

Vanadium concentrations show a dramatic increase in concentration within the black shales. Excello Shale V/Al values are extremely high (> 1.5). While high V concentrations can certainly indicate anoxic systems, V/Al has been deemed a trace element with 'strong euxinic affinity' (Algeo and Maynard, 2004) due to the two-step reduction process, the latter only in the presence of H_2S.

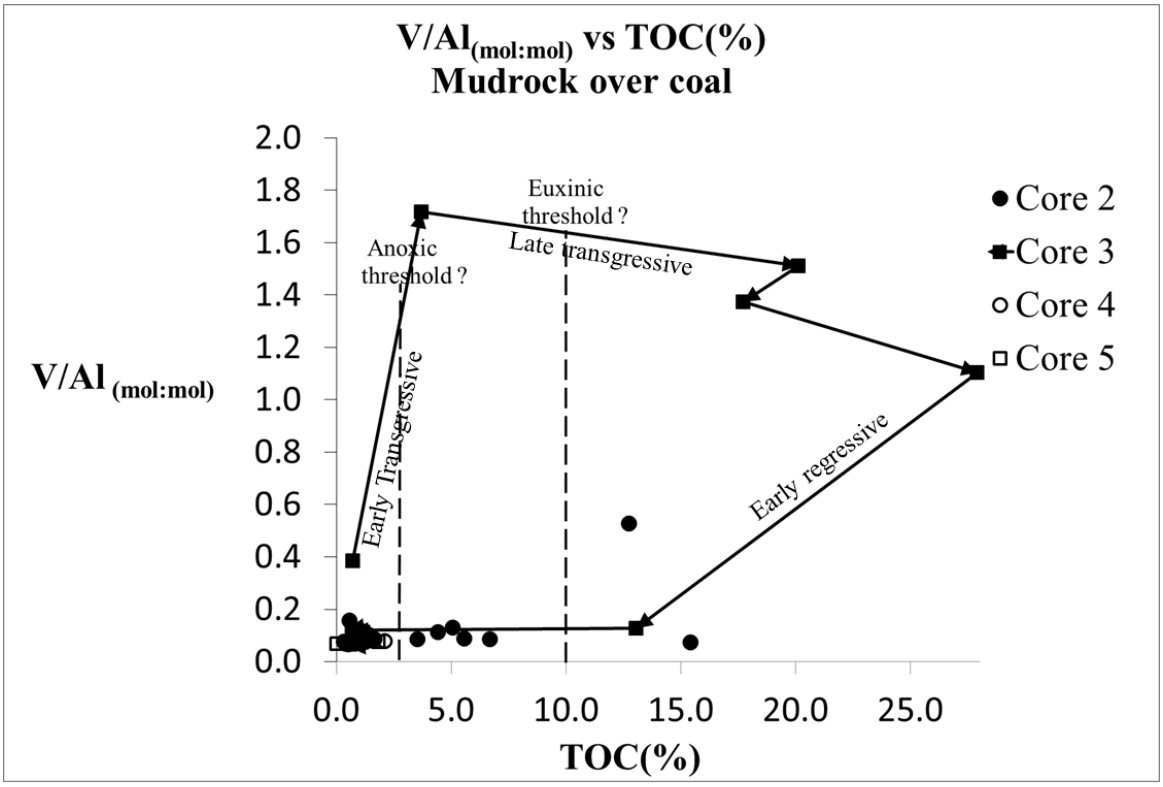

Figure 35: V/Al (mol:mol) is plotted against TOC(%) for mudrocks (black and grey) for Core 2-5. Dashed lines are based on data from Algeo and Maynard, 2004 and compared with Core 3 Excello shale TOC data. These are possible TOC threshold cutoffs for euxinia based on corroborative paleoredox proxies from this study. A depositional loop (solid line with arrows) was observed for V/Al and TOC from the Excello and then on upsection into the grey shale.

Figure 35 shows V/Al concentrations plotted against TOC for all the mudrock superjacent to their respective coal seams. The TOC threshold values are taken from Algeo and Maynard (2004) and based on observed TOC cutoffs associated with assumed euxinic facies of their study and the Excello Shale average TOC in this study. If we assume that these cutoff represent delineations between anoxic and euxinic water columns then V/Al confirms other paleoredox proxies listed, e.g. Mo/Al, C/S and reveals that the entirety of the Excello and the black shale of Core 2 were both deposited in a euxinic water column. All core 4 and 5 values were near zero for both V/Al and TOC and are clumped within the oxic field. Interestingly, a loop was observed for Core 3 that corresponds to a marine flooding event (Fig. 35). As early transgressive waters flooded

the Houchin Creek coal, redox conditions became increasingly anoxic and vanadium was sequestered with organic carbon. Conditions then presumably became euxinic and remained euxinic for the duration of the Excello Shale until returning to anoxic and then fully oxic during the depositional of the grey shale overlying the Excello (i.e. from late transgressive to regressive). Nearshore to offshore interpretations corresponding to this transgressive-regressive event (water depth deepening to shallowing) are thus assumed.

6.8 Paleoredox: Th/U

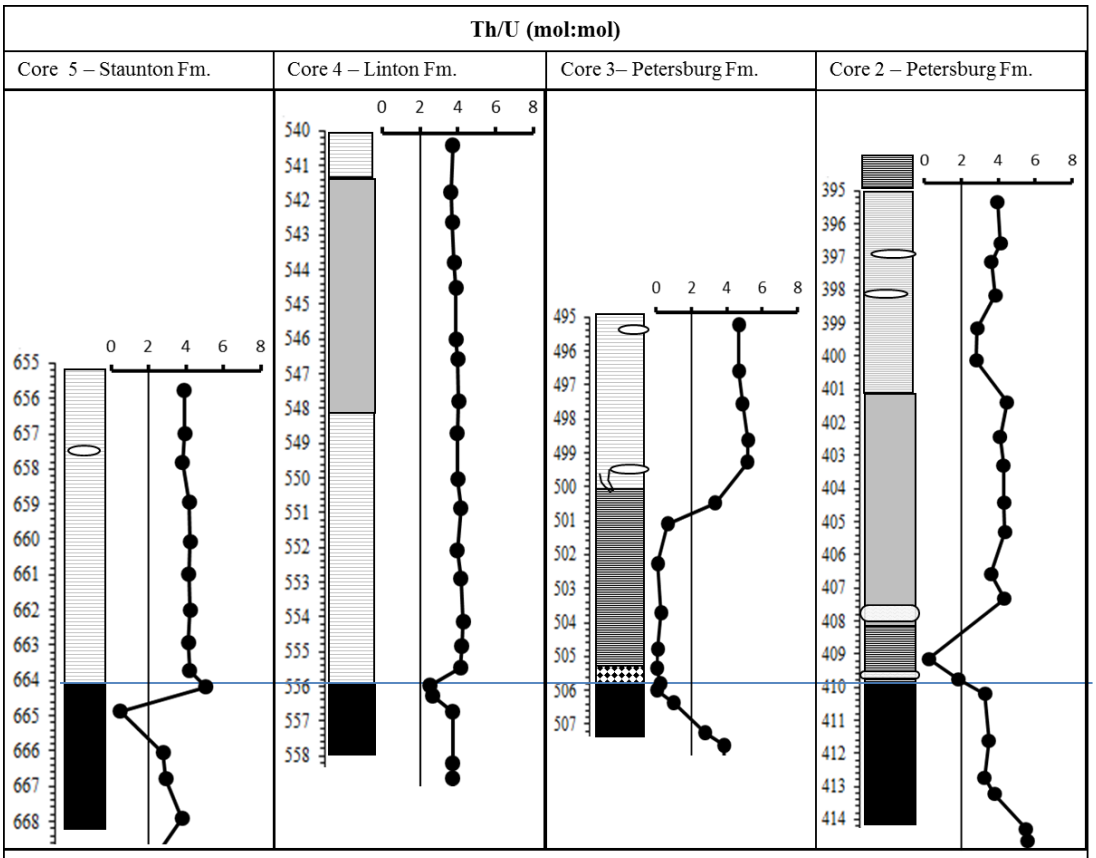

Figure 36: Th/U Comparison between Cores 2-5 – Coal→Mudrock Only

As observed in Figure 36, Th/U values exhibit two clear trends. Although the ratios were all below 7, both black shales of Cores 2 and 3 had values <2, indicating anoxia. The Th/U values are consistently <2 for the top portions of all coal seams, which

suggest that the redox boundary clearly infiltrated into the peat (now coal). All other values for Th/U show an intermediate stage (ranging 3-4) and possibly indicate a dysoxic to oxic system and nearshore interpretation. Such an interpretation would be consistent with previously discussed paleoredox proxies (C/S, Mo/Al, and V/Al). The Th/U ratios provide additional evidence for water column stratification during black shale deposition in Core 2 and Core 3 (Fig. 37). The ratios also indicate that Core 4 and 5 grey shale was deposited below a dysoxic to oxic water column. Arrows indicating nearshore and offshore deposition are based on these interpretations.

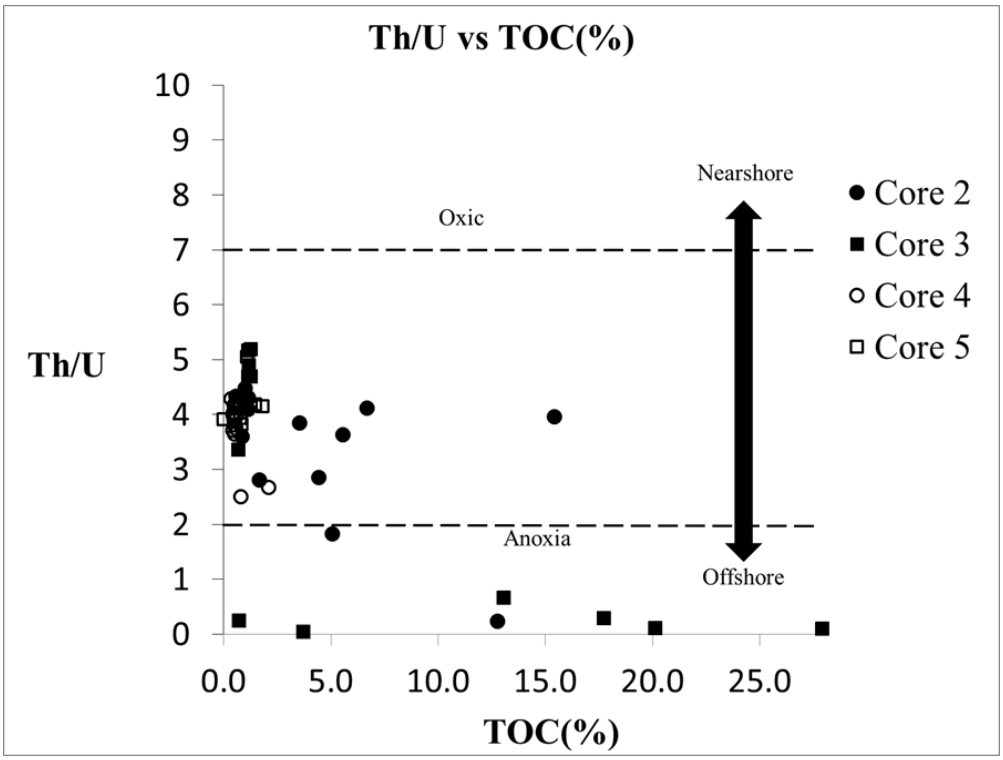

Figure 37: Cores 2-5 shales and mudstone Th/U (mol:mol) values plotted against TOC(%).

6.9 Paleoredox: Iron

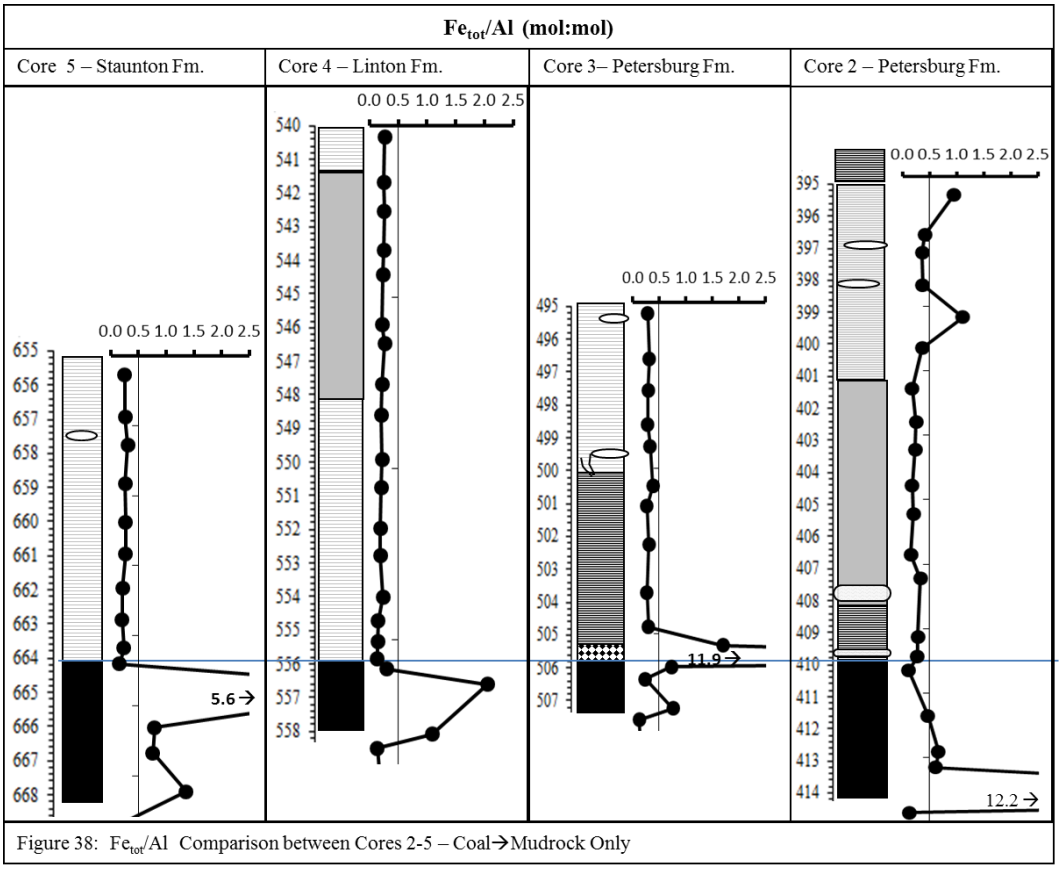

Figure 38: Fe$_{tot}$/Al Comparison between Cores 2-5 – Coal→Mudrock Only

Fe$_{tot}$/Al enrichments are observed in all cores but are associated with the coal/mudrock contacts (Fig. 38). Fe$_{tot}$/Al values are highest in Core 2 at the base of the Springfield coal and correspond to the abundance of szomolnokite detected in this section (Appendix A). Szomolnokite is a secondary mineral produced from the alteration (oxidation and hydration) of pyrite, and thus the two lines of evidence point to a large of amount of pyrite originally present at the base of Core 2. Interestingly however, Fe$_{tot}$/Al values in the black shale of Core 2 are low and do not indicate water column sulfide, whereas other redox proxies have indicated euxinic or at least *near*-euxinic conditions (C/S, Mo/Al, V/Al, Th/U). In addition, core expansion was noted at this interval, albeit much less than the expansion below the coal. Sampling resolution is likely the explanation for this as the expanded portion at the base of the black shale in Core 2 was

not captured as it was at the base of the coal in Core 2. Similar mineralogy and structure, i.e. the presence of a whitish-yellow mineral and expansion, was noted at both intervals (Appendix A). Also surprising was Core 2 *grey* shales crossing over the euxinic threshold (0.5) near the top of the core as the lithology transitioned to more fissile black shale. This does corroborate the interpretation of increasingly anoxic conditions upsection and a probable deepening of the water column near the top of Core 2.

Fe_{tot}/Al is also elevated in Core 3 at the base of the coal suggesting the formation of a sulfidic zone created from sulfate diffusion and reduction within the coal seam. Within the heavily pyritic zone at the base of the Excello shale, Fe_{tot}/Al values increase up to 12 and certainly indicate either a euxinic water column present or a record of pyrite formation within extremely organic-rich sediments. However, above this pyritic section and for the remainder of Excello (504.8-500.6'), Fe_{tot}/Al values are only slightly elevated (avg. 0.3) and do not provide evidence for euxinia as suggested by other proxies. Cores 4 and 5 show high Fe_{tot} values present at the boundary between the respective coal seams and the overlying grey shale but not throughout the rest of the mudrock. This is consistent with the model of sulfate diffusion and subsequent reduction from inundation of sulfate-rich marine waters that percolated through a porous peat-rich stratum. This euxinic state was certainly sub-surface while evidence of water column euxinia is only supported in Core 3.

Figure 39 plots all Fe_{tot} against Al and is adapted from Lyons and Severmann (2006). The dashed line indicates normal shale sedimentation influx. The high ratios in Core 2 and Core 3 values indicate euxinic to near-euxinic conditions suggesting that reactive iron was scavenged from a euxinic water column during syngenetic pyrite

formation. In contrast, all Core 4 and Core 5 values fall near or slightly below the normal shale line. The Fe_{tot}/Al ratios in Core 4 and 5 indicate that detrital influx is the predominant mode of iron delivery. Such values suggest a deltaic or riverine influx of sediment intermingling with marine waters. In addition, the same interpretation can be applied to the grey shales in Core 2 as they fall on or below the normal shale sedimentation rate line as well.

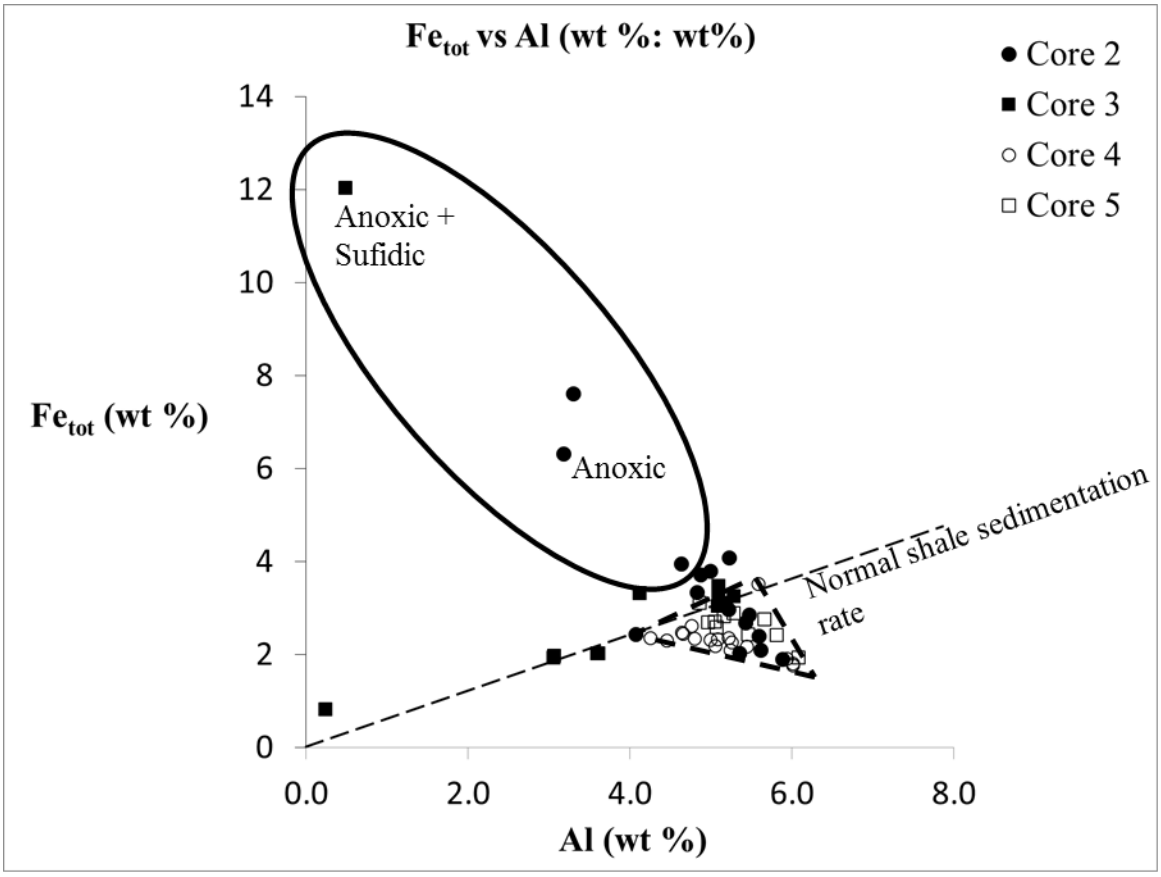

Figure 39: All core shale and mudstone Fe_{tot}/Al values plotted against Al (wt %) to illustrate reactive iron availability. Note the dashed line triangle enclosing all Core 4 and 5 grey shales and falling below normal shale sedimentation and not deposited in an anoxic water column (ellipse). Adapted from Lyons and Severmann, 2006.

6.10 $\delta^{13}C_{org}$

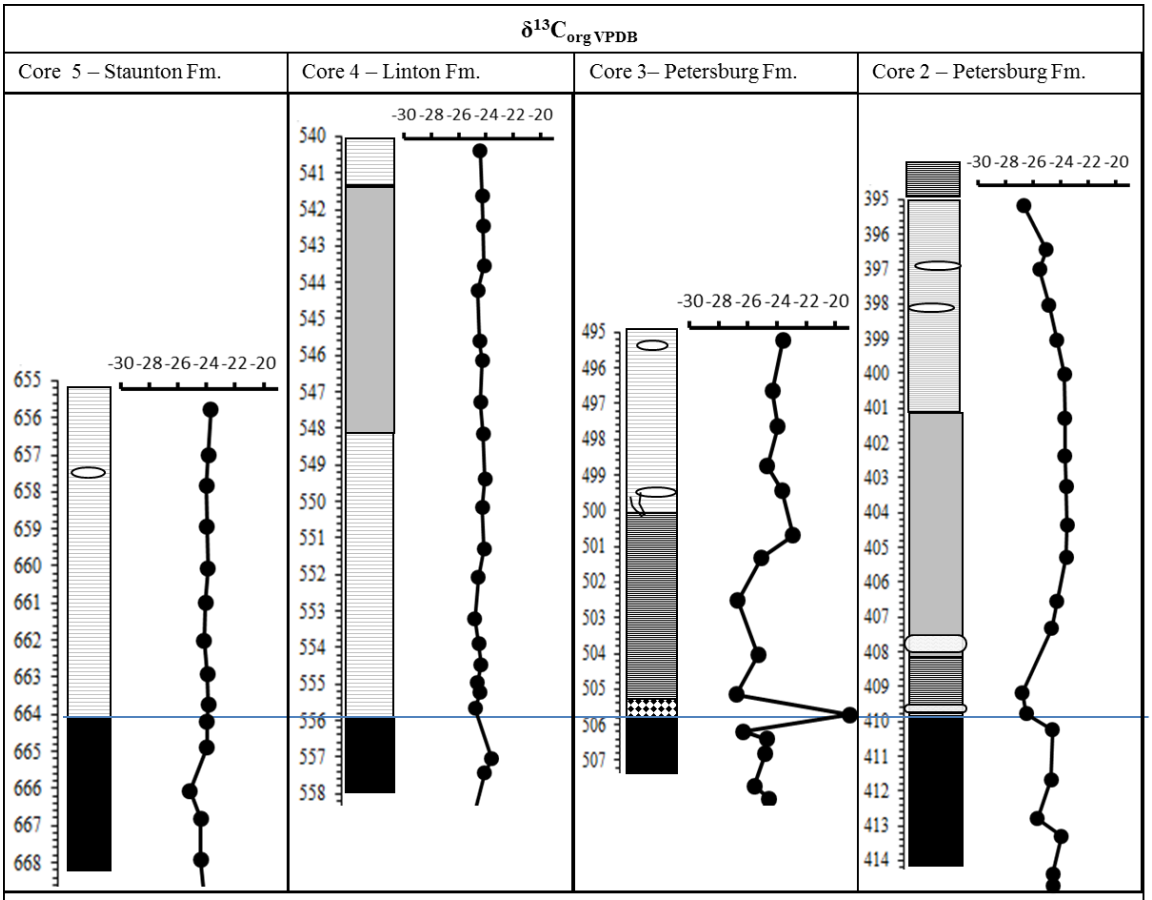

Figure 40: $\delta^{13}C_{org}$ Comparison between Cores 2-5 – Coal→Mudrock Only

Cores 4 and 5 of the Linton and Staunton formations show very little variation with in $\delta^{13}C_{org}$ values while both cores from the Petersburg formation show variations in $\delta^{13}C_{org}$ consistent with the mixing of two endmembers (terrestrial and marine). Above the coal in Core 2, there is a transition from marine-derived organic carbon in black shale ($\delta^{13}C_{org} \approx$ -26.7‰) to terrestrially-derived organic matter in grey shale ($\delta^{13}C_{org} \approx$ -23.6‰), and then to to marine organic matter values in the overlying shales and muds ($\delta^{13}C_{org} \approx$ -26.7‰; Fig. 40, 41). This 'cycle' of marine-terrestrial-marine organic input when compared to trace metal and other geochemical proxies can serve as a 'control' or type section with which to compare other depositional facies and interpretations. It is

important to note that the lowest marine values ($\delta^{13}C_{org}$ -26.8‰) were observed in what are interpreted as the deepest lithofacies present *but* did not match the deepwater marine $\delta^{13}C_{org}$ value of -28‰ as identified in literature (Arthur, et al., 1985; Peters-Kotting, 2006). This corroborates a shallow eastern LPMS that even in the highest magnitude transgressive sequences was still influenced by a significant input of terrestrial organic matter flushed into the basin by surrounding peatlands and river systems. Similar trends in Core 3 show a marine signature in the black shales (average $\delta^{13}C_{org} \approx$ -26‰) followed by an increase in $\delta^{13}C_{org}$ as lithology transitions to grey shale (Fig. 41). This trend is interpreted as indicative of a gradually shallowing water column with more detrital input delivering terrestrial vegetation from deltaic or riverine discharge (Fig. 41).

Linton and Staunton Formation mudstones $\delta^{13}C_{org}$ values do not suggest a marine influence, and remain terrestrially dominated throughout the grey shale and mudstone (Core 4 avg. -24.8‰; Core 5 avg. -24.0‰). The terrestrial input may explain the lack of black shale and marine fauna in these cores. If detrital influx is high in these sections and bringing in terrestrial organic carbon, and the water column even somewhat oxygenated, conditions would not have been conducive for the sequestration of large amounts of organic matter. This is supported by near zero values for TOC in both Core 4 and 5 shales, a strong indication that Linton and Staunton Formation muds were deposited in nearshore environment with marine waters mixed with high detrital and terrestrial influx from deltaic/riverine and organic matter is lost to oxidation and degradation. This interpretation would also explain the small 'nearshore' section of Core 2 and near the top of Core 3 (Fig. 29).

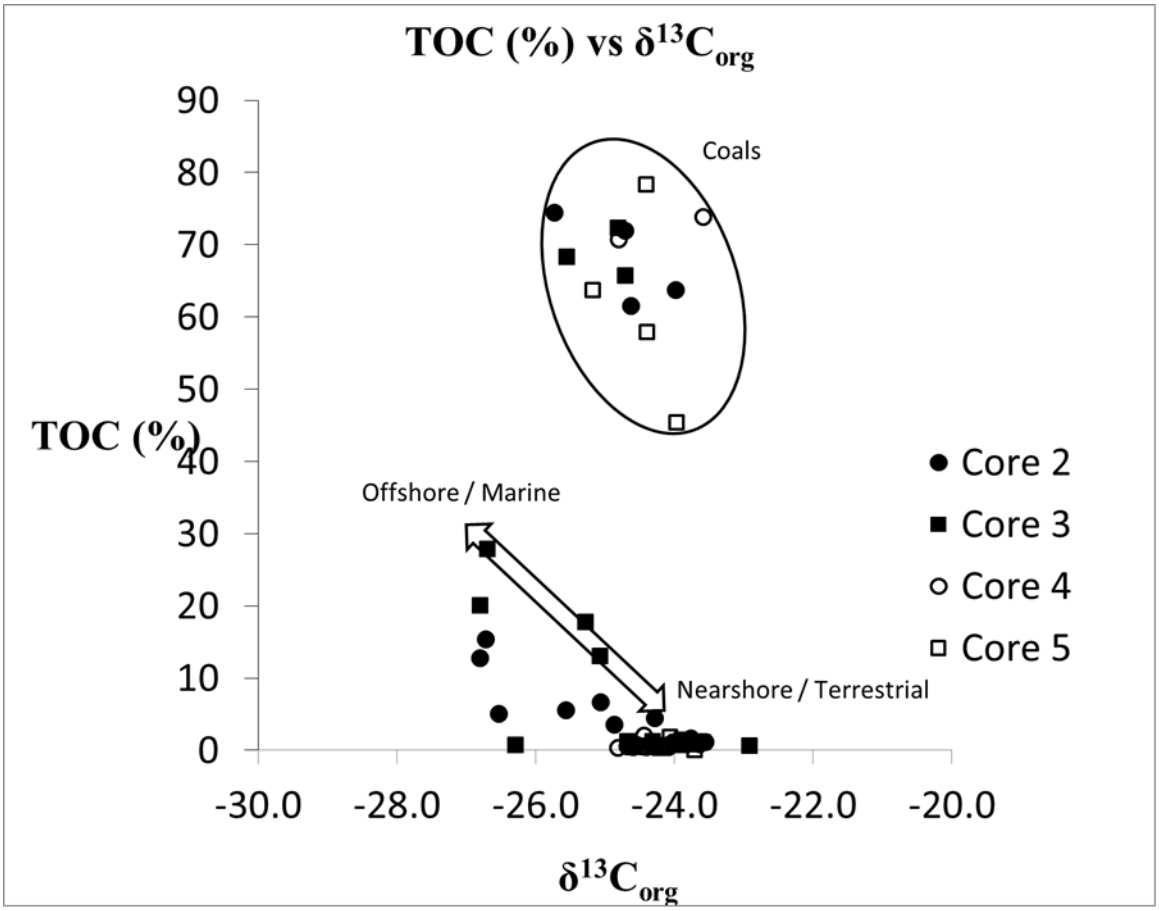

Figure 41: All core TOC(%) values plotted against $\delta^{13}C_{org}$. Note the distinct coal grouping (ellipse) versus the grey and black shales. The arrow represents observed offshore (highstand) and nearshore (lowstand) lithofacies with observed marine and terrestrial organic matter contributions.

Meyers (1994) demonstrated that C/N ratios plotted against $\delta^{13}C_{org}$ delineate four distinctive data fields that represent different types of plant tissue (See Fig. 29). However, these modern values do not take into account two crucial characteristics of ancient (pre-Cretaceous) sediments: (1) the inverse trend in marine and terrestrial $\delta^{13}C_{org}$ and (2) that C4 plants [those plants that utilize the C_4 pathway that fixes CO_2 via the pyruvate (PEP) enzyme producing high $\delta^{13}C$ values (-12‰)] did not exist at this time. Therefore, I propose the following model regarding Pennsylvanian $\delta^{13}C_{org}$ and C/N values (Fig. 42). This model shows three distinct data clusters that are distributed according to facies (coal, black shale, and grey shale) as well as an isotopic 'loop' that

tracks the cyclicity of both a large-scale marine transgressive sequence of the LPMS (outer arrows) and a small-scale marine transgressive sequence (inner arrows).

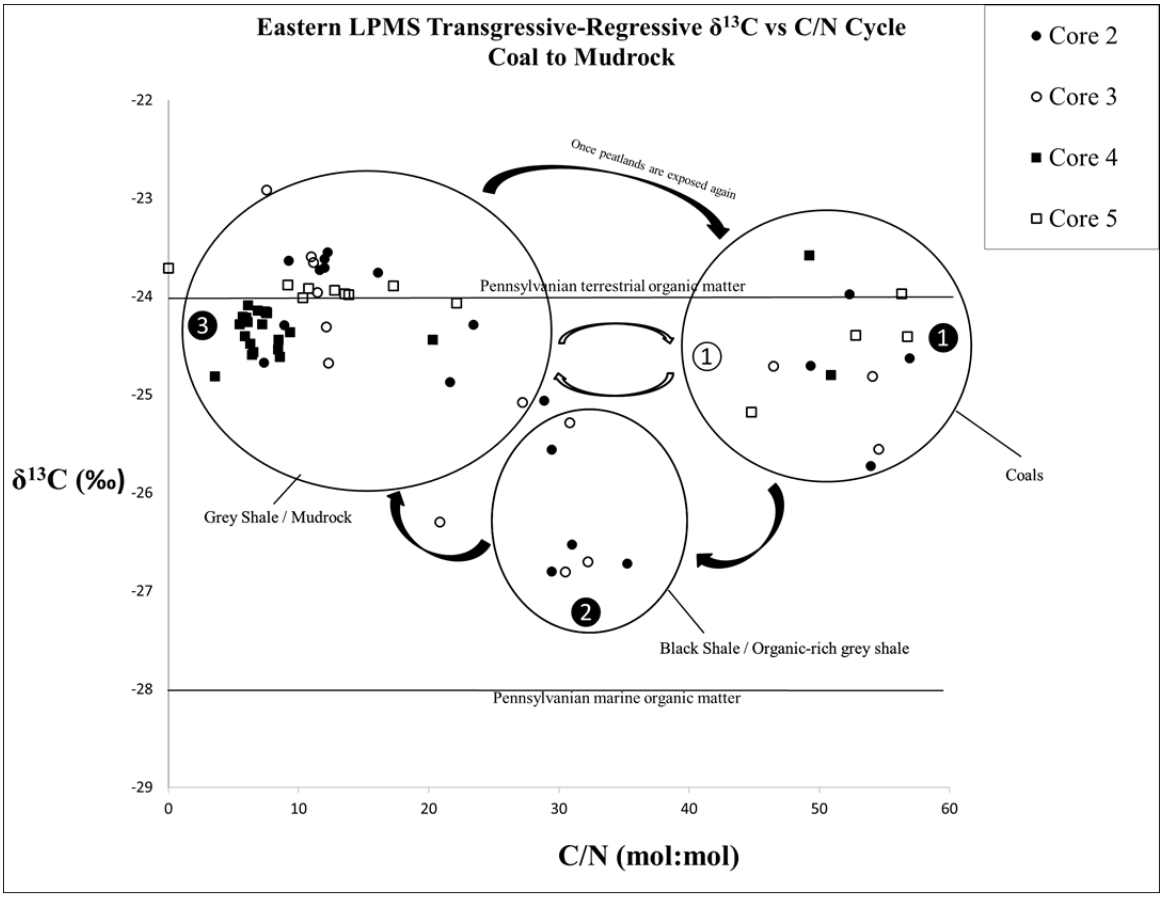

Figure 42: Plot showing a hypothesized model for Eastern LPMS transgressive-regressive organic matter cyclicity. Horizontal lines are marine and terrestrial $\delta^{13}C_{org}$ endmember values. Groupings (ellipses) are core lithofacies. Outer black arrow and black numbers (e.g. ❶) model a large-scale transgressive event with water depths conducive for black shale formation under anoxic/euxinic conditions. Inner arrows and white numerals (e.g. ①) model a lower magnitude transgression and water depths not exceeding critical depths for black shale formation.

Interpretation of the above model is that of two different types of transgressive-regressive sequences. When transgressive events were of sufficient magnitude with marine seawater influx sufficient to raise overall base level of LPMS deltaic/riverine systems and cover the prevalent swamps and peat mires, benthic anoxia developed and conditions were suitable for efficient organic carbon sequestration. This marine flooding event imparted marine C/N and $\delta^{13}C_{org}$ signatures to organic matter preserved in the black shale. As waters regressed and coastlines shifted westward, the bottom waters became

oxygenated, organic matter sequestration lessened, and the organics contained a greater contribution from terrestrial sources. As seawater completely regressed and the environment became once more subaerial, peat aggradation resulted in true terrestrial endmember C/N and $\delta^{13}C_{org}$ values. It is important to note that this model reflects only the coal to mudrock transition in the cores studied, which represent only a portion of a full cyclothemic sequence (Heckel, 1998). While its applicability to a full Pennsylvanian cyclothemic sequence of strata is yet to be determined there is no indication that the core concepts and results modelled would be drastically different.

6.11 Zr (Detrital Influx)

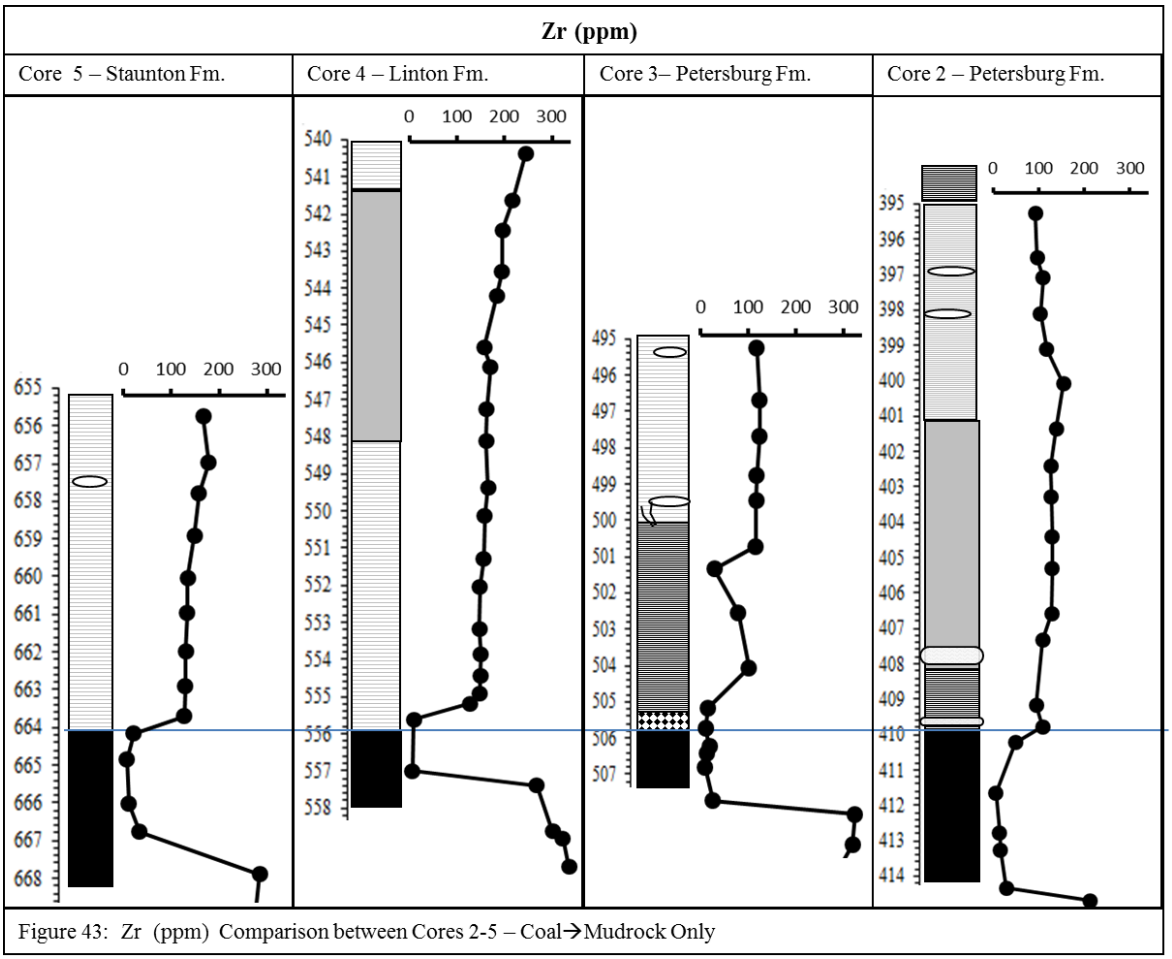

Figure 43: Zr (ppm) Comparison between Cores 2-5 – Coal→Mudrock Only

Figure 43 shows Zr (ppm) concentrations for all four cores for comparison purposes. As a proxy for coarse-grained sediment (silt and sand sized grains), Zr concentrations reveal a higher silt and sand fraction for the grey shales in all four cores, particularly Cores 4 and 5. Baseline Zr concentrations for the black shale in Cores 2 and 3 (generally fissile and very finely grained) averaged 64 ppm. Grey shales had higher Zr concentrations (average 141 ppm). The greater Zr concentration in grey shale is consistent with initial core lithofacies descriptions for the grey shales having a larger percentage of coarser-grains (sand and silt). The trend of Zr concentrations overlying the Springfield coal mirrors the trend in $\delta^{13}C_{org}$ values, already shown to illustrate a type example of offshore-nearshore-offshore organic matter sources (Fig. 40, 43). This increase of ~50 ppm (relative to Core 2 black shale values ~100 ppm) in the section interpreted as the lowstand (deposition nearshore) in the middle of the grey shale section (at ~400.0') and a gradual increase back to a black shale value of around 100 ppm is consistent with the prior highstand-lowstand-highstand interpretation. Core 3 shows the beginning of the same pattern but on a larger scale with much lower values in its marine facies (<25 ppm) but a clear increase in Zr as depth shallows upsection. Core 4 has the highest values and also shows a gradual increase in Zr concentration from the base of the mud to the top of the core, indicating a growing siliciclastic input and large detrital influx consistent with a large deltaic or fluvial input upsection. The grey shale in Core 5 (overlying the Seelyville coal) has Zr concentrations that are consistent with other grey shale concentrations (average 132 ppm versus 141 ppm) for the other cores but still much higher than black shale averages. In all cases grey shale values on average exceed black

shale values and are interpreted to represent a more nearshore coarse-grained influx for this facies coming from LPMS deltas and riverine sediments.

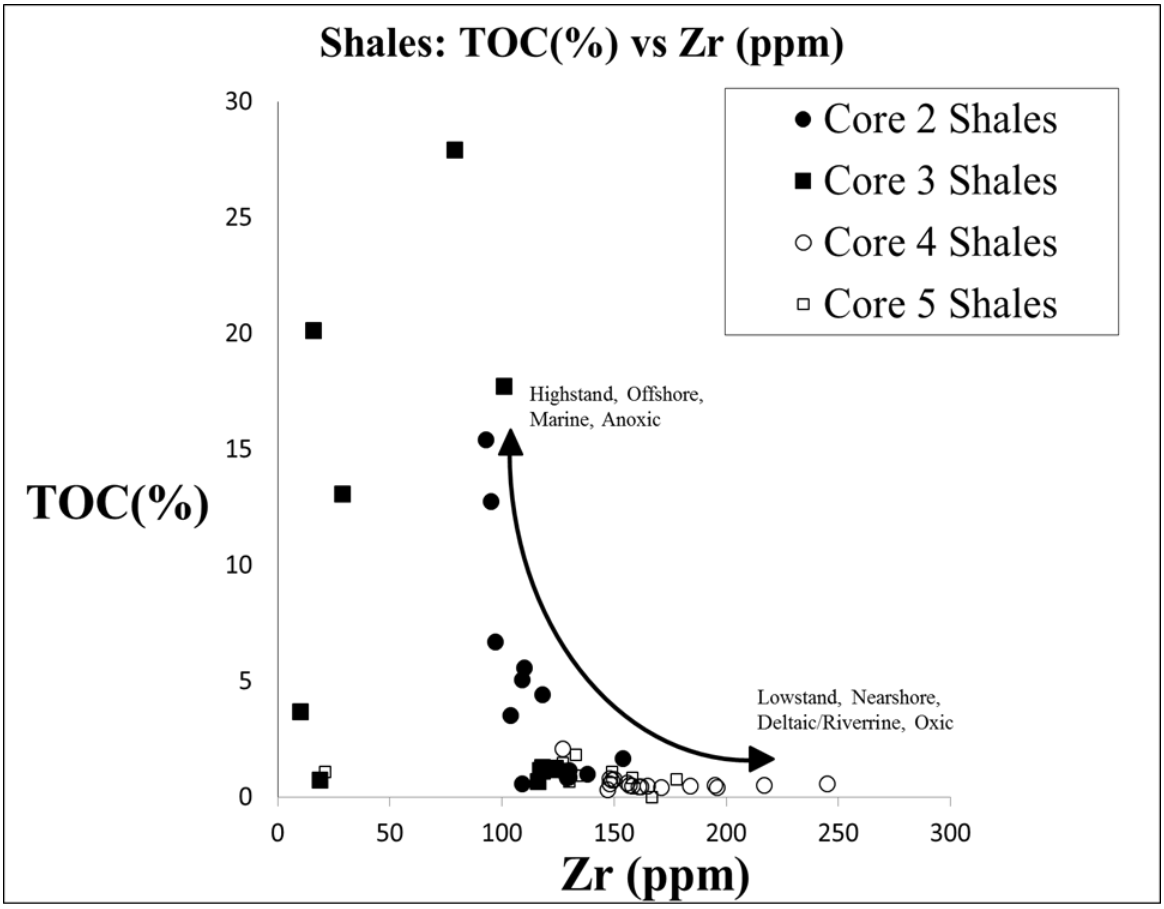

Figure 44: Cross-plot of all shale TOC(%) and Zr (ppm) showing relationship between low and high detrital input on TOC(%) deposition. Arrow indicates oscillation between highstand and lowstand facies.

Figure 44 compares Zr to TOC for all mudrock overlying the coal seams of the four cores. There is a negative correlation between Zr and TOC. This relationship is in agreement with the observe Fe_{tot}/Al:TOC relationship as well; both suggesting that detrital influx can impede both the sequestration of TOC and reduce trace metal concentrations in sediment. The sliding arrow in Figure 44 is an interpretation of the negative correlation based on this and on all previously discussed proxies and interpretations. As Zr (ppm) increases, sedimentation becomes more nearshore, deltaic/riverine influenced and more oxic while sedimentation is more marine and anoxic

as Zr concentrations decrease. This relationship supports the lateral movement of the shoreline and estuarial relationship of LPMS waters over southern Indiana.

6.12 Paleoenvironmental Interpretations

For purposes of illustrating only the effects of the flooding event described heretofore in all four cores (from a subaerial to a subaqueous depositional environment), only the coals and the strata overlying each respective coal seam, those representative of a flooding event, are discussed. All cores are discussed in depositional order beginning with the deepest core (Core 5) and ending with the shallowest core (Core 2), in order to perhaps reveal a changing environment over time for one distinct location (USI Well 1-32).

6.12.1 Paleoenvironmental Interpretation: Cores 5 and 4

Seelyville and Survant Coals (Staunton and Linton Fms.)

Cores 4 and 5 are discussed together and illustrated as similar depositional environments because both show very similar patterns of geochemical, lithological, and paleofaunal evidence which are interpreted to represent similar flooding events, water chemistry, and depositional controls (Fig. 45).

During the Desmoinesian (Staunton Formation and Linton Formation) a relatively small-scale marine flooding event caused by a Gondwanan interglacial period increased LPMS sea level and inundated the low-lying Pennsylvanian peat mires over southern Indiana (Heckel, 1986,1998). Geochemical evidence suggests that seawater sulfate diffused into the peat bogs and sulfide was produced during sulfate reduction and recorded in the TS concentrations and the C/S ratios. These diffusion gradients are

preserved in the geochemical record as massive pyritization bands visible in both the Survant and Seelyville coal seams. The magnitude of this event was not substantial enough to overprint a large influx of clastic sediment and detrital influx as indicated by the Zr, Fe_{tot}/Al records. The sediments deposited after the Seelyville Coal seam, were deposited in fluvial/riverine or deltaic freshwater mixed with marine waters that were dysoxic to oxic as indicated by the C/S ratio, high Mo/Al, low V/Al, Th/U ratios >2, and Fe_{tot}/Al. These waters brought in terrestrial organic matter to the basin, which was then oxidized by aerobic organisms and thus was not sequestered in benthic sediments. This is evidenced by near zero TOC and TIC concentrations, terrestrial $\delta^{13}C_{org}$ signatures, Fe_{tot}/Al ratios and high Zr concentrations (100-300ppm). The lack of black shale deposition is due mainly to relatively shallow water depth (Heckel, 1998) and coastal detrital influx that effectively diluted both metal and TOC concentrations during sedimentation. This higher sedimentation is evidenced by relatively high Zr concentrations, the lack of TOC throughout grey shale deposition, and the near normal shale sedimentation rate for Fe_{tot}/Al. The lack of marine fauna present in the overlying mud is also a result of these same strong fluvial/riverine conditions (Zr, Fe_{tot}/Al). What little organic carbon survived oxidation by organisms and diagenetic degradation was of terrestrial origin based on $\delta^{13}C_{org}$ values of -24‰. Figure 34 shows a proposed depositional model at highstand for both Cores 4 and 5 based on previously discussed geochemical proxies, lithofacies changes and paleofaunal evidence.

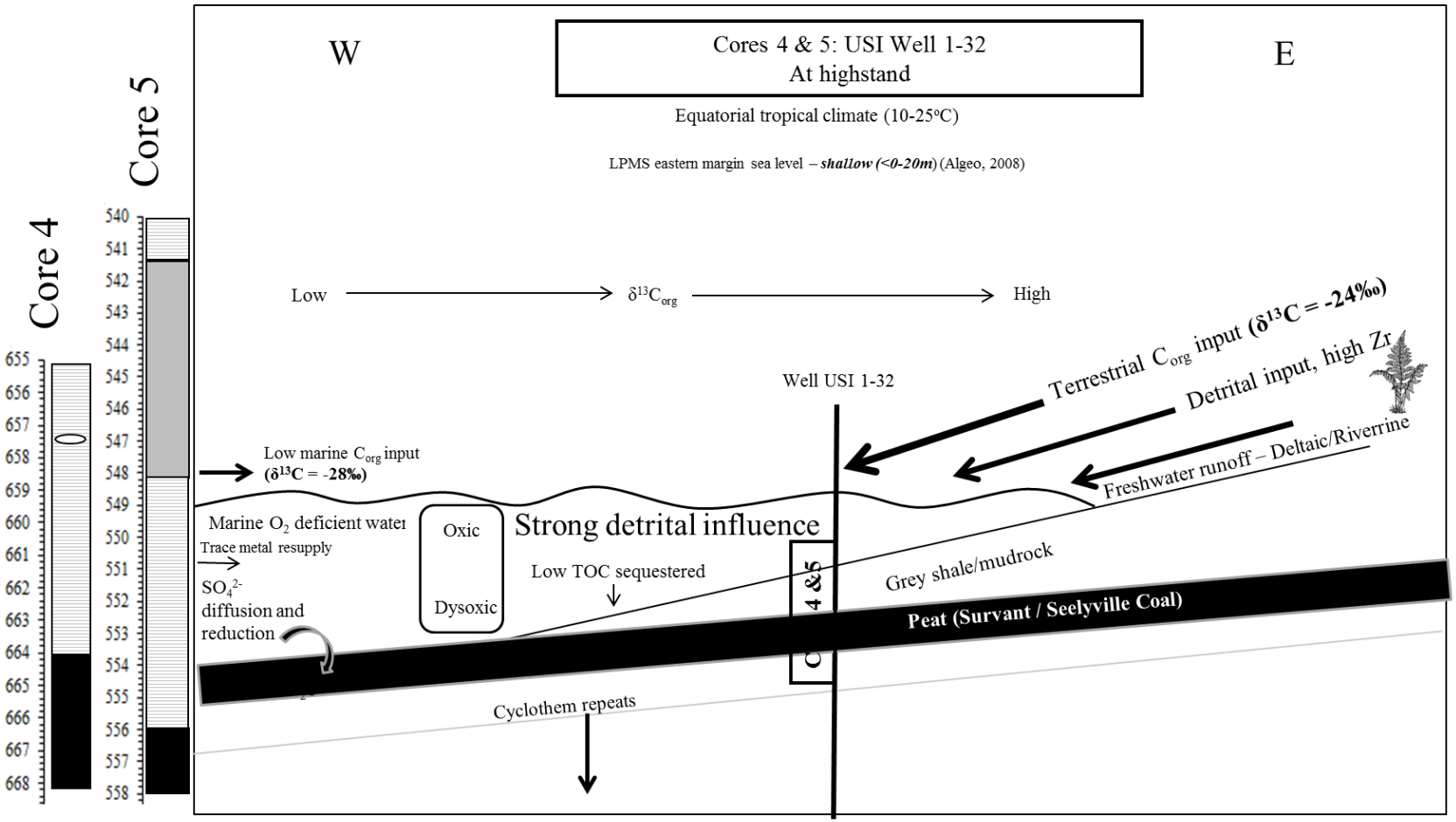

Figure 45: Paleoenvironmental interpretation and depositional model for both Core 4 and 5 coals (Survant and Seelyville) and superjacent grey shale and mudstone.

6.12.2 Paleoenvironmental Interpretation: Core 3

Houchin Creek Coal (Petersburg Fm.)

Deposition above the Houchin Creek coal (Desmoinesian Series, Carbondale Group, Petersburg Formation) was a result of a higher magnitude transgressive marine event (Heckel, 1986, 1998; Fig. 46). These deeper waters, already oxygen deficient due to a distal marine corridor to the Panthalassic Sea, were rich in trace metals (Mo, V, Fe, Th and U), sulfate, marine organic matter and other nutrients. At highstand over southern Indiana and when water depth were sufficient, water column stratification developed. While surface waters remained oxic to dysoxic, benthic waters were anoxic. This water column redox structure is suggested by high TOC%, marine $\delta^{13}C_{org}$ signatures, C/S ratios, trace metal enrichments, and marine fossils. Benthic anoxia then resulted in high organic matter and trace metal sequestration and black shale (Excello) deposition. Benthic euxinia was at least intermittently present and perhaps sustained during black shale deposition as evidenced by all paleoredox proxies including C/S ratios, Mo/Al, V/Al, Th/U, and Fe_{tot}/Al. This interpretation for an at-least intermittent euxinic Excello Shale is consistent with a previous interpretation of the Excello by Ece (1987) and Schultz (2004). Marine sulfate diffusion into the porous peat (later lithified into Houchin Creek coal) is observed and a subsequent reduction to sulfide occurred down through the coal.

As water depths regressed and became shallower, benthic conditions transitioned from euxinic to anoxic and then to dysoxic to near oxic, and the lithology transitioned

from black shale to grey shale upsection. Organic matter transitioned from predominantly marine to terrestrial upsection as the coastline advanced or prograded to the west and Core 3 grey shales were deposited in a nearshore environment. Coarse-grained detrital components (sand and silt) begin to dilute the marine organic matter and TOC concentrations decreased as organic matter was oxidized and consumed.

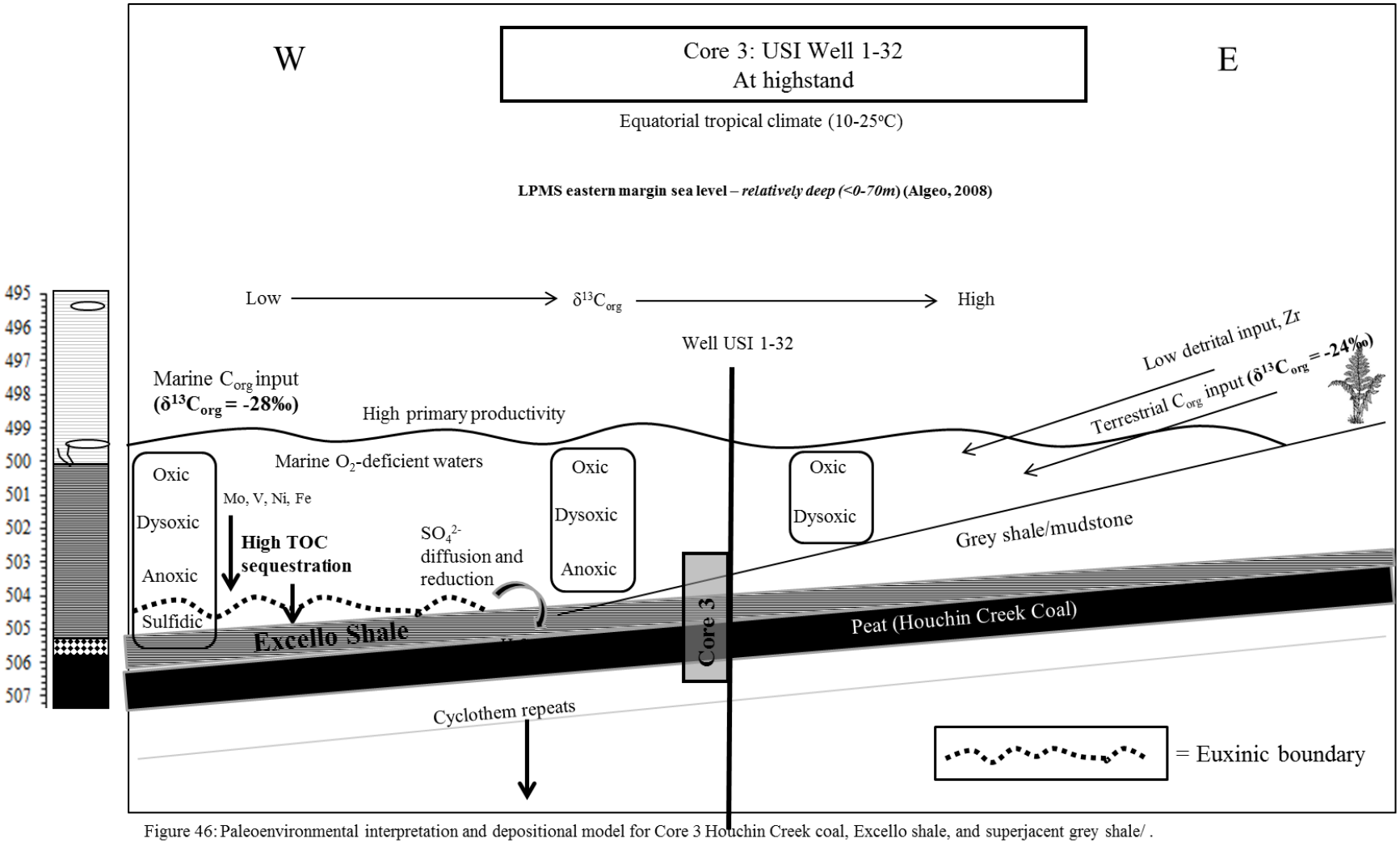

Figure 46: Paleoenvironmental interpretation and depositional model for Core 3 Houchin Creek coal, Excello shale, and superjacent grey shale/ .

6.12.3 Paleoenvironmental Interpretation: Core 2

Springfield Coal (Petersburg Fm.)

Core 2 displays a highstand-lowstand-near highstand sequence of events superjacent to the Springfield coal seam (Fig. 47). An interglacial Gondwanan event increased eustatic sea levels in the LPMS and oxygen-depleted seawater flooded the peat mires in the subtropical environment of Desmoinesian southern Indiana. This is evidenced by the TS inventories at the top of the Springfield coal, the marine isotope signature of the organic carbon (-27‰), and marine fossils. At highstand, water depths brought metal and nutrient-rich seawater over these peatlands. The development of benthic anoxia in turn sequestered of these metals and high amounts of organic carbon in these marine sediments. This is confirmed by the paleoredox proxies C/S, Mo/Al, V/Al, Th/U, and Fe_{tot}/Al. These factors led to the deposition of the black shale overlying the Springfield coal seam. Bottom water redox conditions were also likely near-euxinic to euxinic during times of highstand as evidenced by the same paleoredox proxies and C/S ratios. Organic matter that escaped surface oxidation and degradation was sequestered in benthic sediments as indicated by high TOC values. This transgressive event was of shorter duration than that of Core 3 due to presence of coarse-grained nearshore grey shale deposition overlying the ~12" of black shale deposition. As waters began to recede from the low-lying eastern LPMS shores, sedimentation became more nearshore and oxic, allowing for marine/brackish fauna to flourish as evidenced by a terrestrial $\delta^{13}C_{org}$ signature (-24‰), lower TOC%, and marine fossils. Lowstand for this sequence occurred around the 404.5' well depth, with deposition dominated by freshwater inputs. Possibly another interglacial episode or a decrease in fluvial sedimentation then caused

water depths to increase again and a deepening of the system occurred, repeating the cycle with conditions returning to a more anoxic offshore deeper-water system, with oxygen-depleted waters and benthic anoxia resulting in gradually more fissile grey shale upsection and eventual black shale deposition above Core 2. This is evidenced by the lithology and texture of grey shale (finer) and geochemically by the return to black shale (offshore) values for $\delta^{13}C_{org}$ (near -27‰), gradually increasing TOC% and TIC%, and Zr concentrations (Fig. 47). Figure 47 shows this highstand-lowstand-near highstand sequence as two water levels on the same shoreline. Highstand and near-highstand conditions are represented by the ❶ while lowstand is indicated by the ❷ (Fig. 47).

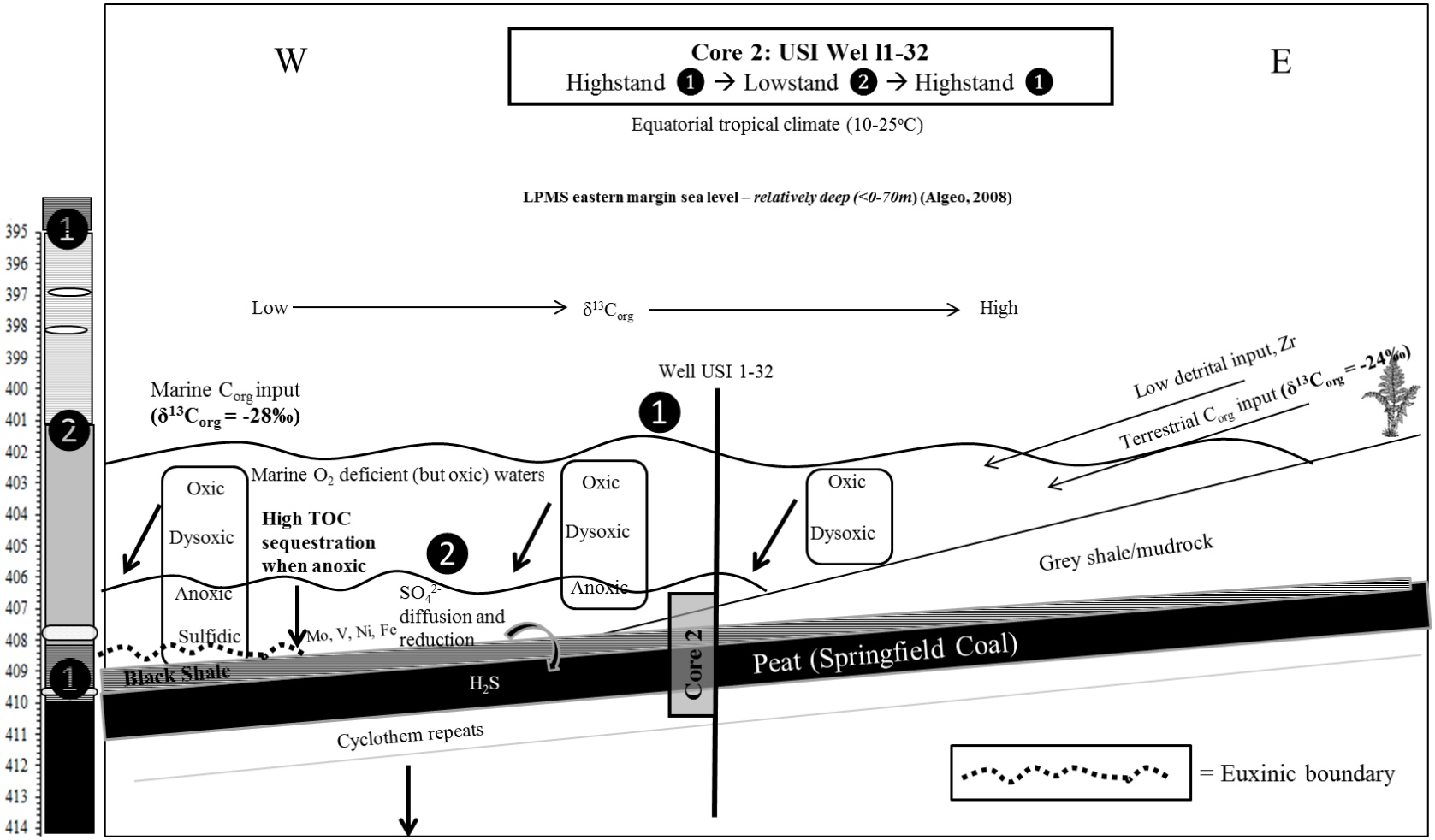

Figure 47: Paleoenvironmental interpretation and depositional model for Core 2 Springfield coal and superjacent black shale and grey mudrock.

7. SUMMARY AND CONCLUSIONS

Core-bearing cores from the Petersburg, Linton, and Staunton Formations all retain a record of marine flooding events. These LPMS transgressions are best recognized in the geochemical signatures of the mudrocks overlying the coal seams and in the sulfur-rich and pyritized bands of the coal itself. The chemostratigraphic changes suggest that the sea-level fluctuations in the older Staunton and Linton Formations (Cores 4 and 5) were smaller in magnitude than those that occurred during the deposition of the Petersburg Formation (Cores 2 and 3). Black shales in the Petersburg Formation were deposited in larger-scale transgressive events that delivered metal and nutrient- rich waters to the eastern shores of the LPMS and Illinois basin. Sufficient water depth at highstand allowed for the development of anoxic and often euxinic bottom waters which allowed for the sequestration of large amounts of organic carbon and trace metals. In smaller-scale transgressive events seen in the muds overlying the coal seams of the Linton and Staunton Formations, water depths were shallower and sedimentation over USI 1-32 was too oxygenated and deltaic/estuarine for water stratification to occur. Combined with nearshore detrital influx from surrounding lowland deltas and rivers, waters were dominated by terrestrial organic carbon signatures and more coarse-grained sedimentation. A fully oxygenated nearshore water column allowed for very little organic carbon sequestration in grey benthic sediments, caused chiefly by the degradation by aerobic organisms.

This study shows the utility of using a combined approach of sedimentology, paleontology, and geochemistry to accurately characterize often-enigmatic facies such as shale and muds in ancient environments, especially those deposited in such a unique

system like the Late Pennsylvanian Midcontinent Sea overlying southern Indiana 300 Ma.

APPENDICES

A. Expanded Core Investigation

A.1 Expanded Section Methods

An X-Ray diffractometer (XRD) was used to determine the mineralogy of three specific portions of Core 2 that had exhibited a 15%-100% volumetric increase upon drying in storage following borehole extraction. Eight samples, from both portions of expanded Core 2 sections and non-expanded Core 2 sections were smeared onto glass slides and run in a Siemens D5000 XRD with a Cu x-ray tube. The range of 2-theta angles scanned was 20-80 degrees and samples were not glycolated. The section with largest observed expansion and visible mineralogical differences (C2-19) was also examined on a JEOL 6060 Field Emission Scanning Electron Microscope (FE-SEM). Portions of the sample were analyzed on an energy dispersive x-ray (Edax) spectrometer to further confirm mineral composition.

A simple dissolution test was conducted on sample C2-19 to determine salt content. Approximately 1.5 g of C2-19 was measured into a vial, which was weighed and then drowned in 18 MΩ water, agitated, and then centrifuged. The supernatant was then pipetted off and the procedure repeated 2 more times. The total time allowed for salt dissolution was <10 minutes. After drying in an oven for 24 hours the sample was reweighed to determine weight loss from dissolution.

A.2 Expanded Section Results

XRD and FE-SEM data for C2-19 revealed the presence of an iron sulfate salt mineral, szomolnokite ($FeSO_4$-H_2O; whitish-yellow mineral) below the coal (Fig. 48).

Szomolnokite is a secondary mineral that only forms from the alteration of sulfide minerals particularly pyrite under highly acidic and arid conditions (Pistorius, 1960; Fig. 48). Quartz was also identified in all samples. A small amount of core expansion was also observed in C2-13, a sample of grey shale section directly superjacent to the black shale in Core 2. XRD analysis did not show the presence of szomolnokite but there was a match to trace amounts of unaltered pyrite.

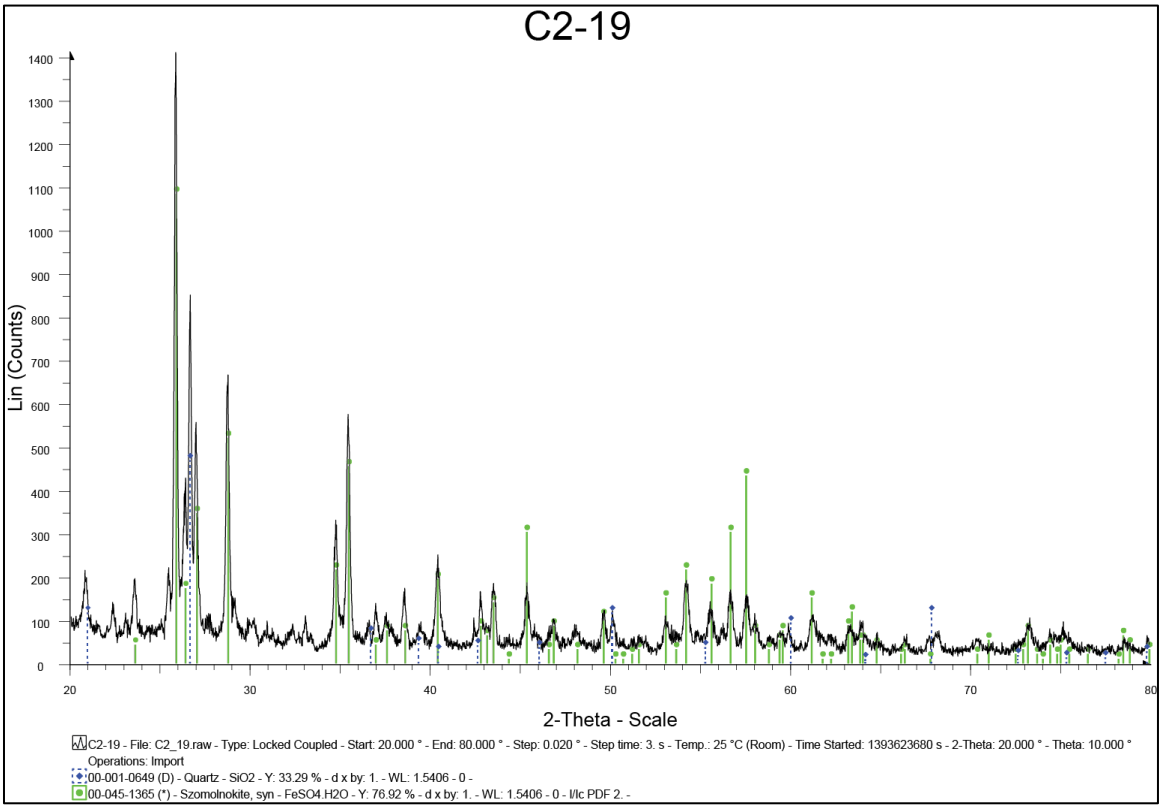

Figure 48: X-ray diffraction patterns for C2-19 with grey solid line match (szomolnokite) and dashed line match (quartz).

A.3 Expanded Section FE-SEM

Several SEM images were taken of portions of C2-19. The images show a powdery mineral (szomolnokite) clustered around shale particles (Fig. 49A). At a much higher magnification, Fig. 49B shows the same light-colored mineral (szomolnokite)

aggregating around an unidentified bladed mineral.

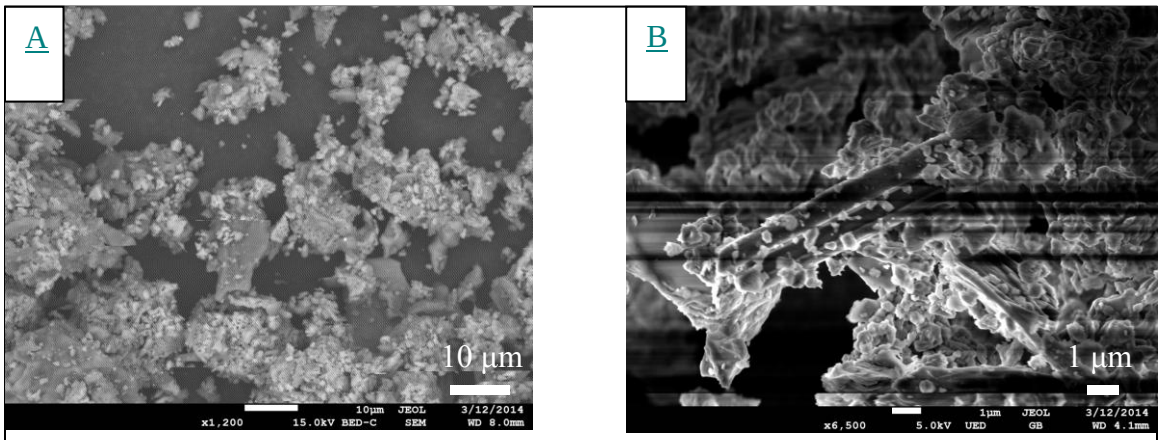

Figure 49: C2-19 EDS Image A) Darker grey and larger pieces of shale underclay covered with lighter colored speckled szomolnokite B) Enhanced SEM image of particles of szomolnokite aggregating around an as yet unknown bladed mineral.

A.4 Electron Dispersive Spectroscopy

A powdered split of C2-19 was analyzed by EDS to determine the elemental composition of targeted minerals. EDS results indicate the light-colored mineral that aggregates around the shale particles (darker platy fragments in Fig. 49A, Fig. 50A) is composed predominantly of Fe, S, and O, with these three elements making up almost 79% of the mass within the targeted area (Table 2). A large proportion of C was also detected (17%) although this is most likely the product of the carbon coating on the sample necessary for sample SEM and EDS preparation (Table 2).

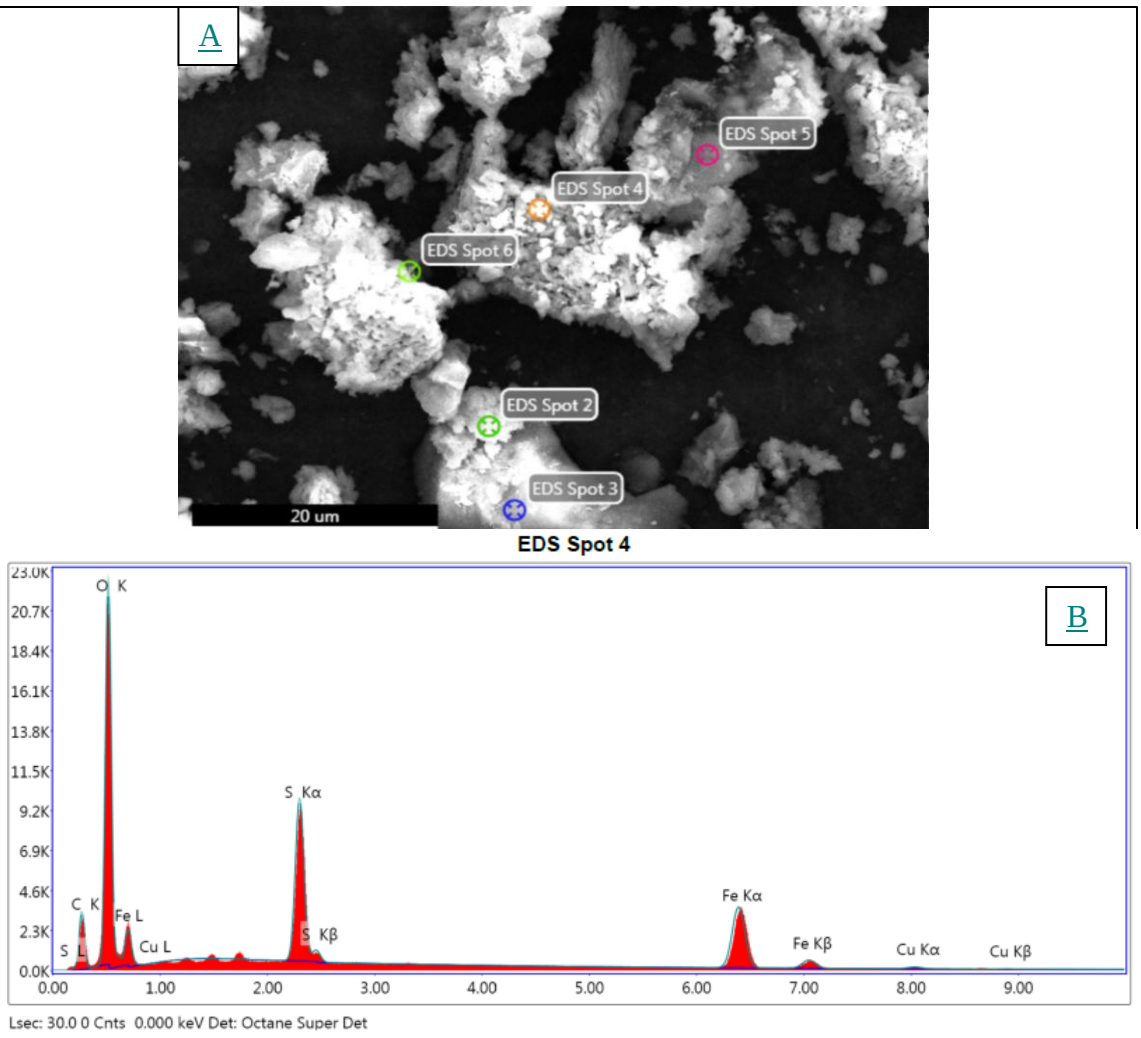

Figure 50: A) C2-19 EDS Image showing Spots 2-6 that were targeted for EDS composition B) EDS spectrum for Spot 4

Table 2: EDS Results for Spot 4 of C2-19

Element	Weight %	Atomic %	Net. Int.	Error %
C	17.31	30.13	1298.91	9.52
O	38.44	50.23	9439.56	7.47
S	11.42	7.45	6018.64	2.73
Fe	30.68	11.49	3407.36	2.74
Cu	2.14	0.7	110.97	16.03

The SEM and EDS results are consistent with the XRD spectrum and point to the presence of a large amount of szomolnokite ($FeSO_4$-H_2O) below the coal. Based on XRD data, the two slightly expanded sections above the coal did not contain szomolnokite, but carried much more of a pyrite signature. These sections were not analyzed by FE-SEM EDS.

A.5 Dissolution Test for C2-19

Table 3: Dissolution Test and Volumetric Calculations for szolmolnokite

	Vial 1	**Vial 2**
Sample + Vial (Before)	1.7234 g	1.429 g
Sample + Vial (After dissolution test)	1.5744 g	1.351 g
% Mass Lost to Dissolution	0.149	0.078
% Mass Lost to Dissolution	**8.6457**	**5.458362**
% Average Mass Lost to Dissolution	**~7 %**	
Volumetric Calculations		
Molar mass of pyrite	119.98 g/mol	
Molar density of pyrite	5.01 g/cm^3	
Molar volume of pyrite	23.9481 cm^3/mol	
Molar mass of szomolnokite	169.93g/mol	
Molar density of szomolnokite	3.1 g/cm^3	
Molar volume of szomolnokite	54.8161 cm3/mol	
Volumetric Increase from pyrite alteration to szomolnokite if 100 % alteration achieved:	**228.9 %**	

Dissolution tests (Table 4) results show an average dissolution of around 7% mass lost from a simple 18 MΩ water rinse, indicating the presence of a soluble mineral. Time

of dissolution was approximately 7 minutes. This solubility test represents a minimum estimate of salt dissolution. It is interesting to note however that szomolnokite only dissolves in water *very slowly* (Pistorius, 1960) but exact dissolution rate information is not known. Whether adequate time was given for full dissolution of the salt during this test is uncertain. Volumetric calculations based on the molar mass of pyrite and molar mass of szomolnokite indicate that if 100% of all pyrite was altered to szomolnokite the resulting volumetric increase would be over 228% (Table 4).

Appendix B: Vanadium and Nickel Paleoredox Proxy

B.1 Paleoredox: Vanadium and Nickel

V and Ni, both redox sensitive trace metals are both preserved preferentially under anoxic conditions, and can serve as proxies for marine anoxia. The metals differ in their uptake into organics and detrital minerals causing a shift in concentrations when high organics and low detrital influences are present. Vanadium normalized to Al was plotted vs. depth to identify periods of anoxic conditions and a combined proxy of V/(V+Ni) was plotted vs. depth to shed light on whether waters were both anoxic and sulfidic (euxinic) according to published threshold values based on previous studies by Lewan and Maynard (1982), Lewan (1984), and Hatch and Levanthal (1991). V/(V+Ni) ratios above 0.84 suggest a euxinic water column, or rather the presence of H_2S in a strongly stratified water column. Ratios from 0.54-0.82 suggest anoxia and a less strongly stratified anoxic water column, and values 0.46-0.60 suggest dysoxic (very little oxygen) conditions in a weakly stratified water column (Hatch and Levanthal, 1991). It is noteworthy to mention however, that these proxy threshold studies were conducted

mainly on petroleum source rocks (black shales) and oils and their applicability to grey shale paleoredox interpretations is less certain.

B.2 Vanadium and Nickel Results

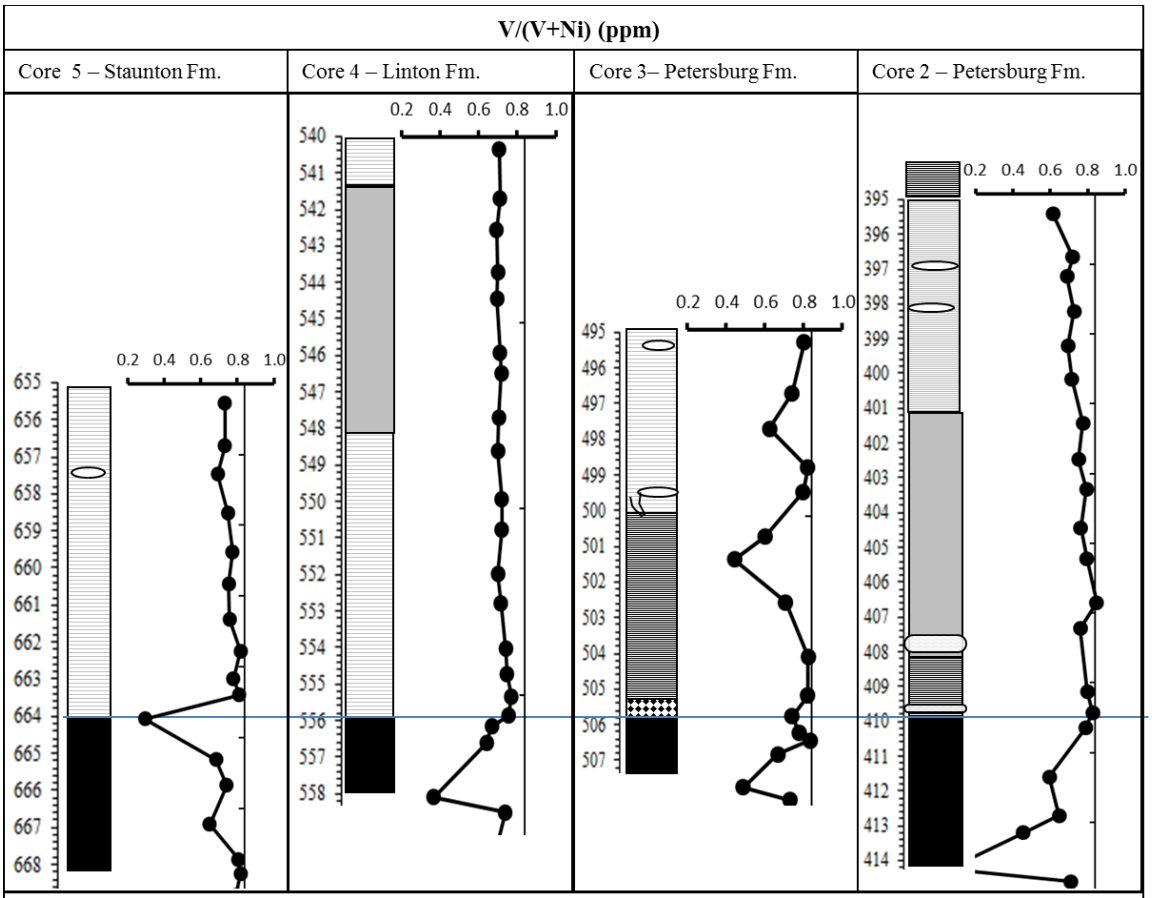

Figure 51: V/(V+Ni) Comparison between Cores 2-5 – Coal→Mudrock Only

Core 5 V/(V+Ni) values outside of the coal are closest to the euxinic threshold (0.81) at the base of the grey shale when transitioning to coal but do not exceed 0.84. Values remain within the anoxia range and become slightly lower upsection.

Core 4 V and Ni values were high enough to generate V/(V+Ni) values in the anoxia range (0.54-0.82) for the entirety of the core above the Survant Coal. Indeed there is very little variation in the V/(V+Ni) values upsection of the coal, ranging between 0.67-0.74. These values decreased very gradually upsection.

Core 3 V/(V+Ni) values approach the 0.84 euxinic threshold with five consecutive values near 0.84, coincident with the high Mo/Al and V/Al values within the black shale. In addition, two high V/(V+Ni) values of 0.82 and 0.80 are observed in the grey shale of Core 2, at 498.7' and 495.35' respectively.

Core 2 V/(V+Ni) ratios cross the euxinic threshold (>0.82) twice, once at the base of the black shale (409.85') and again at the base of the grey shale (406.7'). The rest of all black shale and grey shale values fall in the intermediate and less stratified water column range of 0.54-0.82 except at the very base of the Springfield coal seam (C2-19; 414.4') where a very low ratio is found, 0.051, within the szomolokite underclay section (Fig. 51.)

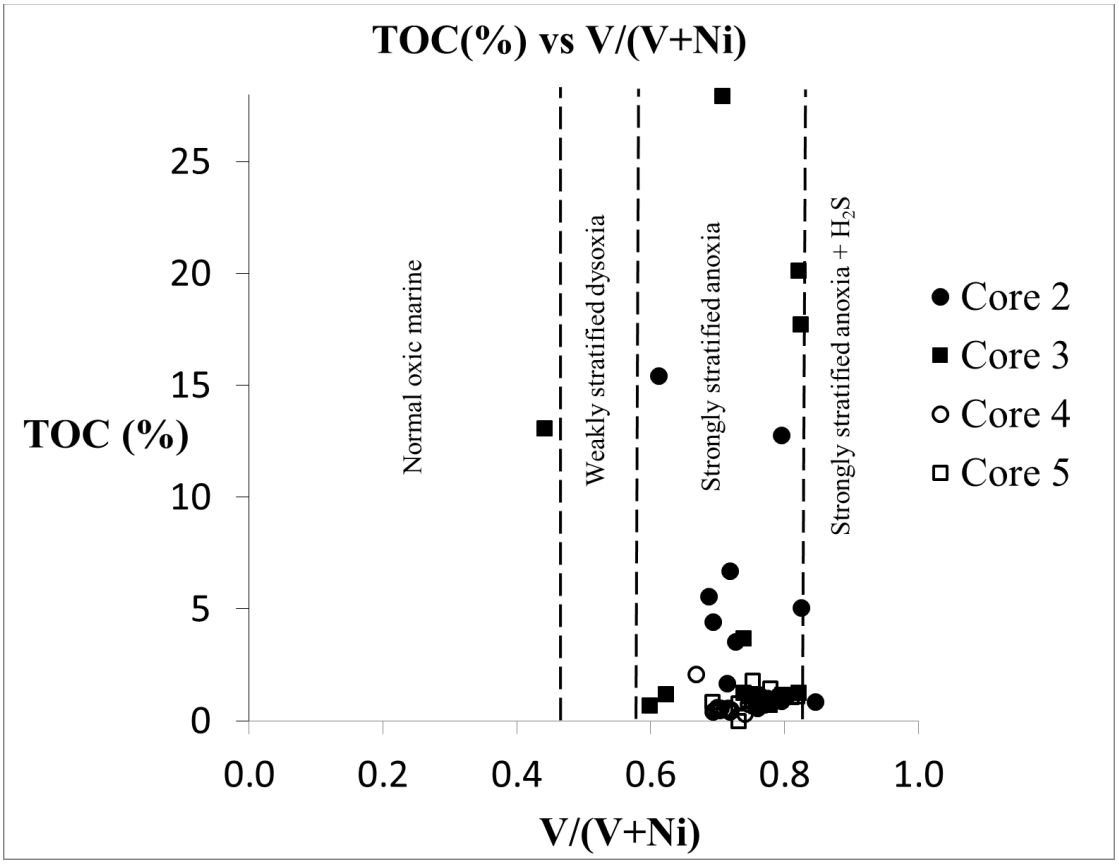

Figure 52: TOC(%) plotted against the combined trace metal paleoredox proxy of V/(V+Ni). Threshold values are taken from Hatch and Levanthal, 1992. Note that according to this proxy all shales and mudstone for all cores were deposited in a strongly stratified anoxic water column, save one value in Core 3.

Core 2 exhibited an increase in V/Al at the same depth as the Mo/Al enrichment (409.25'), within the thinly laminated black shale (Fig. 52). According to these threshold values and paleoredox interpretations, Core 2 displayed two near euxinic episodes, the first was at the transition from coal to black shale at 409.85' and the second occurred immediately above the black shale at 406.7'. All other values for Core 2 fall within the strongly stratified anoxia range. Core 3 values indicate sustained near-euxinic conditions throughout for the first 3 feet of Excello shale deposition with the water column gradually becoming more oxic upsection into the grey shale. However, V/(V+Ni) then return to near euxinic values at the top of the grey shale. These signals does not correspond to other redox proxies, particularly Mo and Fe and may suggest the V/(V+Ni) proxy is not applicable to grey shale. Core 4 values are within the anoxic range for the duration of the mudstone and grey shale upsection from the Survant coal. Core 5 values are similar to Core 4 but show more variation with values approaching a euxinic system directly above the Seelyville coal seam and then decline to anoxia for the remainder of the overlying grey mudstone. V/(V+Ni) values for all cores indicate prolonged anoxia even in waters that other proxies suggest were oxygenated (V/Al, Mo, Fe_{tot}/Al). In fact values falling in the dysoxic range were rarely observed. These interpretations, again, rely on research primarily done on black shales and their use in determining paleoredox conditions prevailing during the deposition of other sediment types, particularly nearshore grey shales, is unknown at this time.

Appendix C: $\delta^{15}N$

C.1 $\delta^{15}N$

Nitrogen isotopic values ($\delta^{15}N$), used in conjunction with $\delta^{13}C_{org}$ for ancient shales can help to support the case for source of organic matter or even shallow to deep/offshore to nearshore parameters. It has been shown that in shales, enriched $\delta^{15}N$ values correspond to times of marine algal influence and thus can help to determine proximity to shoreline and depth of water (Caplan and Bustin, 1998).

C.2 $\delta^{15}N$ Results

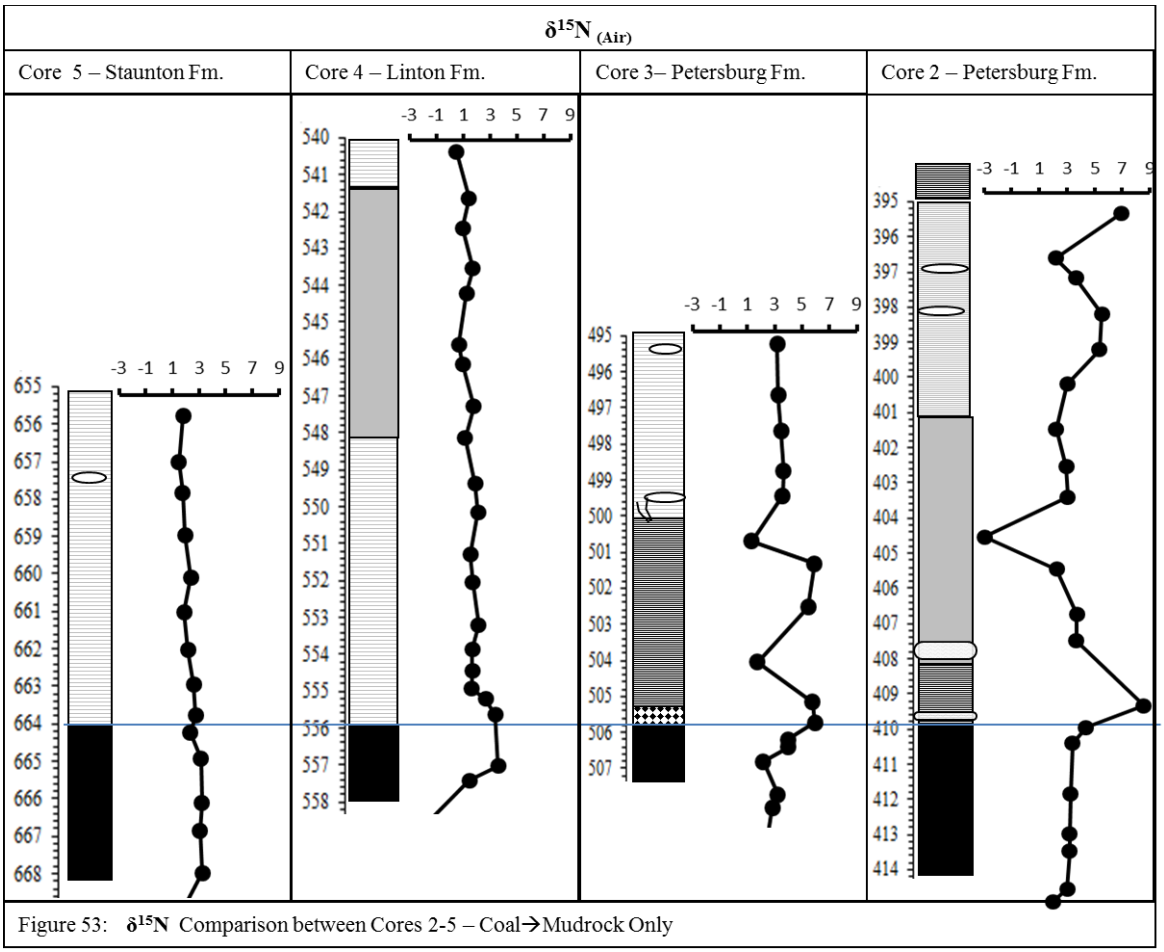

Figure 53: **$\delta^{15}N$** Comparison between Cores 2-5 – Coal→Mudrock Only

Core 5 $\delta^{15}N$ shows little variation upsection but does show a steady and gradual 2‰ decrease in $\delta^{15}N$ from the base of the coal to the top of the core. The Seelyville coal

values are very consistent and averaging 3.2‰. The grey shale values superjacent to the coal seam average 2.1‰ (Fig. 53).

Core 4 $\delta^{15}N$ values within the coal seam (averaging 3.48‰) decrease to an average $\delta^{15}N$ of 1.5‰ within the muddy grey shale. Overall, there is a trend of ^{15}N-depletion from the top of the coal to the top of core.

Core 3 $\delta^{15}N$ values relative to $\delta^{13}C_{org}$ exhibit an antithetic relationship within the black shale, which decrease as $\delta^{13}C_{org}$ increases. At the very top of the coal (~506.0') through the pyritic section and into the base of the black shale there is a pronounced shift from 1‰ to 5‰ in $\delta^{15}N$. With one exception at ~503.8', the black shale is ^{15}N-enriched relative to values observed throughout the grey shale.

Core 2 $\delta^{15}N$ values are inversely proportional to the $\delta^{13}C_{org}$ trends observed above the coal. The highest $\delta^{15}N$ values are within the black shale averaging 6.5‰ and those in the overlying grey mudstone/shale are lower and average 3.2‰. $\delta^{15}N$ for black shale decreases midway through the section of grey shale and then increases where the grey shale becomes more fissile and more organic-rich, mirroring the trend for both TOC and $\delta^{13}C_{org}$.

C.3 $\delta^{15}N$ Discussion

When plotted against each other a trend of nearshore-offshore is observed in the values (Fig. 54) although the mechanisms behind this relationship are as yet undetermined.

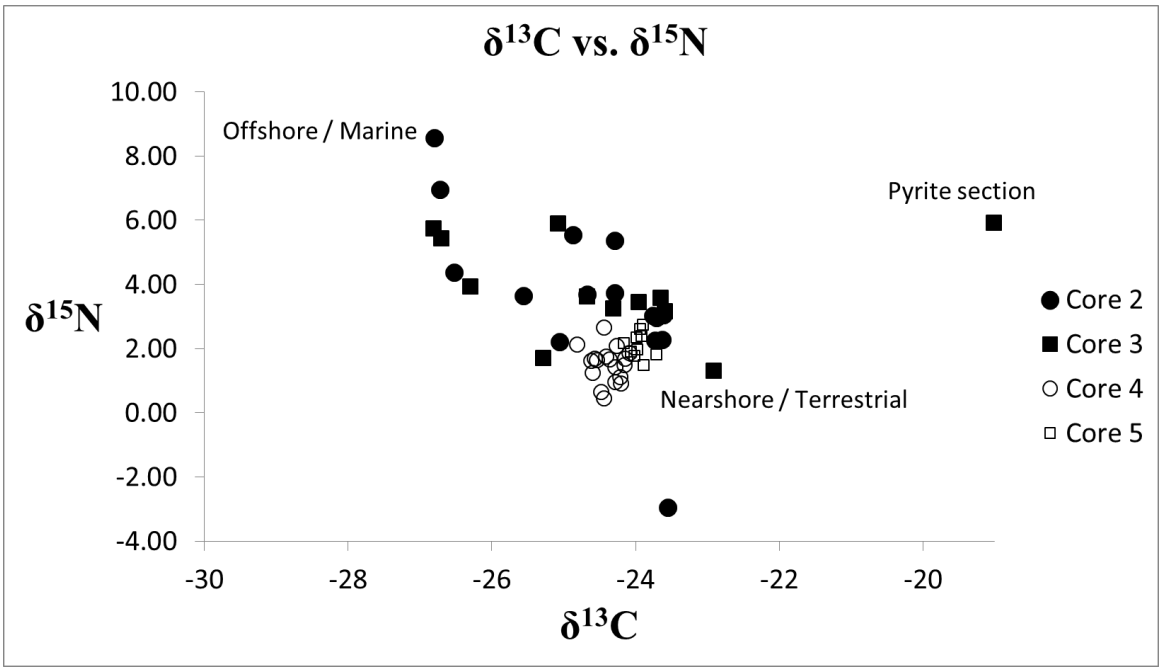

Figure 54: Plot of $\delta^{13}C_{org}$ versus $\delta^{15}N$ for coal and shales for all four cores.

Appendix D: Geochemical Data Tables

D.1 Geochemical Data Table for Core 5 – Petersburg Formation and Springfield Coal

Table 4: Core 5 - Petersburg Formation and Springfield coal Geochemical Data

Sample Name	Depth (ft.)	TC% - Total carbon	TIC (Coulometer)	TOC (= TC - TIC)	TN(%)	TS(%)	Mo (ppm)	Al (mol %)	Mo / Al (mol:mol)	V (ppm)	V/Al (mol:mol)	Th (ppm)	U (ppm)	Th/U (mol:mol)	Fe (wt %)	Fe/Al (mol:mol)	Zr (ppm)	Ni (ppm)	V/V+Ni (ppms)	$\delta^{13}C_{VPDB}$	$\delta^{15}N_{AIR}$	C/N (mol:mol)
C5-1	655.55	0.4	0.56	0	0.07	0.23	2.0	0.19	0.001	128.0	0.068	13.3	3.4	3.91	2.59	0.25	167	47.0	0.73	-23.71	3.48	0
C5-2	656.75	1.35	0.57	0.78	0.1	0.60	2.0	0.18	0.001	125.0	0.068	13.4	3.4	3.94	2.69	0.26	178	46.0	0.73	-23.88	3.30	9.18
C5-3	657.55	1.32	0.49	0.83	0.1	1.97	2.0	0.18	0.001	126.0	0.070	12.6	3.3	3.82	3.11	0.31	158	56.0	0.69	-24.01	2.95	10.31
C5-4	658.65	1.65	0.56	1.09	0.1	0.49	2.0	0.19	0.001	136.0	0.073	14.2	3.4	4.18	2.71	0.26	149	46.0	0.75	-23.97	3.02	13.56
C5-5	659.75	1.65	0.72	0.93	0.09	0.23	2.0	0.20	0.001	153.0	0.078	14.8	3.5	4.23	2.89	0.26	134	45.0	0.77	-23.92	3.14	10.75
C5-6	660.65	2.35	0.54	1.81	0.1	0.89	2.0	0.19	0.001	146.0	0.076	13.7	3.3	4.15	2.83	0.26	133	48.0	0.75	-24.07	3.17	22.13
C5-7	661.65	0.98	0.31	0.67	0.1	0.99	2.0	0.20	0.001	156.0	0.077	15.2	3.6	4.22	2.43	0.21	130	50.0	0.76	-24.17	3.16	7.55
C5-8	662.55	1.58	0.49	1.09	0.09	0.38	2.0	0.22	0.001	194.0	0.090	17.7	4.3	4.12	2.42	0.20	129	43.0	0.82	-23.94	3.08	12.76
C5-9	663.35	1.89	0.44	1.45	0.1	1.77	2.0	0.21	0.001	172.0	0.082	15.5	3.7	4.19	2.76	0.24	127	49.0	0.78	-23.89	3.11	17.27
C5-22	663.8	1.07		1.07	0.09	0.53	2.0	0.23	0.001	188.0	0.083	18.7	3.7	5.05	1.93	0.15	21	44.0	0.81	-23.98	2.57	13.86
C5-10	664.48	45.56	0.15	45.41	0.9	17.80	37.0	0.02	0.153	18.5	0.076	2.3	4.8	0.48	7.66	5.66	7	44.4	0.29	-23.97	-4.79	56.34
C5-11	665.63	63.86	0.13	63.73	1.49	2.37	2.0	0.01	0.021	7.9	0.083	0.9	0.3	2.77	0.42	0.79	11	3.7	0.68	-25.18	4.97	44.77
C5-12	666.35	78.66	0.27	78.39	1.52	2.39	2.0	0.01	0.018	11.5	0.105	1.3	0.5	2.91	0.47	0.76	33	4.0	0.74	-24.41	-0.07	56.78
C5-13	667.45	58.19	0.23	57.96	1.24	7.64	7.0	0.04	0.019	30.4	0.082	3.3	0.9	3.80	2.79	1.36	285	16.5	0.65	-24.39	-0.55	52.80
C5-14	668.45	1.99	0.08	1.91	0.1	0.38	2.0	0.21	0.001	124.0	0.059	18.2	7.4	2.46	0.89	0.08	277	30.0	0.81	-24.16	3.54	34.21
C5-15	668.85	2.35	0.08	2.27	0.1	0.30	2.0	0.21	0.001	135.0	0.065	17.8	8.8	2.02	0.76	0.07	273	30.0	0.82	-23.65	3.09	44.07
C5-16	669.45	0.61	0.07	0.54	0.04	0.38	2.0	0.21	0.001	136.0	0.066	18.2	9.1	2.00	0.78	0.07	257	35.0	0.80	-24.09	3.53	10.43
C5-17	670.15	0.32	0.09	0.23	0.03	2.66	2.0	0.20	0.001	127.0	0.064	16.4	13.0	1.26	1.78	0.16	265	92.0	0.58	-23.85	3.30	4.38
C5-18	671.25	1.01	0.28	0.73	0.09	0.93	2.0	0.19	0.001	128.0	0.066	16.2	7.7	2.10	1.45	0.13	252	39.0	0.77	-24.48	3.47	14.17
C5-19	672.55	0.67	0.43	0.24	0.12	1.04	2.0	0.20	0.001	135.0	0.069	15.7	7.1	2.21	1.78	0.16	257	36.0	0.79	-23.90	3.11	4.68
C5-20	673.45	0.7	0.31	0.39	0.11	1.28	2.0	0.20	0.001	131.0	0.064	16.4	5.7	2.88	1.51	0.13	260	62.0	0.68	-23.82	3.20	7.52
C5-21	674.75	1.21	0.30	0.91	0.1	1.08	2.0	0.20	0.001	137.0	0.067	15.5	7.0	2.21	1.20	0.11	164	38.0	0.78	-23.89	2.84	17.76

D.2 Geochemical Data Table for Core 4 – Petersburg Formation and Houchin Creek Coal

Table 5: Core 4 - Petersburg Formation and Houchin Creek coal Geochemical Data

Sample Name	Depth (ft.)	TC% - Total carbon	TIC (Coulometer)	TOC (= TC - TIC)	TN(%)	TS(%)	Mo (ppm)	Al (mol %)	Mo / Al (mol:mol)	V (ppm)	V/Al (mol:mol)	Th (ppm)	U (ppm)	Th/U (mol:mol)	Fe (wt %)	Fe/Al (mol:mol)	Zr (ppm)	Ni (ppm)	V/V+Ni (ppms)	$\delta^{13}C_{VPDB}$	$\delta^{15}N_{AIR}$	C/N (mol:mol)
C4-1	540.35	1.44	0.66	0.57	0.06	0.16	2.0	0.16	0.001	110.0	0.070	11.6	3.1	3.74	2.35	0.27	245	46.0	0.71	-24.44	3.13	8.44
C4-2	541.65	1.19	0.55	0.50	0.06	0.11	2.0	0.17	0.001	120.0	0.073	11.3	3.1	3.65	2.29	0.25	217	49.0	0.71	-24.28	3.09	7.21
C4-3	542.5	1.38	0.65	0.41	0.07	0.15	2.0	0.17	0.001	120.0	0.070	11.5	3.1	3.71	2.48	0.26	196	53.0	0.69	-24.21	2.96	5.72
C4-4	543.65	1.33	0.58	0.49	0.07	0.17	2.0	0.17	0.001	119.0	0.069	11.8	3.1	3.81	2.44	0.25	195	51.0	0.70	-24.14	2.75	6.85
C4-5	544.35	1.16	0.53	0.47	0.07	0.17	2.0	0.18	0.001	121.0	0.068	11.3	2.9	3.90	2.34	0.24	184	53.0	0.70	-24.59	3.25	6.41
C4-6	545.8	1.05	0.49	0.51	0.07	0.10	2.0	0.19	0.001	125.0	0.067	10.9	2.8	3.89	2.32	0.22	157	51.0	0.71	-24.48	3.11	6.28
C4-7	546.35	1.23	0.60	0.42	0.07	0.51	2.0	0.18	0.001	125.0	0.071	11.2	2.8	4.00	2.61	0.26	171	49.0	0.72	-24.28	3.21	5.46
C4-8	547.55	1.06	0.46	0.46	0.08	0.12	2.0	0.19	0.001	135.0	0.070	12.1	3	4.03	2.35	0.22	162	57.0	0.70	-24.41	2.00	5.89
C4-9	548.45	0.48	0.42	0.46	0.07	0.23	2.0	0.19	0.001	131.0	0.070	11.9	3	3.97	2.19	0.21	161	56.0	0.70	-24.22	2.67	5.99
C4-10	549.75	0.49	0.46	0.48	0.08	0.16	2.0	0.19	0.001	133.0	0.071	12.4	3.1	4.00	2.32	0.22	165	52.0	0.72	-24.09	3.34	6.12
C4-11	550.55	1.71	0.39	0.49	0.1	0.25	2.0	0.19	0.001	139.0	0.071	12.1	2.9	4.17	2.26	0.21	158	54.0	0.72	-24.26	3.19	6.07
C4-12	551.75	1.98	0.32	0.60	0.1	0.13	2.0	0.19	0.001	135.0	0.069	11.9	3	3.97	2.09	0.19	156	58.0	0.70	-24.15	3.37	7.42
C4-13	552.55	1.21	0.35	0.56	0.1	0.09	2.0	0.20	0.001	146.0	0.072	12.9	3.1	4.16	2.17	0.19	148	58.0	0.72	-24.57	3.26	6.52
C4-14	553.75	0.48	0.65	0.32	0.07	0.05	2.0	0.20	0.001	154.0	0.077	13.3	3.1	4.29	2.70	0.24	147	54.0	0.74	-24.81	3.53	3.57
C4-15	554.45	0.51	0.12	0.76	0.08	0.33	2.0	0.22	0.001	156.0	0.071	13.9	3.3	4.21	1.91	0.15	150	53.0	0.75	-24.54	3.43	8.42
C4-23	555.05	0.68		0.72	0.09	0.15	2.0	0.22	0.001	154.0	0.069	14.9	3.6	4.14	1.80	0.14	149		0.77	-24.36	2.06	9.33
C4-16	555.55	0.57	0.09	0.79	0.07	0.14	2.0	0.22	0.001	153.0	0.069	1.0	0.4	2.50	1.76	0.14	148	50.0	0.75	-24.62	3.33	8.56
C4-24	555.85	1.83		2.09	0.11	4.99	2.0	0.21	0.001	163.0	0.079	0.8	0.3	2.67	3.52	0.30	127		0.67	-24.44	2.73	20.31
C4-17	556.3	75.85	0.24	70.69	1.64	4.85	2.0	0.01	0.016	11.2	0.089	15.3	4.1	3.73	1.44	2.05	9	7.0	0.64	-24.80	2.18	50.89
C4-18	557.75	58.74	0.17	73.86	1.39	2.76	2.0	0.01	0.020	12.4	0.122	9.7	2.6	3.73	0.62	1.09	6	27.0	0.37	-23.58	2.52	49.22
C4-19	558.15	0.38	0.08	1.11	0.07	0.34	2.0	0.21	0.001	129.0	0.062	9.7	2.6	3.73	1.57	0.13	268	46.0	0.74	-24.11	2.92	15.95
C4-20	559.45	0.22	0.07	0.45	0.08	1.10	2.0	0.11	0.002	64.0	0.059	13.3	3.6	3.69	1.28	0.21	301	31.0	0.67	-24.92	0.64	16.60
C4-21	559.65	0.35	0.07	0.73	0.08	1.00	2.0	0.11	0.002	68.0	0.060	13.3	3.4	3.91	1.39	0.22	323	33.0	0.67	-25.01	1.43	20.71
C4-22	560.45	0.49	0.38	1.83	0.07	0.82	2.0	0.15	0.001	113.0	0.076	13.4	3.4	3.94	2.39	0.29	336	44.0	0.72	-24.26	3.43	23.78

D.3 Geochemical Data Table for Core 3 – Linton Formation and Survant Coal

Table 6: Core 3 - Linton Formation and Survant coal Geochemical Data

Sample Name	Depth (ft.)	TC% - Total carbon	TIC (Coulometer)	TOC (= TC - TIC)	TN(%)	TS(%)	Mo (ppm)	Al (mol %)	Mo / Al (mol:mol)	V (ppm)	V/Al (mol:mol)	Th (ppm)	U (ppm)	Th/U (mol:mol)	Fe (wt %)	Fe/Al (mol:mol)	Zr (ppm)	Ni (ppm)	V/V+Ni (ppms)	$\delta^{13}C_{VPDB}$	$\delta^{15}N_{AIR}$	C/N (mol:mol)
C3-1	495.35	2.08	0.95	1.13	0.10	0.05	2.0	0.19	0.001	154.0	0.081	12.2	2.6	4.69	3.11	0.29	118	38.0	0.80	-23.59	3.49	10.98
C3-2	496.70	2.31	1.06	1.25	0.10	0.25	2.0	0.19	0.001	178.0	0.094	13.6	2.9	4.69	3.35	0.32	124	63.0	0.74	-24.31	3.46	12.12
C3-3	497.65	1.59	0.41	1.18	0.10	2.72	2.0	0.20	0.001	155.0	0.079	13.7	2.8	4.89	3.26	0.30	124	94.0	0.62	-23.96	3.34	11.44
C3-4	498.70	2.22	0.95	1.27	0.11	0.07	2.0	0.19	0.001	183.0	0.097	16.1	3.1	5.19	3.04	0.29	118	40.0	0.82	-24.68	3.81	12.31
C3-5	499.35	2.31	1.16	1.15	0.11	0.46	2.0	0.19	0.001	215.0	0.114	18.1	3.5	5.17	3.48	0.33	117	55.0	0.80	-23.65	4.03	11.13
C3-6	500.55	1.79	1.11	0.68	0.09	4.45	12.0	0.15	0.008	182.0	0.119	14.1	4.2	3.36	3.33	0.39	116	122.0	0.60	-22.92	3.97	7.53
C3-7	501.15	13.65	0.59	13.06	0.50	2.35	14.0	0.13	0.011	171.0	0.128	11.5	17.3	0.66	2.02	0.27	29	216.0	0.44	-25.08	5.94	27.20
C3-8	502.30	28.31	0.40	27.91	1.03	3.31	712.0	0.11	0.627	1253.0	1.104	8.9	91.4	0.10	1.97	0.31	79	520.0	0.71	-26.70	5.46	32.23
C3-9	503.75	18.02	0.29	17.72	0.67	2.92	348.0	0.13	0.260	1838.0	1.374	9.9	34.4	0.29	2.03	0.27	101	393.0	0.82	-25.28	5.45	30.85
C3-10	504.80	20.66	0.54	20.12	0.70	2.74	233.0	0.11	0.206	1710.0	1.511	8.5	80.5	0.11	1.93	0.31	16	373.0	0.82	-26.81	4.56	30.47
C3-11	505.35	13.35	9.66	3.69	0.05	0.44	68.0	0.01	0.779	150.0	1.718	1.5	32.7	0.05	0.83	1.70	10	53.0	0.74	-19.01	-0.75	22.67
C3-12	505.80	5.65	4.94	0.71	0.01	20.00	71.0	0.02	0.391	70.0	0.386	1.7	6.9	0.25	12.03	11.88	19	20.0	0.78	-26.30	0.88	20.83
C3-13	506.00	66.15	0.39	65.76	1.40	3.45	36.4	0.02	0.221	41.0	0.268	1.5	24.0	0.06	0.67	0.73	13	8.9	0.83	-24.71	2.71	46.48
C3-14	506.38	72.48	0.15	72.33	1.50	2.36	7.1	0.01	0.051	11.0	0.089	1.1	1.1	1.00	0.19	0.25	9	6.3	0.67	-24.81	2.36	54.07
C3-15	507.25	68.40	0.09	68.31	1.42	4.35	2.7	0.03	0.009	32.0	0.113	2.5	0.9	2.78	1.20	0.76	26	33.4	0.49	-25.55	-1.29	54.56
C3-16	507.60	2.18	0.09	2.09	0.13	0.35	2.0	0.13	0.001	68.0	0.051	11.9	3.1	3.84	0.96	0.13	325	25.0	0.73	-24.53	2.80	20.36
C3-17	508.40	0.42	0.09	0.33	0.08	0.60	2.0	0.14	0.001	89.0	0.064	12.0	3.1	3.87	1.18	0.15	319	34.0	0.72	-25.85	4.41	4.55
C3-18	509.30	0.51	0.41	0.10	0.06	0.81	2.0	0.12	0.002	85.0	0.068	10.4	2.6	4.00	1.20	0.17	277	33.0	0.72	-26.52	3.80	2.04
C3-19	510.55	0.01	0.07	0.00	0.01	0.44	2.0	0.11	0.002	62.0	0.058	8.3	2.0	4.15	0.86	0.14	222	27.0	0.70	-28.53	1.86	0.00
C3-20	511.45	0.01	0.09	0.00	0.01	0.76	2.0	0.10	0.002	67.0	0.064	8.6	2.0	4.30	1.00	0.17	236	27.0	0.71	-28.31	1.74	0.00
C3-21	512.55	0.24	0.30	0.00	0.01	2.55	2.0	0.09	0.002	54.0	0.061	6.6	1.5	4.40	1.78	0.36	200	23.0	0.70	-29.04	0.62	0.00
C3-22	513.55	0.63	0.67	0.00	0.00	1.28	2.0	0.08	0.002	46.0	0.056	5.9	1.4	4.21	1.38	0.30	199	23.0	0.67	-28.21	-0.04	0.00
C3-23	514.05	5.61	5.46	0.15	0.01	0.82	2.0	0.09	0.002	69.0	0.081	7.4	2.3	3.22	3.06	0.64	181	19.0	0.78	-27.71	2.08	4.37
C3-24	514.80	0.00	0.09	0.00	0.02	2.64	2.0	0.13	0.002	90.0	0.068	11.6	2.8	4.14	1.90	0.26	365	38.0	0.70	-29.18	1.32	0.00
C3-25	515.40	0.01	0.10	0.00	0.02	2.80	2.0	0.13	0.002	87.0	0.069	12.1	2.9	4.17	1.95	0.28	447	34.0	0.72	-29.44	1.75	0.00

D.4 Geochemical Data Table for Core 2 – Staunton Formation and Seelyville Coal

Table 7: Core 2 - Staunton Formation and Seelyville coal Geochemical Data

Sample Name	Depth (ft.)	TC% - Total carbon	TIC (Coulometer)	TOC (= TC - TIC)	TN(%)	TS(%)	Mo (ppm)	Al (mol %)	Mo / Al (mol:mol)	V (ppm)	V/Al (mol:mol)	Th (ppm)	U (ppm)	Th/U (mol:mol)	Fe (wt %)	Fe/Al (mol:mol)	Zr (ppm)	Ni (ppm)	V/V+Ni (ppms)	$\delta^{13}C_{VPDB}$	$\delta^{15}N_{AIR}$	C/N (mol:mol)
C2-1	395.55	18.41	3.00	15.41	0.38	0.49	2.0	0.12	0.002	87.0	0.074	9.5	2.4	3.96	6.31	0.96	93	55.0	0.61	-26.72	7.05	35.24
C2-2	396.80	8.10	1.41	6.68	0.23	0.25	2.0	0.17	0.001	148.0	0.086	13.6	3.3	4.12	3.94	0.41	97	58.0	0.72	-25.06	4.17	28.87
C2-3	397.35	6.50	0.95	5.55	0.20	1.36	2.0	0.19	0.001	165.0	0.089	13.8	3.8	3.63	3.79	0.37	110	75.0	0.69	-25.56	5.95	29.44
C2-4	398.35	4.78	1.26	3.52	0.16	0.52	2.0	0.19	0.001	168.0	0.087	14.6	3.8	3.84	4.08	0.38	104	63.0	0.73	-24.87	3.89	21.62
C2-5	399.35	7.56	3.14	4.42	0.14	1.26	2.0	0.12	0.002	138.0	0.113	10.0	3.5	2.86	7.61	1.11	118	61.0	0.69	-24.29	5.17	23.42
C2-6	400.30	2.58	0.92	1.66	0.10	1.32	2.0	0.18	0.001	155.0	0.086	13.2	4.7	2.81	3.71	0.37	154	62.0	0.71	-23.76	3.31	16.10
C2-7	401.55	1.21	0.21	0.99	0.09	0.53	2.0	0.20	0.001	151.0	0.076	13.0	2.9	4.48	2.03	0.18	138	44.0	0.77	-23.73	2.91	11.60
C2-8	402.60	1.63	0.50	1.13	0.10	0.97	2.0	0.20	0.001	164.0	0.081	13.1	3.2	4.09	2.85	0.25	127	55.0	0.75	-23.71	2.92	11.97
C2-9	403.45	1.73	0.60	1.13	0.10	0.25	2.0	0.20	0.001	163.0	0.081	13.7	3.2	4.28	2.68	0.24	128	43.0	0.79	-23.62	3.50	11.99
C2-10	404.55	1.35	0.20	1.15	0.10	0.37	2.0	0.21	0.001	160.0	0.077	13.8	3.2	4.31	2.09	0.18	130	50.0	0.76	-23.55	3.65	12.24
C2-11	405.45	1.42	0.55	0.87	0.10	0.42	2.0	0.21	0.001	175.0	0.084	14.4	3.3	4.36	2.39	0.21	130	45.0	0.80	-23.64	3.44	9.24
C2-12	406.70	1.11	0.27	0.84	0.11	0.40	2.0	0.22	0.001	236.0	0.108	16.9	4.7	3.60	1.90	0.16	129	43.0	0.85	-24.29	3.56	8.89
C2-13	407.45	1.79	1.22	0.57	0.08	5.01	6.0	0.18	0.003	281.0	0.157	15.6	3.6	4.33	3.33	0.33	109	89.0	0.76	-24.67	3.35	7.33
C2-14	409.25	12.88	0.13	12.75	0.46	3.74	196.0	0.15	0.130	796.0	0.527	11.2	47.8	0.23	2.43	0.29	95	204.0	0.80	-26.80	8.99	29.45
C2-21	409.85	5.05		5.05	0.19	4.50	15.0	0.19	0.008	254.0	0.131	14.2	7.8	1.82	2.97	0.27	109	54.0	0.82	-26.53	4.37	31.00
C2-15	410.30	61.57	0.06	61.51	1.20	1.77	6.7	0.05	0.011	34.7	0.065	3.6	1.2	3.27	0.35	0.12	49	9.3	0.79	-24.63	3.69	56.93
C2-16	411.70	72.01	0.08	71.93	1.67	2.51	2.1	0.01	0.023	9.0	0.102	0.7	0.3	3.50	0.23	0.47	6	6.2	0.59	-24.70	1.89	49.34
C2-17	412.80	74.55	0.07	74.48	1.63	3.38	1.5	0.02	0.012	13.9	0.082	1.3	0.4	3.25	0.63	0.66	14	7.6	0.65	-25.73	3.10	53.95
C2-18	413.30	64.37	0.68	63.69	1.29	3.03	1.1	0.02	0.016	15.9	0.087	1.9	0.5	3.80	0.63	0.62	16	19.0	0.46	-23.98	2.24	52.31
C2-19	414.35	0.41	0.06	0.35	0.02	20.00	5.0	0.03	0.033	15.0	0.055	2.2	0.4	5.50	18.44	12.20	29	279.0	0.05	-24.59	-4.05	1.95
C2-20	414.70	0.60	0.05	0.55	0.13	0.80	2.0	0.19	0.001	133.0	0.069	15.1	2.7	5.59	1.45	0.13	213	55.0	0.71	-24.57	4.28	4.89

8. REFERENCES

Adams, John AS, and Charles E. Weaver. "Thorium-to-uranium ratios as indicators of sedimentary processes: example of concept of geochemical facies." AAPG Bulletin 42.2 (1958): 387-430.

Affolter and Hatch, 2002 Affolter, Ronald H., ed. *Resource assessment of the Springfield, Herrin, Danville, and Baker coals in the Illinois Basin*. US Department of the Interior, US Geological Survey, 2002Algeo, T. J., & Scheckler, S. E., 1998. Terrestrial-marine teleconnections in the Devonian: links between the evolution of land plants, weathering processes, and marine anoxic events. Philosophical Transactions of the Royal Society of London. Series B: Biological Sciences, 353(1365), 113-130.

Algeo, T. J., Schwark, L., & Hower, J. C., 2004. High-resolution geochemistry and sequence stratigraphy of the Hushpuckney Shale (Swope Formation, eastern Kansas): implications for climato-environmental dynamics of the Late Pennsylvanian Midcontinent Seaway. Chemical Geology, 206(3), 259-288.

Algeo, T. J., Lyons, T. W., Blakey, R. C., & Over, D. J., 2007. Hydrographic conditions of the Devono–Carboniferous North American Seaway inferred from sedimentary Mo–TOC relationships. Palaeogeography, Palaeoclimatology, Palaeoecology, 256(3), 204-230.

Algeo, T. J., & Maynard, J. B., 2004. Trace-element behavior and redox facies in core shales of Upper Pennsylvanian Kansas-type cyclothems. Chemical geology, 206(3), 289-318.

Algeo, T. J., & Lyons, T. W., 2006. Mo–total organic carbon covariation in modern anoxic marine environments: Implications for analysis of paleoredox and paleohydrographic conditions. Paleoceanography, 21(1).

Algeo, T. J., Heckel, P. H., Maynard, J. B., Blakey, R., & Rowe, H., 2008. Modern and ancient epicratonic seas and the superestuarine circulation model of marine anoxia. Dynamics of Epeiric Seas: Sedimentological, Paleontological and Geochemical Perspectives: Geological Association of Canada Special Publications, 48, 7-38.

Algeo, T. J., & Heckel, P. H., 2008. The Late Pennsylvanian midcontinent sea of North America: a review. Palaeogeography, Palaeoclimatology, Palaeoecology, 268(3), 205-221.

Archer, Allen W., and Erik P. Kvale. "Origin of gray-shale lithofacies ("clastic wedges") in US midcontinental coal measures (Pennsylvanian): an alternative explanation." *Geological Society of America Special Papers* 286 (1993): 181-192.

Arthur, M. A., Dean, W. E., & Claypool, G. E., 1985. Anomalous ^{13}C enrichment in modern marine organic carbon. Letters to Nature, Vol. 315; 216-218.

Barker, C. E., Dallegge, T. A., & Clark, A. C. 2003. USGS coal desorption equipment and a spreadsheet for analysis of lost and total gas from canister desorption measurements. US Department of the Interior, US Geological Survey.

Berner, R. A., & Raiswell, R., 1983. Burial of organic carbon and pyrite sulfur in sediments over Phanerozoic time: a new theory. Geochimica et Cosmochimica Acta, 47(5), 855-862.

Berner, Z. A., Puchelt, H., Noeltner, T., & Kramar, U. 2013. Pyrite geochemistry in the Toarcian Posidonia Shale of south-west Germany: Evidence for contrasting trace-element patterns of diagenetic and syngenetic pyrites. Sedimentology, 60(2), 548-573.

Boggs, Sam. *Principles of sedimentology and stratigraphy*. Vol. 23117923. New Jersey: Prentice Hall, 1995.

Broach, C., & Elliott, W.S. Jr., 2011. Sedimentological Examination of Lithofacies Associated with Coal Seams of the Linton and Petersburg Formations (Pennsylvanian) in Vanderburgh County, Indiana: Implications for Coal Formation and Origins of Coal-Bed Methane; Poster. GSA Northeastern (46th Annual) and North-Central (45th Annual) Joint Meeting (20–22 March 2011).

Broach, C., Gilhooly, W. III, Smith, C., Elliott, W.S., Jr., Voegerl, R., 2012, Paleoenvironmental History of Five Late Middle Pennsylvanian Cores (Carbondale Group) from the Illinois Basin, Southwest Indiana: A Combined Geochemical and Geophysical Approach. 2012 GSA Annual Meeting in Charlotte; Poster (4-7 November).

Busch, R. M., & Rollins, H. B., 1984. Correlation of Carboniferous strata using a hierarchy of transgressive-regressive units. Geology, 12(8), 471-474.

Buschbach, T. C., & Kolata, D. R., 1991. Regional setting of Illinois basin. Interior cratonic basins: American Association of Petroleum Geologists Memoir, 51, 29-55.

Calvert, S. E., Bustin, R. M., & Ingall, E. D., 1996. Influence of water column anoxia and sediment supply on the burial and preservation of organic carbon in marine shales. Geochimica et Cosmochimica Acta, 60(9), 1577-1593.

Canfield, D. E., 1994. Factors influencing organic carbon preservation in marine sediments. Chemical Geology, 114(3), 315-329.

Canfield, D. E., & Farquhar, J., 2012. The global sulfur cycle. Fundamentals of Geobiology, 49-64.

Caplan, M. L., & Bustin, R. M., 1999. Palaeoceanographic controls on geochemical characteristics of organic-rich Exshaw mudstones: role of enhanced primary production. Organic Geochemistry, 30(2), 161-188.

Caplan, M. L., & Marc Bustin, R., 2001. Palaeoenvironmental and palaeoceanographic controls on black, laminated mudstone deposition: example from Devonian–Carboniferous strata, Alberta, Canada. Sedimentary Geology, 145(1), 45-72.

Castro, P., & Huber, M. E., 2003. Marine biology 4th edn.

Coveney, Raymond M., and Nelson R. Shaffer. "Sulfur-isotope variations in Pennsylvanian shales of the midwestern United States." *Geology* 16.1 (1988): 18-21.

Coveney Jr, R. M., & Glascock, M. D., 1989. A review of the origins of metal-rich Pennsylvanian black shales, central USA, with an inferred role for basinal brines. Applied Geochemistry, 4(4), 347-367.

Coveney, Raymond M., W. Lynn Watney, and Christopher G. Maples. "Contrasting depositional models for Pennsylvanian black shale discerned from molybdenum abundances." *Geology* 19.2 (1991): 147-150.

Davies, S. J., Leng, M. J., Macquaker, J. H. S., & Hawkins, K., 2012. Sedimentary process control on carbon isotope composition of sedimentary organic matter in an ancient shallow-water shelf succession. Geochemistry, Geophysics, Geosystems, 13(11).

Dean, W. E., Piper, D. Z., & Peterson, L. C., 1999. Molybdenum accumulation in Cariaco basin sediment over the past 24 ky: A record of water-column anoxia and climate. Geology, 27(6), 507-510.

Demaison, G. J., and G. Tn Moore. "Anoxic environments and oil source bed genesis." *Organic Geochemistry* 2.1 (1980): 9-31.

Dimichele, William A., and W. John Nelson. "Small-scale spatial heterogeneity in Pennsylvanian-age vegetation from the roof shale of the Springfield Coal (Illinois Basin)." *Palaios* (1989): 276-280.

DiMichele, William A., Hermann W. Pfefferkorn, and Tom L. Phillips. "Persistence of Late Carboniferous tropical vegetation during glacially driven climatic and sea-level fluctuations." *Palaeogeography, Palaeoclimatology, Palaeoecology* 125.1 (1996): 105-128.

Doveton, J. H., & Merriam, D. F., 2004. Borehole petrophysical chemostratigraphy of Pennsylvanian black shales in the Kansas subsurface. Chemical geology, 206(3), 249-258.

Dypvik, H., & Harris, N. B., 2001. Geochemical facies analysis of fine-grained siliciclastics using Th/U, Zr/Rb and (Zr+ Rb)/Sr ratios. Chemical Geology, 181(1), 131-146.

Ece, O. I., 1987. Petrology of the Desmoinesian Excello black shale of the midcontinent region of the United States. Clays and Clay Minerals, 35(4), 262-270.

Eggert, Donald L. "The Leslie Cemetery and Francisco distributary fluvial channels in the Petersburg Formation (Pennsylvanian) of Gibson County, Indiana, USA." *Sedimentology of Coal and Coal-Bearing Sequences* (1984): 309-315.

Falcon-Lang, H. J., 2004. Pennsylvanian tropical rain forests responded to glacial-interglacial rhythms. Geology, 32(8), 689-692.

Faure, G., 1998. Principles and applications of geochemistry (Vol. 2). Upper Saddle River, NJ: Prentice-Hall.

Fielding, C. R., Frank, T. D., & Isbell, J. L., 2008. The late Paleozoic ice age—a review of current understanding and synthesis of global climate patterns. Geological Society of America Special Papers, 441, 343-354.

Frank, T. D., Birgenheier, L. P., Montañez, I. P., Fielding, C. R., & Rygel, M. C., 2008. Late Paleozoic climate dynamics revealed by comparison of ice-proximal stratigraphic and ice-distal isotopic records. Geological Society of America Special Papers, 441, 331-342.

Eble, Cortland F. "Desmoinesian coal beds of the Eastern Interior and surrounding basins: the largest tropical peat mires in earth history." *Extreme Depositional Environments: Mega End Members in Geologic Time* 370 (2003): 127.

Hammer, O, Harper, D.A.T., Ryan, P.D., 2001, PAST: Paleontological Statistics software package for educational and data analysis. Palaeontologia Electronica 4(1); 9 pp.

Hassan, K. M., Swinehart, J. B., & Spalding, R. F., 1997. Evidence for Holocene environmental change from C/N ratios, and $\delta^{13}C$ and $\delta^{15}N$ values in Swan Lake sediments, western Sand Hills, Nebraska. Journal of Paleolimnology, 18(2), 121-130.

Hayes, J. M., 2004. An introduction to isotopic calculations. Woods Hole Oceanogr. Inst., Woods Hole, Mass.

Hatch, J. R., & Leventhal, J. S., 1992. Relationship between inferred redox potential of the depositional environment and geochemistry of the Upper Pennsylvanian (Missourian) Stark Shale Member of the Dennis Limestone, Wabaunsee County, Kansas, USA. Chemical Geology, 99(1), 65-82.

Heckel, Philip H. "Sea-level curve for Pennsylvanian eustatic marine transgressive-regressive depositional cycles along midcontinent outcrop belt, North America." Geology 14.4 (1986): 330-334.

Heckel, Philip H., Martin R. Gibling, and Norman R. King. "Stratigraphic model for glacial-eustatic Pennsylvanian cyclothems in highstand nearshore detrital regimes." *The Journal of geology* 106.4 (1998): 373-384.

Heckel, P. H., 2008. Pennsylvanian cyclothems in Midcontinent North America as far-field effects of waxing and waning of Gondwana ice sheets. Resolving the Late Paleozoic ice age in time and space, 441, 275.

Helz, G. R., Miller, C. V., Charnock, J. M., Mosselmans, J. F. W., Pattrick, R. A. D., Garner, C. D., & Vaughan, D. J., 1996. Mechanism of molybdenum removal from the sea and its concentration in black shales: EXAFS evidence. Geochimica et Cosmochimica Acta, 60(19), 3631-3642.

Hetzel, A., Böttcher, M. E., Wortmann, U. G., & Brumsack, H. J., 2009. Paleo-redox conditions during OAE 2 reflected in Demerara Rise sediment geochemistry (ODP Leg 207). Palaeogeography, Palaeoclimatology, Palaeoecology, 273(3), 302-328.

Hoffman, E. L., 1992. Instrumental neutron activation in geoanalysis. Journal of Geochemical Exploration, 44(1), 297-319.

Hurtgen, M. T., Lyons, T. W., Ingall, E. D., & Cruse, A. M., 1999, Anomalous enrichments of iron monosulfide in euxinic marine sediments and the role of H_2S in iron sulfide transformations: examples from Effingham Inlet, Orca Basin, and the Black Sea. American Journal of Science, 299(7-9), 556-588.

Jacobson, R. J., 1983. Stratigraphic Correlations of Seelyville, De Koven, and Davis Coals (Desmoinesian) of Illinois Basin Coalfield: ABSTRACT. AAPG Bulletin, 67(9), 1456-1456.

Jones, Bryn, and David AC Manning. "Comparison of geochemical indices used for the interpretation of palaeoredox conditions in ancient mudstones." *Chemical Geology* 111.1 (1994): 111-129.Lewan, M. D., 1984. Factors controlling the proportionality of vanadium to nickel in crude oils. Geochimica et Cosmochimica Acta, 48(11), 2231-2238.

Lewan, M. D., 1986, Stable carbon isotopes of amorphous kerogens from Phanerozoic sedimentary rocks. Geochimica et Cosmochimica Acta, 50(8), 1583-1591.

Loucks, R. G., & Ruppel, S. C., 2007. Mississippian Barnett Shale: Lithofacies and depositional setting of a deep-water shale-gas succession in the Fort Worth Basin, Texas. AAPG bulletin, 91(4), 579-601.

Lyons, T. W., & Severmann, S., 2006. A critical look at iron paleoredox proxies: New insights from modern euxinic marine basins. Geochimica et Cosmochimica Acta, 70(23), 5698-5722.

Mastalerz, M., Drobniak, A., & Sowder, K. H., 2010. Coal of Indiana. Indiana Geological Survey.

Maynard, J. B.,1981. Carbon isotopes as indicators of dispersal patterns in Devonian-Mississippian shales of the Appalachian Basin. Geology, 9(6), 262-265.

Meybeck, M. 1979. Major elements contents of river water and dissolved inputs to the oceans. Revue de Geologie Dynamique et de Geographie Physique 21: 215-246

Meyers, P. A., 1994. Preservation of elemental and isotopic source identification of sedimentary organic matter. Chemical Geology, 114(3), 289-302.

Middelburg, J. J., 1991. Organic carbon, sulphur, and iron in recent semi-euxinic sediments of Kau Bay, Indonesia. Geochimica et Cosmochimica Acta, 55(3), 815-828.

Millero, Frank J., et al. "The composition of Standard Seawater and the definition of the Reference-Composition Salinity Scale." *Deep Sea Research Part I: Oceanographic Research Papers* 55.1 (2008): 50-72.

Murphy, A. E., Sageman, B. B., Hollander, D. J., Lyons, T. W., & Brett, C. E., 2000. Black shale deposition and faunal overturn in the Devonian Appalachian Basin: Clastic starvation, seasonal water-column mixing, and efficient biolimiting nutrient recycling. Paleoceanography, 15(3), 280-291.

Peters-Kottig, W., Strauss, H., & Kerp, H., 2006. The land plant $\delta^{13}C$ record and plant evolution in the Late Palaeozoic. Palaeogeography, Palaeoclimatology, Palaeoecology, 240(1), 237-252.

Phillips, T. L., Peppers, R. A., & DiMichele, W. A., 1985. Stratigraphic and interregional changes in Pennsylvanian coal-swamp vegetation: environmental inferences. International Journal of Coal Geology, 5(1), 43-109.

Phillps, Tom L., and William A. DiMichele. "A transect through a clastic-swamp to peat-swamp ecotone in the Springfield Coal, Middle Pennsylvanian age of Indiana, USA." *Palaios* 13.2 (1998): 113-128.

Pistorius, C. W. F. T., 1960, Lattice constants of $FeSO_4.H_20$ (artificial szomolnokite) and NiSiO4.H2O, Bulletin de la Societe Chimique de Belgique 69: 570-574.

Raiswell, R., & Berner, R. A.,1985, Pyrite formation in euxinic and semi-euxinic sediments. American Journal of Science, 285(8), 710-724.

Rimmer, S. M., Thompson, J. A., Goodnight, S. A., & Robl, T. L., 2004. Multiple controls on the preservation of organic matter in Devonian–Mississippian marine black shales: geochemical and petrographic evidence. Palaeogeography, Palaeoclimatology, Palaeoecology, 215(1), 125-154.

Rygel, M. C., Fielding, C. R., Frank, T. D., & Birgenheier, L. P., 2008. The magnitude of Late Paleozoic glacioeustatic fluctuations: a synthesis. Journal of Sedimentary Research, 78(8), 500-511.

Schultz, Richard B., and Raymond M. Coveney Jr. "Time-dependent changes for Midcontinent Pennsylvania black shales, USA." *Chemical geology* 99.1 (1992): 83-100.

Schultz, R. B., 2004. Geochemical relationships of Late Paleozoic carbon-rich shales of the Midcontinent, USA: a compendium of results advocating changeable geochemical conditions. Chemical geology, 206(3), 347-372.

Scott, C., & Lyons, T. W., 2012. Contrasting molybdenum cycling and isotopic properties in euxinic versus non-euxinic sediments and sedimentary rocks: refining the paleoproxies. Chemical Geology, 324, 19-27.Schultz, R. B., & Coveney Jr, R. M., 1992. Time-dependent changes for Midcontinent Pennsylvania black shales, USA. Chemical geology, 99(1), 83-100.

Strąpoć, D., Mastalerz, M., Schimmelmann, A., Drobniak, A., & Hedges, S., 2008. Variability of geochemical properties in a microbially dominated coalbed gas system from the eastern margin of the Illinois Basin, USA. International Journal of Coal Geology, 76(1), 98-110.

Treworgy, Colin G., and Russell J. Jacobson. "Paleoenvironments and distribution of low-sulfur coal in Illinois." *Illinois Department of Energy and Natural Resources, STATE GEOLOGICAL SURVEY DIVISION, Ninth International Congress on Carboniferous Stratigraphy and Geology*. 1979.

Tribovillard, N., Algeo, T. J., Lyons, T., & Riboulleau, A., 2006. Trace metals as paleoredox and paleoproductivity proxies: an update. Chemical Geology, 232(1), 12-32.

White, T., & Arthur, M. A., 2006, Organic carbon production and preservation in response to sea-level changes in the Turonian Carlile Formation, US Western Interior Basin. Palaeogeography, Palaeoclimatology, Palaeoecology, 235(1), 223-244.

CURRICULUM VITAE

Clinton M. Broach

EDUCATION

M.S. Geology, IU - Indiana University Purdue University Indianapolis
December, 2014 GPA: 3.5

B.S. Geology, USI - University of Southern Indiana
May, 2011 AGPA: 3.7/4.0 Geology GPA: 3.9/4.0

IUGFS Alumnus - Judson Mead Geologic Field Station, Cardwell, MT
Summer 2010

B.A. History, Purdue University
May, 2004 GPA: 2.8

Honors Diploma, Evansville North High School
May 1997 GPA: 3.9

HONORS / AWARDS / MEMBERSHIPS

- Imperial Barrel Award (AAPG), 2012
  4th Place – Eastern Region, IUPUI Team member
    - 1st team ever assembled at IUPUI
    - Experience in seismic and well log interpretation along with 2D and 3D seismic manipulation with SMT Kingdom
- Walter F. Sill Memorial Scholarship for Academic Excellence in Geology, USI, 2010
    - **Highest award given for Geology majors.**
- J.R. Dick Harris Memorial Scholarship, USI, 2010 – Award for outstanding Junior or Senior planning a career in petroleum or environmental geology.
- Walter F. Sill Field Camp Award, USI, 2010
- Judson Mead Geologic Field Station Scholarship, IU, 2010
- Graduated *Magna Cum Laude* with Academic Honors Diploma, 1997
- AAPG and GSA member since 2008

RESEARCH

2012-2014- MS Thesis

Geochemical analysis of four Late Middle Pennsylvanian cores from Southern Indiana

- **Oral Presentation: 2013 AAPG ACE – 5-22-13** ***Geochemical Analysis of Late Middle Pennsylvanian Cores (Carbondale Group) from the Illinois Basin, Southern Indiana***
- Poster: National GSA, Nov. 2012: *Paleoenvironmental history of five Late Middle Pennsylvanian cores (Carbondale group) from the Illinois basin, southwest Indiana: A combined geochemical and geophysical approach*
- **Thesis research co-sponsored by Weatherford International Ltd., Geoscience Development, Dr. Christopher Smith**

2010-2011– Undergraduate Independent Research Project

Sedimentological examination of lithofacies associated with coal seams of the Linton and Petersburg Formations (Pennsylvanian) in Vanderburgh County, Indiana: Implications for coal formation and origins of Coal-Bed Methane.

- Poster: GSA Regional Conference in Pittsburgh, PA on March, 2011.

2010 - Field investigation into the presence of Pre-Wisconsin age (Illinoian) glacial till in Vanderburgh County via Giddings soil probe.

PROFESSIONAL EXPERIENCE

- **Professional Intern – Chevron ETC, Houston, TX 6-13 – 8-13**

  Reservoir Characterization Unit, Reservoir Management Technology Services; Team Lead: Nicole Champenoy

  Complete a full geological and geochemical play assessment of the Ft. Worth basin Barnett Shale. Compile and organize existing internal data on the Barnett, update and add to all well and geochemical data from external sources, build new complete structure, isopach, TOC and other necessary geochemical and geotechnical parameter maps/grids to determine total GIP, et al. potential. Write geological section for Ft. Worth Barnett Playbook Summary. Develop proficiencies in *ArcGIS*, *Petra*, and *Spotfire* to accomplish internship objectives.
- **Exploration Intern, CountryMark Energy Resources, Indianapolis, IN 5-12 – 8-12**

  Built SMT Kingdom seismic database – Imported over 600 2D and 3D seismic SGY files and corresponding SP data. Created bedrock elevation maps to assist geophysicists for seismic and gravity survey mapping. Generate 3D maps of Ordovician reef structures with *Surfer* for field analogue analysis
- **Research and Teaching Assistant, IUPUI, IN** 1-12 – 5-14

  Advisor: Dr. Bill Gilhooly III -- Conducting thesis research. Coursework: Isotope Geochemistry, Introduction to GIS, Geochemistry, Advanced Geological Problems, Geomicrobiology, Data Analysis and Techniques for Geologists, Seismic Analysis (As team member for 2012 AAPG IBA)

  Classes taught: Labs for Physical Geology, Historical Geology, Env. Geology

- **Senior Mudlogger – Schlumberger, Geoservices - Offshore** 7-11 – 1-12
  Offshore mudlogger in Gulf of Mexico Platforms: Transocean DD1 (Operator - BHP Billiton) and the drillship Discoverer Americas (Operator – Anadarko). Responsibilities included monitoring drilling parameters, e.g. ROP, Drill String torque, BHA and Strings calc., WOH, WOB, and all mud pit volumes to ensure downhole pressure equilibrium is maintained. Also routinely take real-time mud gas readings, sample drill cuttings, and describe lithology and examine for HC show. Training: Well Control School, Mudlogging, Advanced Mudlogging, HUET, SafeGulf, and OSHA Offshore. Experience with VigiGraphics and other Geoservices software.
- **Geologist, Independent Contractor with Buck Creek Resources.** 1-11 – 3-11
  Alongside chief coal geologist Penny Meighan drill and core the WKY 9 (Springfield) coal seam throughout western Kentucky to prove coal reserves and assess the geological potential for a proposed underground Buck Creek coal mine. Main job duties included rig-site sedimentological and structural core description with focus on coal volume and floor and roof integrity
- **Lab Technician, Standard Laboratories, Inc.** 10-09 – 05-11
  11-09 to 5-10 Special Labs Technician – Conducted Chlorine PPM analysis, BTU count via calorimeter bomb, % Sulfur, % Moisture, Fusion Ash count, some supervisory duties.
  5-10 – 5-11 – Coal Preparation with focus on quality control
  Core specialist – Organize and analyze core samples for coal seams, describe, and process core samples for lab work.
- **Summer Internship, Energy Systems Group (ESG)** 6-09 – 9-09 **– CBM (coal bed methane) exploration project for USI**
  Selected by USI faculty and hired by ESG to work on joint venture between USI and ESG. Project drilled approx. 700' well on USI property and conducted Coal Bed Methane testing according to USGS canister and manometer methods to determine whether natural gas extraction and production was a geologically feasible and economically viable revenue source for USI.
- **4 years of remodeling and construction estimating and design experience prior to Geology career**

SKILLS / EXPERIENCE / MEMBERSHIPS

Field and Field Equipment Experience: Offshore mudlogging and engineering, Drilling and wellsite management, Geologic mapping, Coring Extraction, Core Analysis, Giddings Soil Probe drilling, Vibracore sediment sampling, Environmental stream gauging and analysis, Slug testing, Water well monitoring, Coal Bed Methane (CBM) well drilling and natural gas extraction

Laboratory Experience: Mass spectrometry, Stable Isotope Calibration and Coulometry, General geochemistry laboratory analysis, Rock preparation and thin section, Petrographic Microscopy and mineral identification, Particle Size Analysis - Malvern Mastersizer, Fluoroscope, Cuttings Analysis, Bomb calorimetry, Fusion Oven, Moisture gas ovens, LECO sulfur analyzer, Dry

sieving, Mechanical Sieving via sieve shakers, Wet sieving, Chemical Float/Sink Density testing, Baldor crushers, Baldor pulverizers, et al.

Software: *Petra*, *ArcGIS*, *Spotfire*, *IHS (SMT) Kingdom*, *Surfer*, *VigiGraphics* (Geoservices), All Microsoft Office software (*Word*, *Excel*, *PowerPoint*, *Access*). Various pricing software. Limited experience with *AutoCAD 14* design, UNIX programming, *20-20 Design*, and *Chief Architect* design software.

Memberships: Member of GSA (Geological Society of America), AAPG (American Association of Petroleum Geologists)